

CARLSON, Paul E.

MEASUREMENT OF SNOWFALL BY RADAR

Department of Meteorology

Doctor of Philosophy

ABSTRACT

Two aspects of one major snowstorm were analysed using 3-cm radar observations taken at a number of heights: (i) the correlation of radar returns taken at low heights with snowfall measurements at the ground, (ii) the variation of radar returns with height, and with time.

For 20 grid points within 42-miles range, the ratio of amounts measured by radar at 5000 ft to amounts measured at the ground had a log-normal distribution, the standard deviation corresponding to ratio 1.3 and its reciprocal. It was found that useful measurements of snowfall amount could be derived from radar observations out to 100-miles range, and that the variation of snowfall rate at a point could be determined from observations taken earlier along the trajectory of the snow falling toward that point.

Radar data from greater heights showed that more than 95% of the snow that fell within 100-miles range had been generated below 20 000 ft, and that the growth of snow with distance fallen varied in space and time. Thus in regions north of the radar half the growth was at heights between 10 000 ft and 5000 ft; in regions south of the radar half the growth was between 15 000 and 10 000 feet.

MEASUREMENT OF SNOWFALL BY RADAR

P.E. Carlson

MEASUREMENT OF SNOWFALL BY RADAR

P.E. Carlson, M.A.

A thesis submitted to the Faculty of Graduate
Studies and Research in partial fulfilment of the
requirements for the degree of Doctor of Philosophy.

Department of Meteorology,
McGill University,
Montreal, P.Q.

March 1970

Preface

The historical sequence of work that led to the present study is outlined in Chapter 1. Apart from certain sections of Chapter 5, where results of similar work in rain are used for comparison, the remainder of the thesis describes the results of research carried out by the author.

Acknowledgements

The author is indebted to the Meteorological Service of Canada for educational leave with financial support which made this research possible.

The stimulating guidance and supervision provided by Professors J.S. Marshall and K.L.S. Gunn are gratefully acknowledged. Discussions with them and other members of the Stormy Weather Group were helpful at many stages.

The work reported in this thesis is based on records from the CPS-9 weather-radar system operated by McGill University at Montreal International Airport. Mr. M. Claassen and Mr. P. Seidenfuss provided technical assistance relating to that system.

Data extraction and processing were carried out by Mrs. Evelyn Pearl, Mrs. Shanta Chervu, and Mrs. Sandra McBride. Their assistance was indispensable.

The efforts of Miss Ursula Seidenfuss, who drafted and photographed the diagrams, and from Miss Arlene Milburn and Mrs. Suzette Loroway, who typed preliminary drafts and final text, are sincerely appreciated.

TABLE OF CONTENTS

1. Introduction	1
1.1 Background	1
1.2 Radar equation for distributed precipitation particles	2
1.3 Relationships between radar reflectivity and snowfall rate	3
2. The Snowstorm of 6-8 February 1964	9
3. Mapping of Snowfall Amounts	14
3.1 Climatological	14
3.2 Radar	17
4. Comparison of Snowfall Amounts	24
4.1 Radar/climat ratio	24
4.2 Short-range data	26
4.3 Medium-range data	28
4.4 Long-range data	30
4.5 Asymmetrical pattern of radar measurements	32
5. Comparison with Other Results	36
5.1 Rain in Illinois	37
5.2 Rain in Indiana	40
5.3 Rain in New Jersey	43
5.4 Snow at Montreal	46
5.5 Accuracy of radar measurements	48
6. Variation of Snowfall Rates at a Point	50
6.1 Gauge-measured rates	50
6.2 Snow trails and trajectories	52
6.3 Radar-derived rates	56
6.4 Comparison of gauge-measured and radar-measured rates	59
7. Variation of Radar-derived Snow Parameters with Height	60
7.1 Grid-point values of snowfall amount	60
7.2 Variation of radar amount with height	62
7.3 Duration of snow exceeding given rates	63
7.4 Variation with time of averaged snowfall parameters	65
8. Conclusions	70
References	73
Appendix 1	A1
Appendix 2	All

1. Introduction

1.1 Background

Radar was first used during World War II for remote detection and tracking of military targets. Those operations were hampered at times by the appearance of large, slow-moving areas of clutter on the radar displays. Investigators soon verified that this type of clutter resulted from radar detection of precipitation. Concurrent theoretical developments indicated that radar was potentially a quantitative tool for remote measurement, as well as detection, of precipitation.

Precipitation is an unusual radar target in being a patterned continuum of distributed particles. In most radar operations, the patterned continuum of sea or ground clutter, or precipitation is the undesirable background from which the desired point targets must be discriminated. In weather-radar operations, the undesirable background of sea or ground clutter must be suppressed, or eliminated, to permit unambiguous detection, and measurement, of radar-signal returns from precipitation.

Early efforts to measure rainfall using 3-cm radars (i.e. operating at wavelength 3 cm) verified that attenuation became appreciable in moderate rain, and severe in heavy rain. Thus, attenuation severely limited the accuracy of 3-cm radar measurements through intervening rain. Attempts to develop attenuation-correction circuits met with limited success; mainly because radar calibrations could not be maintained within the extremely narrow limits that were necessary for attenuation corrections to be reliable. Negligible attenuation occurs at wavelengths > 8 cm, and 10-cm radars are often used for applications that require reliable performance in rain.

In dry (cold) snow, attenuation is negligible at wavelengths > 3 cm; however, in wet (melting) snow, attenuation is severe at wavelength 3 cm, and even at 5 cm (Gunn and East, 1954). Therefore, weather radars operating at wavelength 3 cm should be capable of providing remote measurements in snow as long as wet snow situations are avoided.

The efforts to date, toward measurement of snowfall by radar, have involved comparison of gauge-measured snowfall rates at a few points with concurrent radar measurements in the falling snow above those points (Langille and Thain, 1951; Kodaira and Inaba, 1955; Austin, 1963). Although the results obtained in each case indicate a significant correlation between radar and surface observations, there is insufficient evidence to ascertain the reliability of snowfall measurements by radar.

1.2 Radar equation for distributed precipitation particles

The average power received by a radar from precipitation is given by

$$\bar{P}_r = \frac{C |K|^2 Z}{r^2} \quad (1.1)$$

where

$Z = \sum D^6$, radar reflectivity, the sum of the sixth powers of the diameters of the precipitation particles per unit volume ($\text{mm}^6 \text{m}^{-3}$),

$|K|^2$ is a dielectric factor (0.93 for water, 0.20 for ice),

r is the range,

and C is a calibration factor that takes into account the operating characteristics of the radar.

This generally-accepted form of the radar equation (Battan, 1959) is based on assumptions that the radar beam is entirely filled with uniform precipitation, and that there are no losses by attenuation along the radar beam.

The CPS-9 radar (wavelength 3.2 cm) used in this study is equipped with a circuit to correct for the variation of received power with the inverse square of range. The calibration factor C has been established, and the performance of the radar is routinely monitored, by means of electronic tests. The quantity actually displayed on the radar maps may be described as thresholded values of $\frac{P_r r^2}{C}$, or $|K|^2 Z$ (equivalent radar reflectivity).

The radar reflectivity of a snowflake is not necessarily related to its physical size, but to its mass. For convenience, this is expressed in terms of the diameter of the water drop to which the snowflake would melt. Thus, radar reflectivity is defined as $Z = \sum D^6$, both for rain and for snow.

1.3 Relationships between radar reflectivity and snowfall rate

Measurements of radar reflectivity Z in falling snow are converted to radar measurements of snowfall rate R , through the use of statistical Z - R relationships. Several Z - R relationships have been derived from size distributions of snowflakes observed in samples of falling snow taken near the ground (Imai, Fujiwara, Ichimura, and Toyama, 1955; Gunn and Marshall, 1958; Ohtake, 1968).

The relationship used in this study is $Z = 2000 R^{2.0}$ (Gunn and Marshall, 1958), where Z is in $\text{mm}^6 \text{m}^{-3}$ and R is in mmw h^{-1} (mmw: millimetres of water). Gunn and Marshall used a brushed angora-wool surface and dyed filter papers to obtain size distributions of aggregate snowflakes for 20 samples taken on 10 different days during one winter season. Horizontal size distributions for each of the samples were converted to spatial size distributions using a relationship between fallspeed of aggregate flakes (v) and

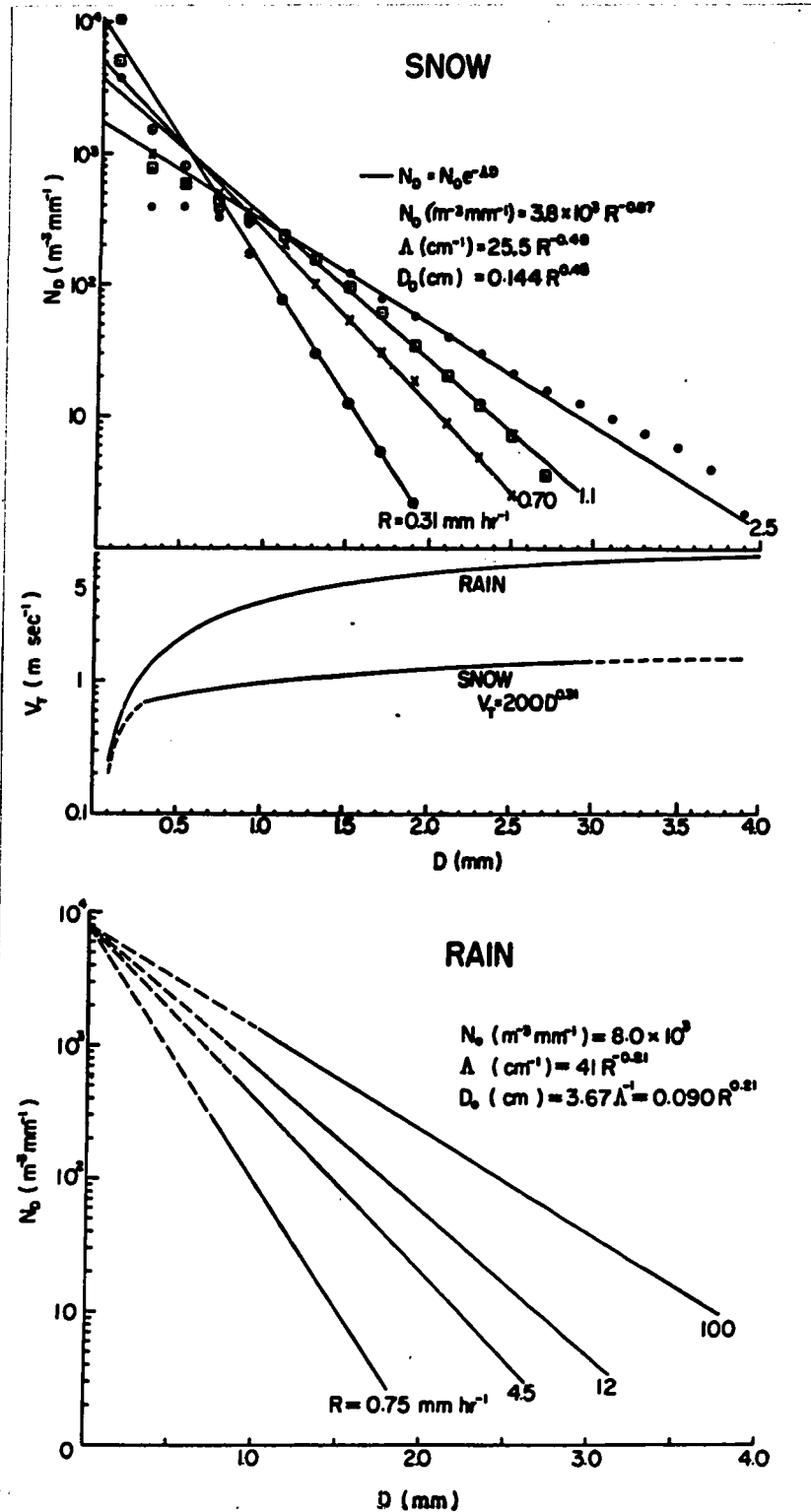


Figure 1.1. Top: averaged size distributions of aggregate snowflakes $N_D = N_0 e^{-\Lambda D}$ (after Gunn and Marshall, 1958)
 Middle: fallspeeds of raindrops (from Gunn and Kinzer, 1949) and snowflakes (from Langleben, 1954)
 Bottom: average rain distributions given by Marshall and Palmer's (1948) equation.

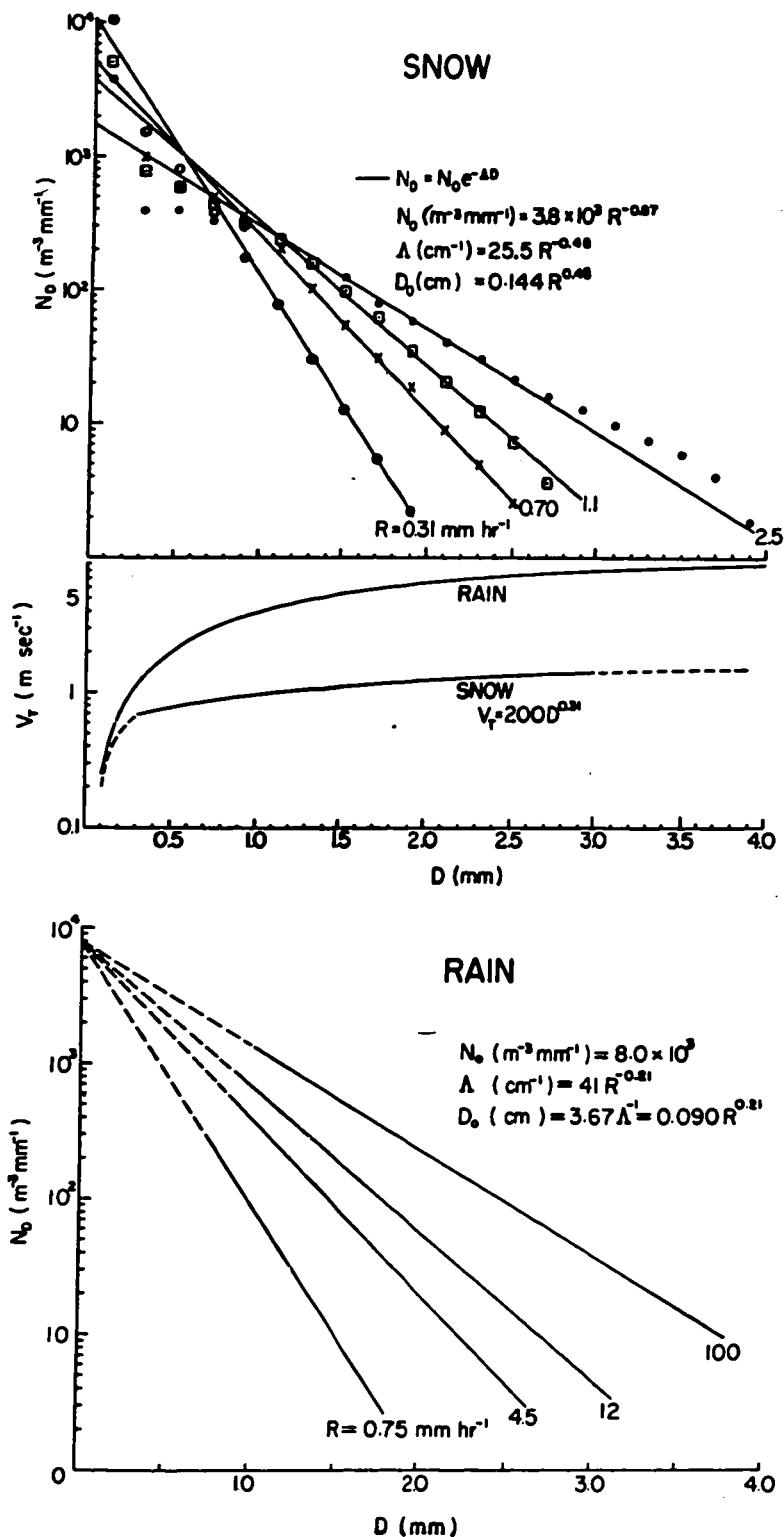


Figure 1.1. Top: averaged size distributions of aggregate snowflakes $N_D = N_0 e^{-\Lambda D}$ (after Gunn and Marshall, 1958)
 Middle: fallspeeds of raindrops (from Gunn and Kinzer, 1949) and snowflakes (from Langleben, 1954)
 Bottom: average rain distributions given by Marshall and Palmer's (1948) equation.

diameter of melted snowflakes (D) based on work by Langleben (1954) i.e. $v = 200 D^{0.31}$, where v is in cm sec^{-1} and D is in cm . Values of Z and R obtained from each sample were plotted on a log-log scale, and fitted by eye to obtain an average relationship, $Z = 2000 R^{2.0}$, for aggregate snowflakes.

Gunn and Marshall also reported averaged size distributions of aggregate snowflakes at snowfall rates 0.31, 0.70, 1.1, and 2.5 mmw h^{-1} . These are shown in Figure 1.1 along with corresponding M-P (Marshall and Palmer, 1948) distributions for rain. In each case, averaged data were fitted by inverse exponentials of the form $N_D = N_0 e^{-\Lambda D}$ and indicated relationships between N_0 , Λ , and precipitation rate, R , were determined by the respective authors. The range of snowfall rates is much smaller than the range of rainfall rates, as might be expected; but the range of diameters of melted flakes is greater than the range of rain-drop diameters at comparable precipitation rates.

The central portion of Figure 1.1 gives the fallspeeds of raindrops (Gunn and Kinzer, 1949) and aggregate snowflakes (Langleben, 1954), each as a function of diameter. Except for diameters less than 1 mm, snowflakes fall at one-fifth the speed of raindrops with the same diameter.

Imai, Fujiwara, Ichimura, and Toyama (1955) used an automatic sampler for continuous observation of the size distribution of falling snowflakes during one two-hour period. Snowfall rates were mostly in the range 0.1 to 1 mmw h^{-1} . Fallspeeds of snowflakes, and diameters of melted flakes were also measured: the resulting data were in close agreement with those of Langleben (1954) and they used $v(\text{cm sec}^{-1}) = 207 D^{1/3}$ (D in cm) to convert horizontal size distributions into corresponding spatial distributions. Imai et al (1955) calculated Z and R values for each minute of record. For the

first 20 minutes, the snow was composed mainly of single crystals with relatively few aggregate flakes and the Z-R data fell about the locus $Z = 600 R^{1.8}$. For the remainder of the period, the snow was composed mainly of aggregate flakes with relatively few single crystals and the Z-R data fell about the locus $Z = 2100 R^{1.8}$ (averaging the loci, $Z = 2400 R^{1.8}$ and $Z = 1800 R^{1.8}$, reported by Imai et al).

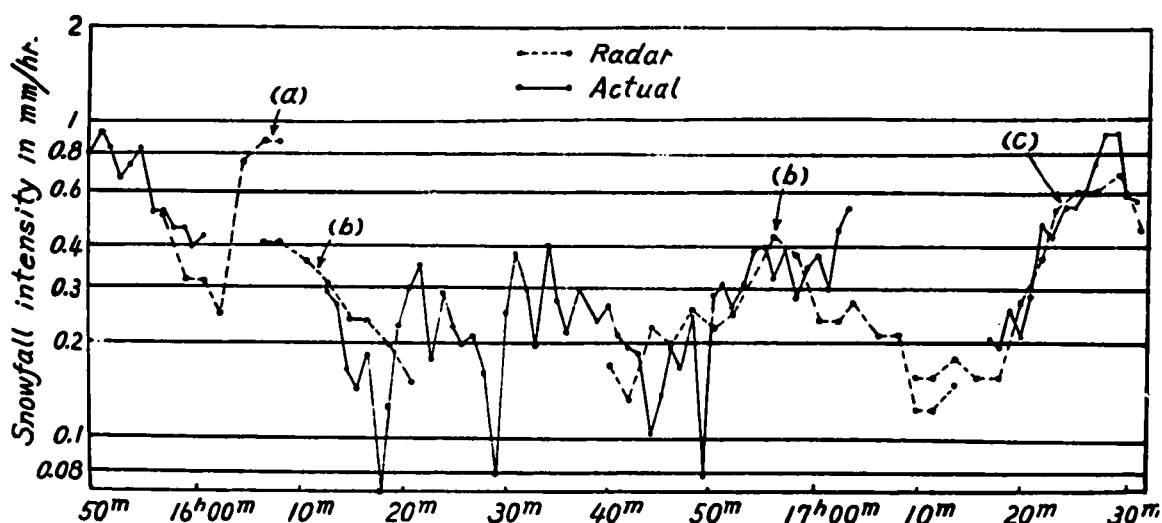


Figure 1.2. Comparison of radar-measured snowfall rates (mmw h^{-1}) with actual (sampler-measured) rates (after Kodaira and Inaba, 1955)

a) $Z = 600 R^{1.8}$ b) $Z = 2400 R^{1.8}$ c) $Z = 1800 R^{1.8}$

Kodaira and Inaba (1955) used a 3-cm radar to measure radar-signal power from the falling snow over the snowflake sampler during its operation by Imai et al (1955). Measured values of P_r at one-minute intervals were converted to radar snowfall rates, using a modified form of the radar equation and the Z-R relationships derived by Imai et al. Snowfall rates measured by the sampler and by radar (Figure 1.2) proved to be comparable, but the Japanese authors were concerned about the rapid variations in size distribution of snowflakes, and resultant Z-R relationships, over the two-hour period.

first 20 minutes, the snow was composed mainly of single crystals with relatively few aggregate flakes and the Z-R data fell about the locus $Z = 600 R^{1.8}$. For the remainder of the period, the snow was composed mainly of aggregate flakes with relatively few single crystals and the Z-R data fell about the locus $Z = 2100 R^{1.8}$ (averaging the loci, $Z = 2400 R^{1.8}$ and $Z = 1800 R^{1.8}$, reported by Imai et al).

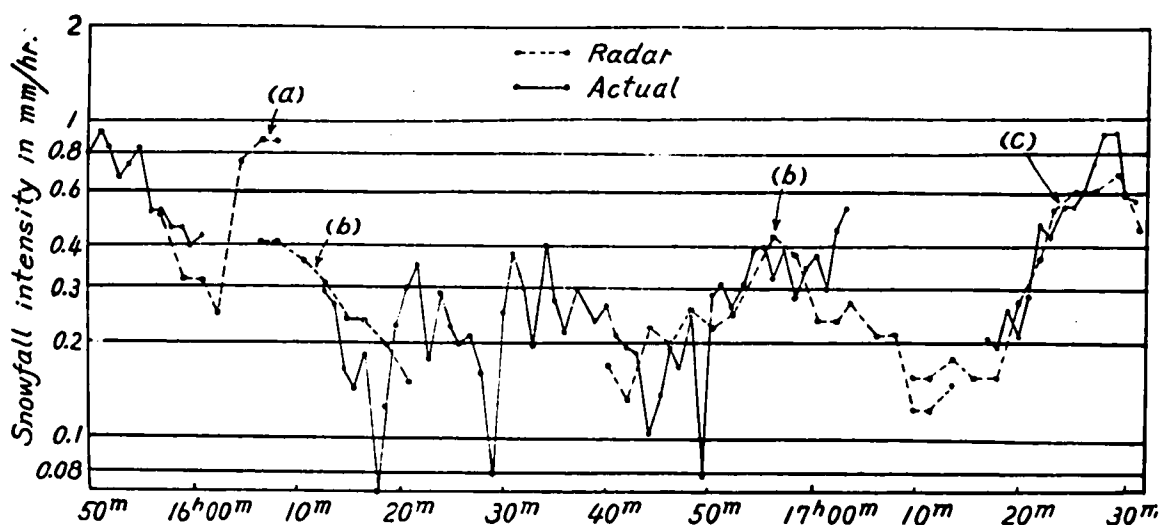


Figure 1.2. Comparison of radar-measured snowfall rates (mmw h^{-1}) with actual (sampler-measured) rates (after Kodaira and Inaba, 1955)

a) $Z = 600 R^{1.8}$ b) $Z = 2400 R^{1.8}$ c) $Z = 1800 R^{1.8}$

Kodaira and Inaba (1955) used a 3-cm radar to measure radar-signal power from the falling snow over the snowflake sampler during its operation by Imai et al (1955). Measured values of P_r at one-minute intervals were converted to radar snowfall rates, using a modified form of the radar equation and the Z-R relationships derived by Imai et al. Snowfall rates measured by the sampler and by radar (Figure 1.2) proved to be comparable, but the Japanese authors were concerned about the rapid variations in size distribution of snowflakes, and resultant Z-R relationships, over the two-hour period.

Ohtake (1968) used a brushed angora-wool surface and dyed filter papers to obtain simultaneous observations of size distributions in snow and rain, above and below the melting layer. His observations cover a four-day period during which the dominant crystal-type in the snow above the melting layer varied from time to time. Because of uncertainties regarding the fallspeed of precipitation particles in the vicinity of the melting layer, Ohtake mainly dealt with horizontal, rather than spatial, size distributions. Later he used the fallspeed relation $v(\text{cm sec}^{-1}) = 200 D^{0.31}$ (D in cm), for snowflakes of all crystal types, to obtain the Z-R relationships given in Table 1. These relationships were reported verbally at the 13th Conference on Radar Meteorology (Montreal, 1968).

Table 1 - Z-R Relationships for Snow

<u>Dominant Crystal-type</u>	<u>Z-R Relationship</u>
Plane dendrite	$Z = 2000 R^{1.6}$
Spatial dendrite	$Z = 1700 R^{1.6}$
Column and thick plate	$Z = 370 R^{1.4}$
Bullet	$Z = 860 R^{1.8}$
Needle	$Z = 860 R^{1.7}$

Ohtake's Z-R relationships for dendritic snow are similar to those reported by Gunn and Marshall (1958) and Imai et al (1955) for aggregate snowflakes. The relationships for bullet-shaped, and needle-shaped, crystals fall between the relationship $Z = 600 R^{1.8}$ reported by Imai et al (1955) for single-crystal snow, and the relationship $Z = 1000 R^{1.6}$ (Austin, 1963). Upon inclusion of the dielectric factor, the latter relationship allows radar data for snow to be processed in the same manner as that for rain, using $Z = 200 R^{1.6}$.

Austin (1963) compared snowfall rates measured by gauges and by radar, using $Z = 1000 R^{1.6}$, in nine New England snowstorms. She found that no adjustment of the relationship was required for six of those storms. For the other three storms, comprised mainly of light snow, with maximum rates between 0.5 and 4.0 mmw h⁻¹, some upward adjustment of radar-derived rates was required.

In the present case, two aspects of one major snowstorm are analysed using 3-cm radar data taken at a number of heights: (a) correlation of low-level radar returns with measurements of new-fallen snow at climatological stations, (b) variation of radar returns with height, and with time.

2. The Storm of 6-8 February 64

Two separate snowfalls, which occurred in the Montreal area from 6-8 February 64, were produced by a large, complex extra-tropical cyclone. The first snowfall was associated with an occluding frontal wave that moved northeastward along the Atlantic coast toward the Bay of Fundy, while the second snowfall was associated with a pressure trough that later moved northeastward along the St. Lawrence Valley from eastern Lake Ontario to Quebec City.

The situation at 0700EST 6 February (1200GMT), approximately 14 hours before the onset of the first snowfall at Montreal, is depicted in Figure 2.1. The surface map shows three low-pressure centres, each located about 600 miles from Montreal, which were moving rapidly on converging paths toward the New England states. The northernmost low (L1) was associated with an arctic frontal wave that had moved from southern Alberta to central Lake Superior in 24 hours. Arctic air was pouring southward across the Canadian Prairies into the American plains states. The leading edge of the arctic air mass already extended from Lake Superior to northern Texas. This arctic cold front advanced across the Mississippi Valley and eastern United States until it reached the Atlantic coast some 42 hours later. The second low (L2), centred over Ohio, was the remnant of a cold low that had stagnated over western Texas until 24 hours before; it then accelerated rapidly northeastward. The southernmost low (L3), centred over North Carolina, was associated with a frontal wave that had formed in southern Texas three days before. For 48 hours it had moved slowly eastward toward the Mississippi delta, and then accelerated along a curving path into the Carolinas.

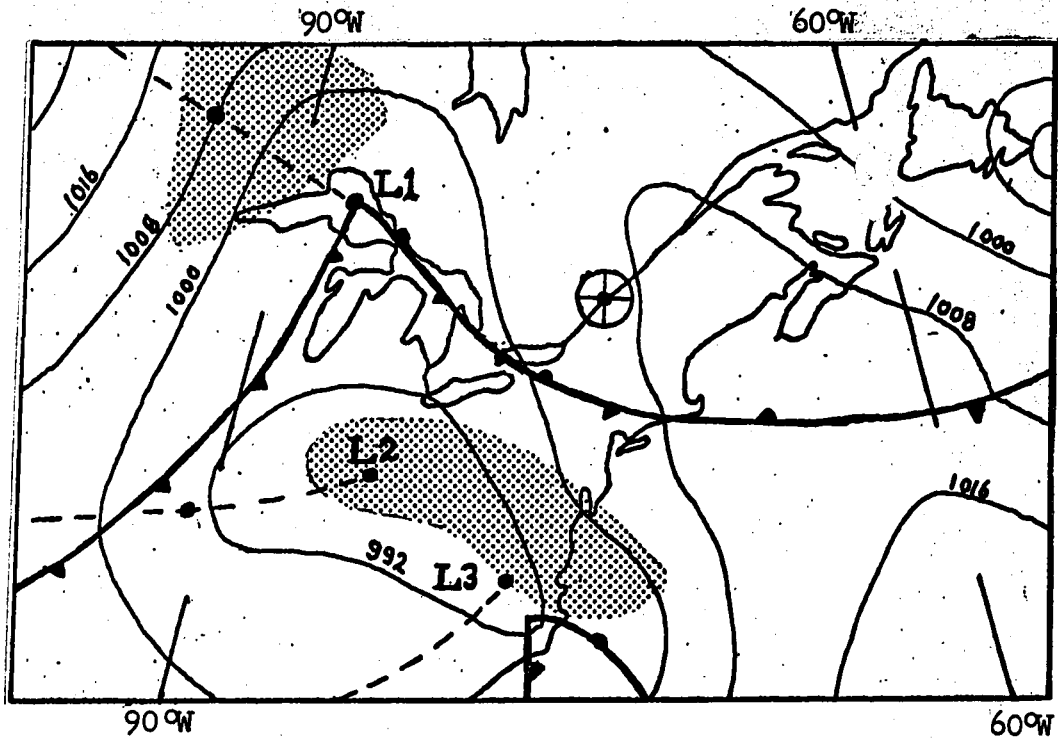


Figure 2.1. Synoptic map for 0700EST 6 February. Isobars at 8-mb (millibar) intervals, positions of low-pressure centres at 12-hour intervals (●---●), and fronts (—▲—).
 ⊕ Montreal (MTL) [shaded area] area of precipitation

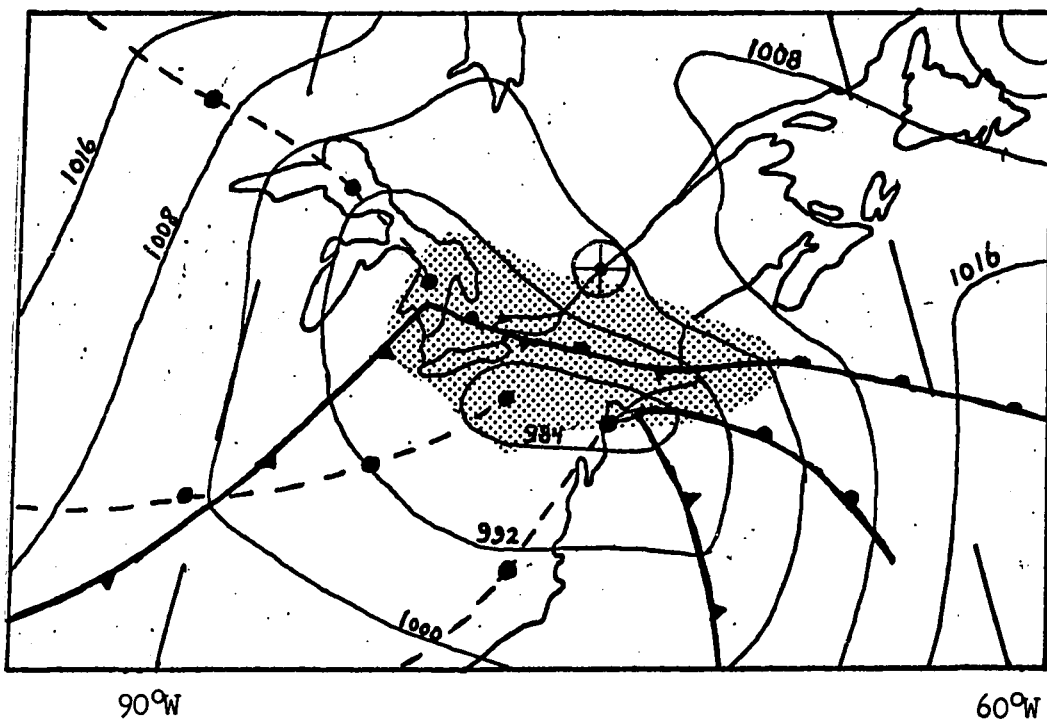


Figure 2.2. As above, for 1900EST 6 February (07/0000GMT).

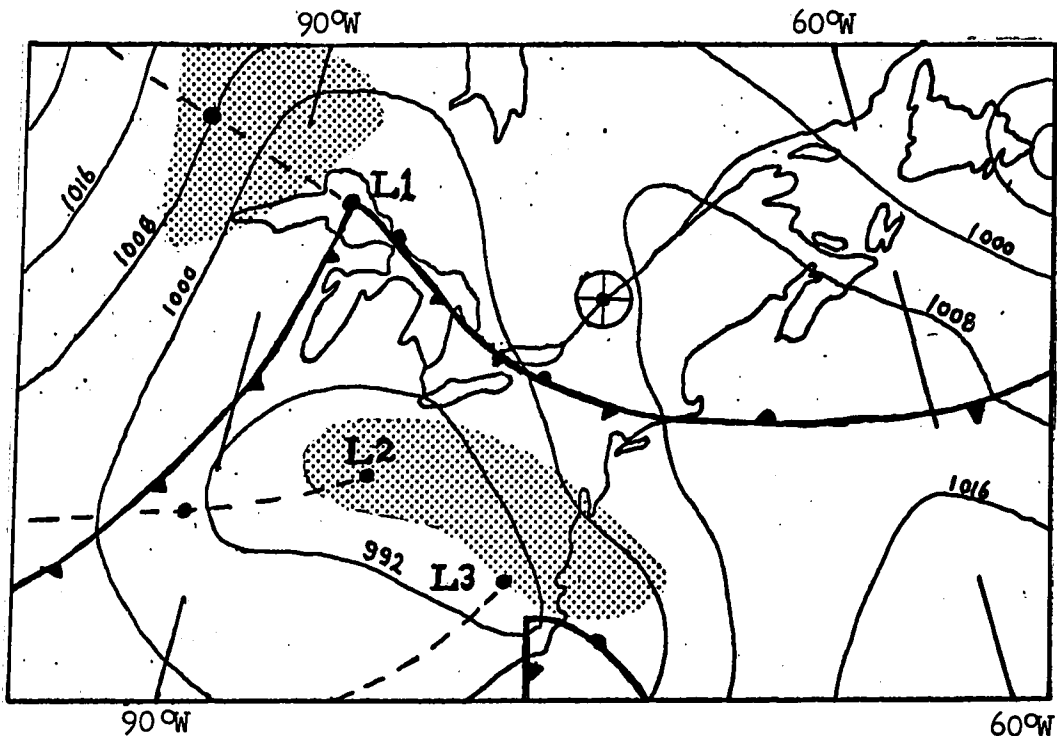


Figure 2.1. Synoptic map for 0700EST 6 February. Isobars at 8-mb (millibar) intervals, positions of low-pressure centres at 12-hour intervals (●- -●), and fronts (—▲—).
 ⊕ Montreal (MTL) [shaded area] area of precipitation

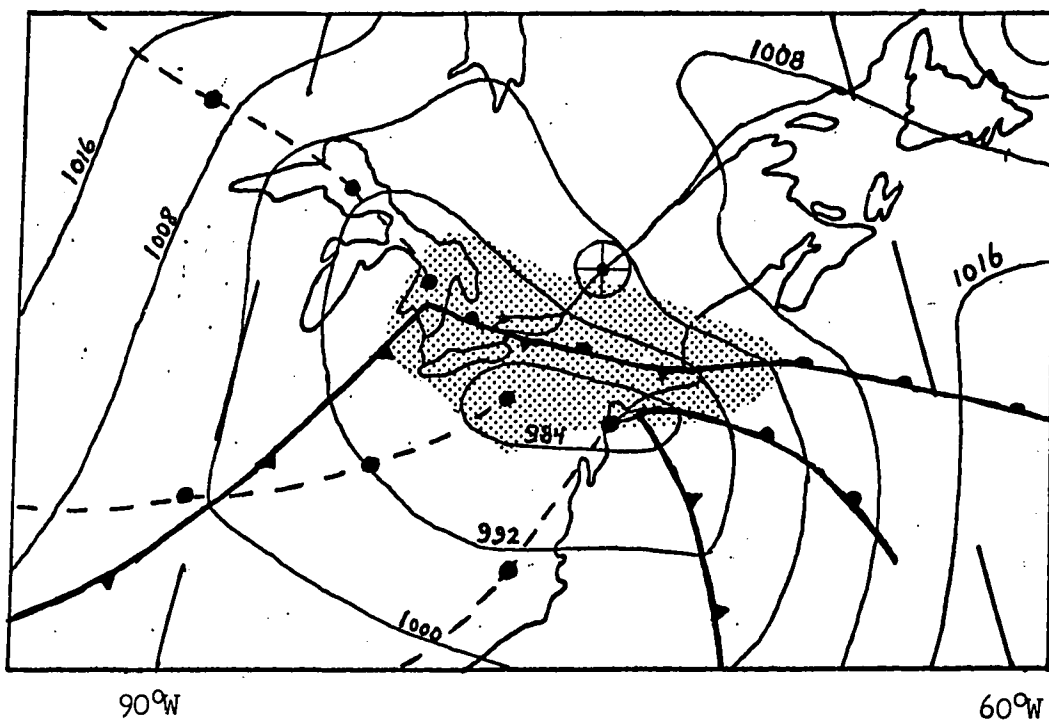


Figure 2.2. As above, for 1900EST 6 February (07/0000GMT).

The situation at 1900EST 6 February (07/0000GMT), approximately 2 hours before the onset of the first snowfall at Montreal, is depicted in Figure 2.2. The surface map shows that the three lows (L1, L2, and L3) comprised a large cyclonic circulation encompassing the eastern United States, Ontario, and a large portion of southern Quebec. The edge of a large area of precipitation had advanced to an east-west line just south of Montreal. The low over northern Lake Huron (L1) was decelerating and turning eastward. The low near Washington, D.C. (L3), and its occluding frontal wave, were advancing northeastward along the coast at an average speed of 30 mi h^{-1} . The central pressure of this low had dropped 8 mb in 12 hours, from 988 to 980 mb. The remnant of the cold low from Texas (L2) was located in northeastern Pennsylvania and was rapidly losing its identity as a closed low at the surface, although it remained identifiable on the 850-mb and 700-mb maps.

Figure 2.3 shows the situation at 0700EST 7 February, after the first snowfall had ended at Montreal. The low over Georgian Bay (L1) was moving eastward slowly, while the low on the Maine coast (L3) was moving northeastward at 30 mi h^{-1} toward the Bay of Fundy. The surface pressure trough, across the St. Lawrence Valley southwest of Montreal, was maintained as a weak, but identifiable feature linking the main cyclonic centres (L1 and L3) for approximately 12 hours. During that period, it moved northeastward along the St. Lawrence Valley, and generated a second snowfall in the Montreal area 8 to 12 hours after the first snowfall had ended.

Figure 2.4 shows the situation at 1900EST 7 February (08/0000GMT), during the second snowfall at Montreal.

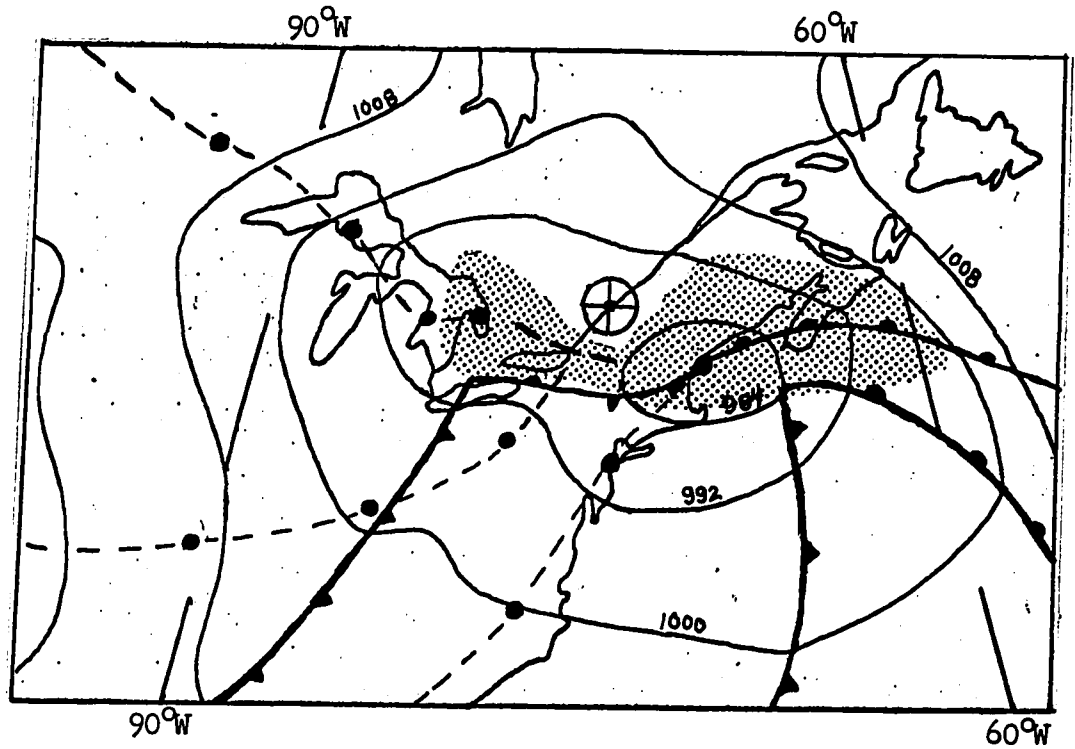


Figure 2.3. Synoptic map for 0700EST 7 February (07/1200GMT).
Parameters as indicated for Fig. 2.1.

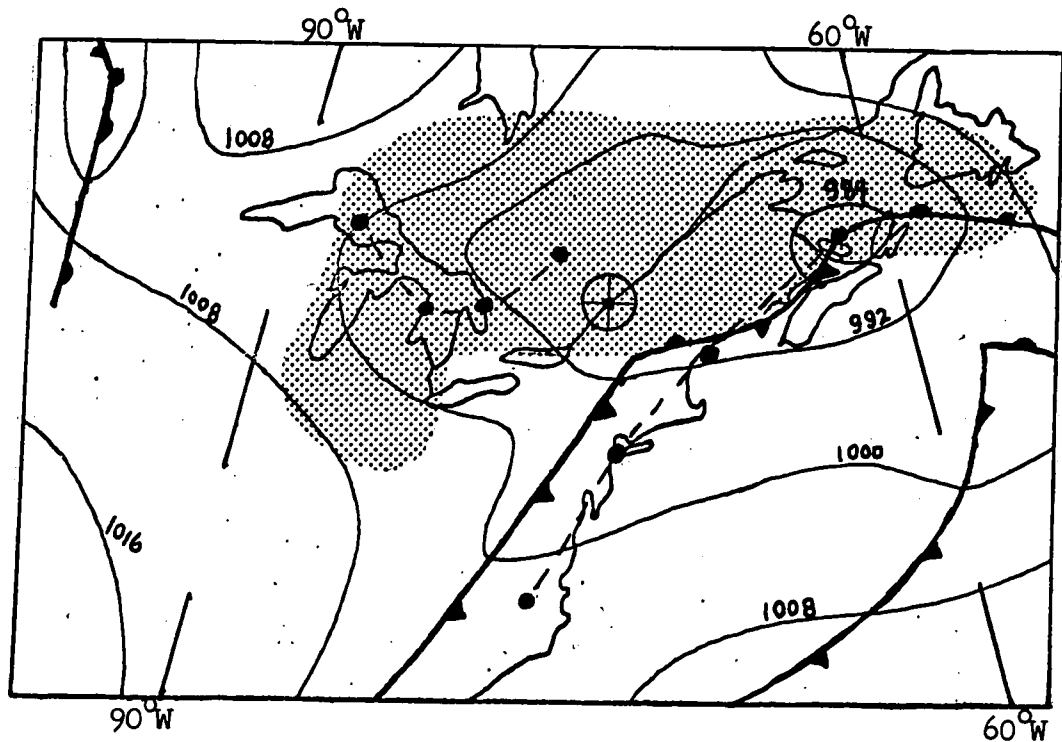


Figure 2.4. Synoptic map for 1900EST 7 February (08/0000GMT).
Parameters as indicated for Fig. 2.1.

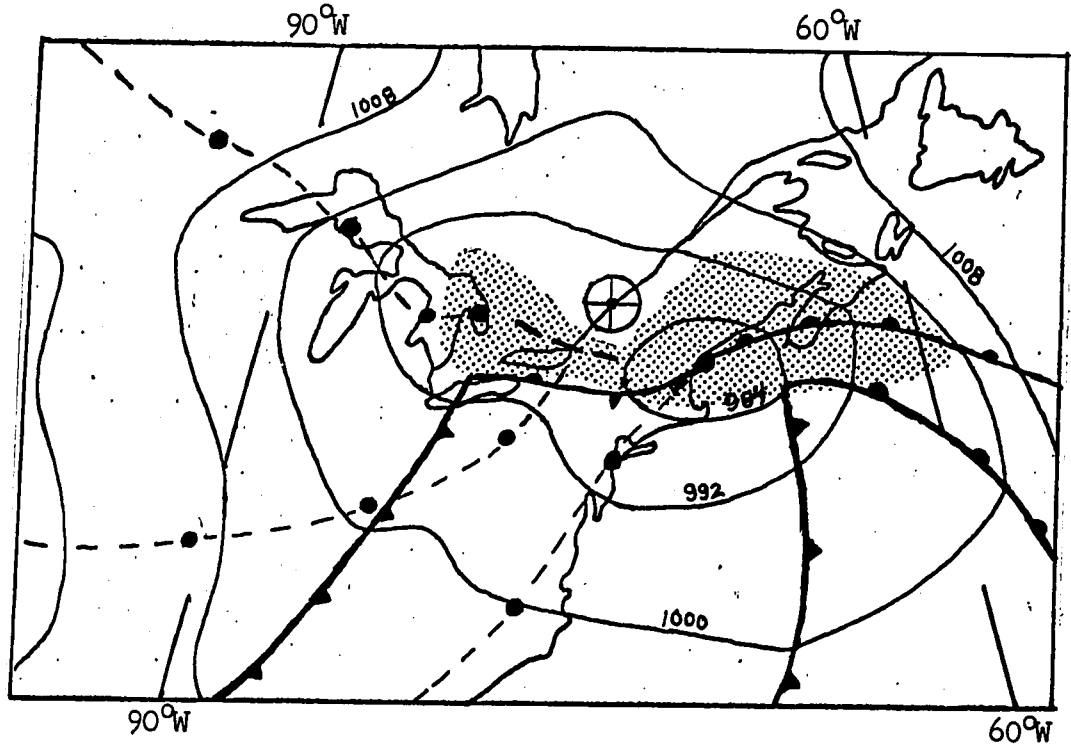


Figure 2.3. Synoptic map for 0700EST 7 February (07/1200GMT).
Parameters as indicated for Fig. 2.1.

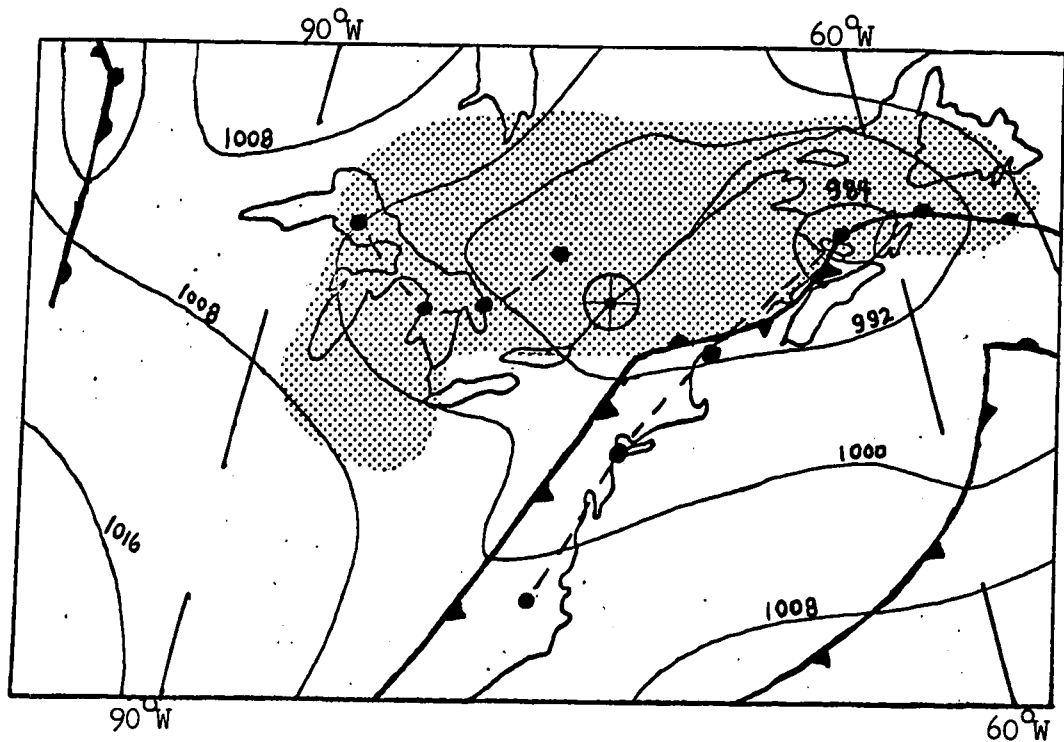


Figure 2.4. Synoptic map for 1900EST 7 February (08/0000GMT).
Parameters as indicated for Fig. 2.1.

Synoptic maps at 6-hour intervals, and intermediate 3-hourly maps, provided basic information regarding motion of pressure systems and related weather parameters for the period under study.¹

Upper-air data (temperature, dewpoint, wind speed and direction) were obtained from analysed maps for pressure levels 850, 700, and 500 millibars at 12-hour intervals.¹ In the absence of specific data in the immediate vicinity of Montreal, it was necessary to interpolate between radiosonde and rawinsonde stations at Maniwaki and Seven Islands (Quebec), Albany and Buffalo (New York), Portland and Caribou (Maine). Temperatures reported by these stations for pressure level 850 mb (height 4 to 5 thousand feet) ranged from zero to -4°C at 1900EST 6 February, from -1 to -6°C at 0700EST and from -4 to -8°C at 1900EST 7 February.

¹Meteorological data, in the form of analysed maps, were kindly supplied by the Montreal (Public and Aviation) Weather Forecast Office, and the Central Analysis Office, Meteorological Service of Canada.

3. Mapping of Snowfall Amounts

3.1 Climatological

Routine measurements of new-fallen snow are taken at 140 stations located within 100 miles of Montreal International Airport, the location of the radar used in this study. The geographical distribution of these stations, relative to the radar site, is shown in Figure 3.1. Most of the stations are climatological stations operated by unpaid volunteers, who record total rainfall amount and/or ruler-measured amount of new-fallen snow every 24 hours. Snowfall amounts, measured in tenths of inches, are converted to amounts of water assuming a standard-snow density such that 1 inch of snow yields a tenth of an inch of water on melting. Generally, there is no information about the actual density of the new-fallen snow, or the rate at which it accumulated during 24-hour periods between observations. The climatological data used in this study were obtained from monthly summaries published by the Canadian Meteorological Service, and by the U.S. Department of Commerce, Environmental Science Services Administration.

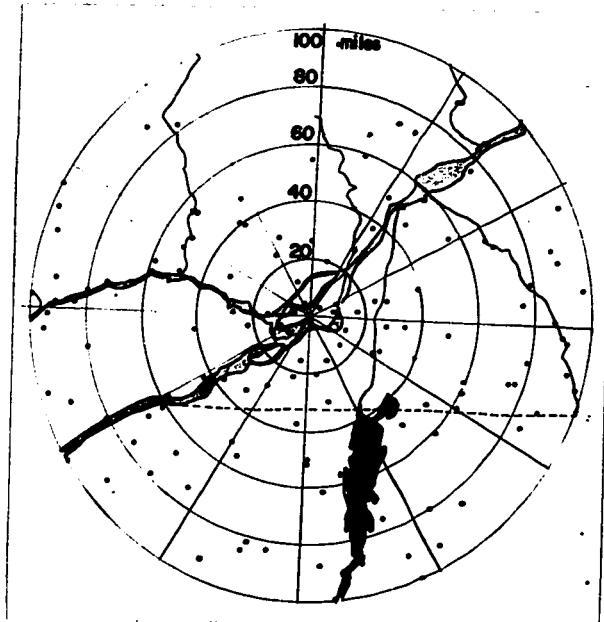


Figure 3.1. Geographical distribution of climatological stations near Montreal.

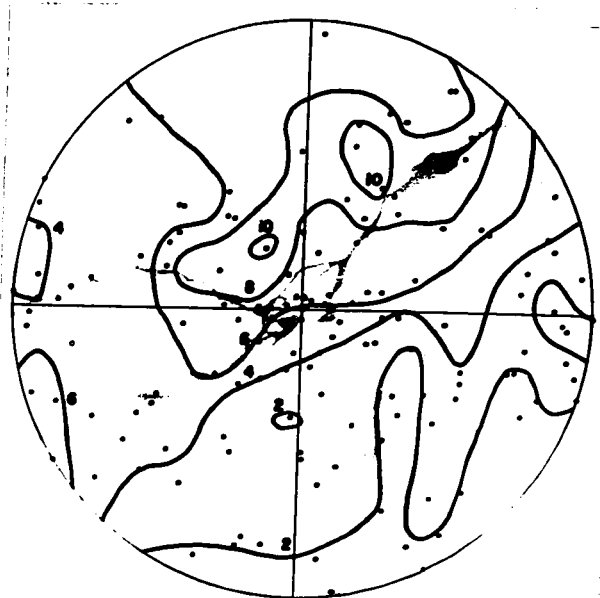


Figure 3.2. Climat isohyets (intervals of 2 inches of snow).

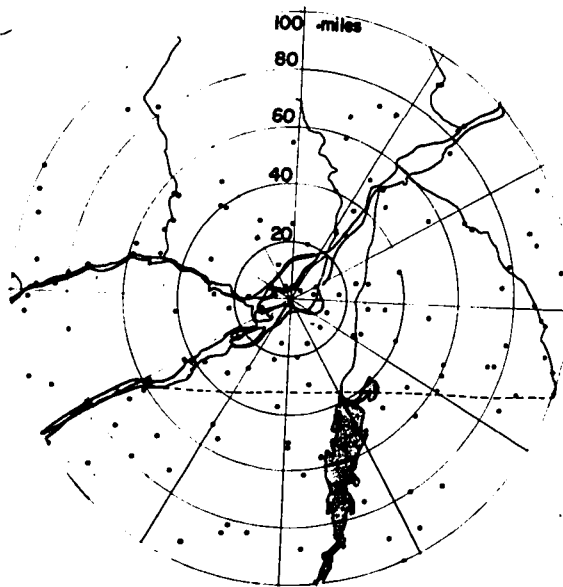


Figure 3.1. Geographical distribution of climatological stations near Montreal.



Figure 3.2. Climat isohyets (intervals of 2 inches of snow).

Climatological observations are not necessarily taken at the same time of day at all stations. Daily amounts of precipitation were recorded between 0700 and 0900EST at the majority of stations (~60%), between 1500 and 1700EST at others (~25%), and at midnight at the remaining stations. The disparity in times of observation did not create any serious problem in this study, as it was unlikely that any significant amount of snow fell in the 24 hours before 1700EST 6 February, or the 24 hours after 0900EST 8 February. However, such non-uniform times of observation coupled with a time resolution of 24 hours could cause problems in other circumstances.

The total amount of new-fallen snow reported by each station, during the 48-hour period under study, was plotted on a map and the resulting data were analysed to obtain the climat isohyets of Figure 3.2. A moderate degree of subjective smoothing was exercised in order to eliminate small-scale irregularities from the analysis. Four stations reported more than 10 inches of snow in two small areas, northeast and northwest of the radar site. Twenty stations, generally in the southeast quadrant, reported less than 2 inches of snow. Between these maxima and minima in snowfall amount, the isohyets roughly parallel the St. Lawrence River and the strongest gradient in snowfall amount occurs in the vicinity of Montreal Island, where the climatological stations are relatively close together.

Twelve of the 140 stations were equipped with recording snowgauges (actually, heated tipping-bucket raingauges), but detailed records were available from only two of them. One of those stations was located too close to the radar, i.e. less than 10 miles, for the radar data to be reliable. The variation of snowfall rate with time at the other station is compared with corresponding radar data taken in the falling snow above the gauge (Chapter 6).

3.2 Radar

The distribution of precipitation over an area of 55,000 mi² around Montreal is routinely and automatically mapped at six heights every 22.5 minutes by the McGill CPS-9 weather radar and its constant-altitude PPI (CAPPI) display system. The CAPPI display system involves three major developments, each associated with the person responsible for it. There is electronic generation of CAPPI (T.W.R. East, 1958), there is grey-scale representation of thresholded signal strength (T.H. Legg, 1960), and there is areal integration in conjunction with facsimile reproduction (M. Wein, 1965).

In normal operations, facsimile maps are produced by scanning a radar film record as it emerges from a rapid-access processor. Production of a sequence of CAPPI maps at six heights occupies 22.5 minutes, and there is a lag of no more than 7½ minutes between completion of observations at a given CAPPI height and completion of the corresponding facsimile map.

Earlier studies of this snowstorm (Gunn, Carlson, and Feldman, 1966; Carlson, 1968) were based on CAPPI maps produced by scanning the film record from the rapid-access processor. However, operation of another display tube and camera during 1963-64 had provided an archival film record, which involved normal rather than rapid-access processing.

The present study is based on a set of CAPPI maps that was produced by scanning the archival film record. The principal reason for this change was the belated finding that the response of the display tube in the rapid-access system to uniform test signals was much less uniform over the area of coverage than that of the other display tube (Appendix I). In both cases,

mappings of the non-uniformities, which give relative sensitivity of the display tubes as a function of position were used to correct the radar data.

The radar data of this study were obtained from 100 sets of CAPPI maps covering the two snowfalls during the period under study. Each set contains six CAPPI maps for six separate heights, i.e. 5, 10, 15, 20, 25, and 30 thousand feet. No snow was detected at the latter two heights during the course of this storm. The radar coverage of the two snowfalls was complete, with the exception of two periods (1½-2 hours each) in which faulty operation of a switch in the display system caused intermittent blanking of segments on the CAPPI maps. These deficiencies were offset, as much as possible, through interpolation on individual maps and interpolation between preceding and succeeding maps.

The general approach to obtaining an isohyetal mapping over an extensive area for an extended period of time from radar data, may be summarized as follows. Precipitation rate is determined and mapped from radar observations taken at low heights at regular intervals. Then each rate is multiplied by the interval between observations to yield an amount: adding these amounts one arrives at a radar isohyetal map for as long a period as required.

In the present case, data extracted from the 5000-ft CAPPI maps were used to produce an isohyetal map. Figure 3.3. shows a sample map for height 5000 ft during this snowstorm. The circle, at 100-miles range, encompasses the area under study. The quantity displayed is equivalent radar reflectivity, i.e. $|K|^2 Z = \frac{P_r r^2}{C}$, in thresholded shades of grey. There is provision for displaying as many as 6 thresholds on each CAPPI map, which actually appears as a pair of facsimile maps with alternate thresholds displayed on left-hand

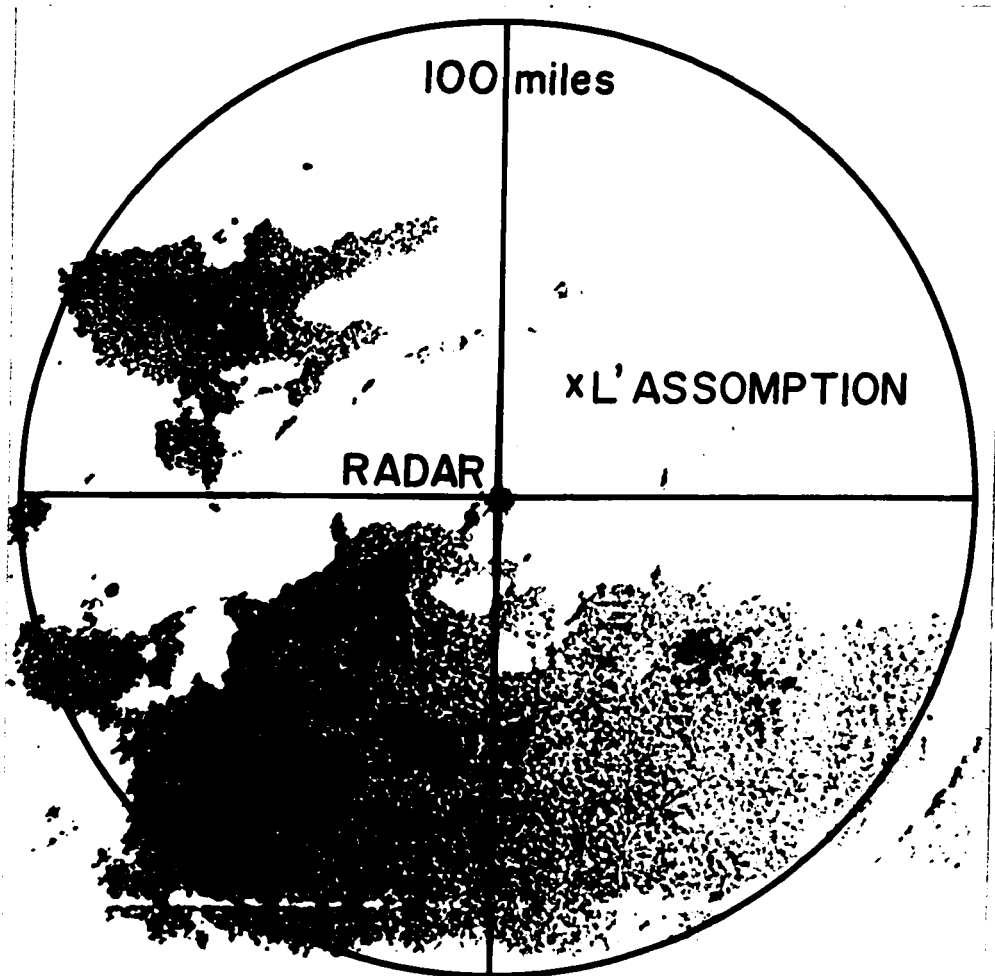


Figure 3.3. CAPPI map for height 5000 ft, thresholds 1 (light grey-shade), and 3 (medium grey-shade) appear (actual scale, for facsimile maps produced from archival film record).

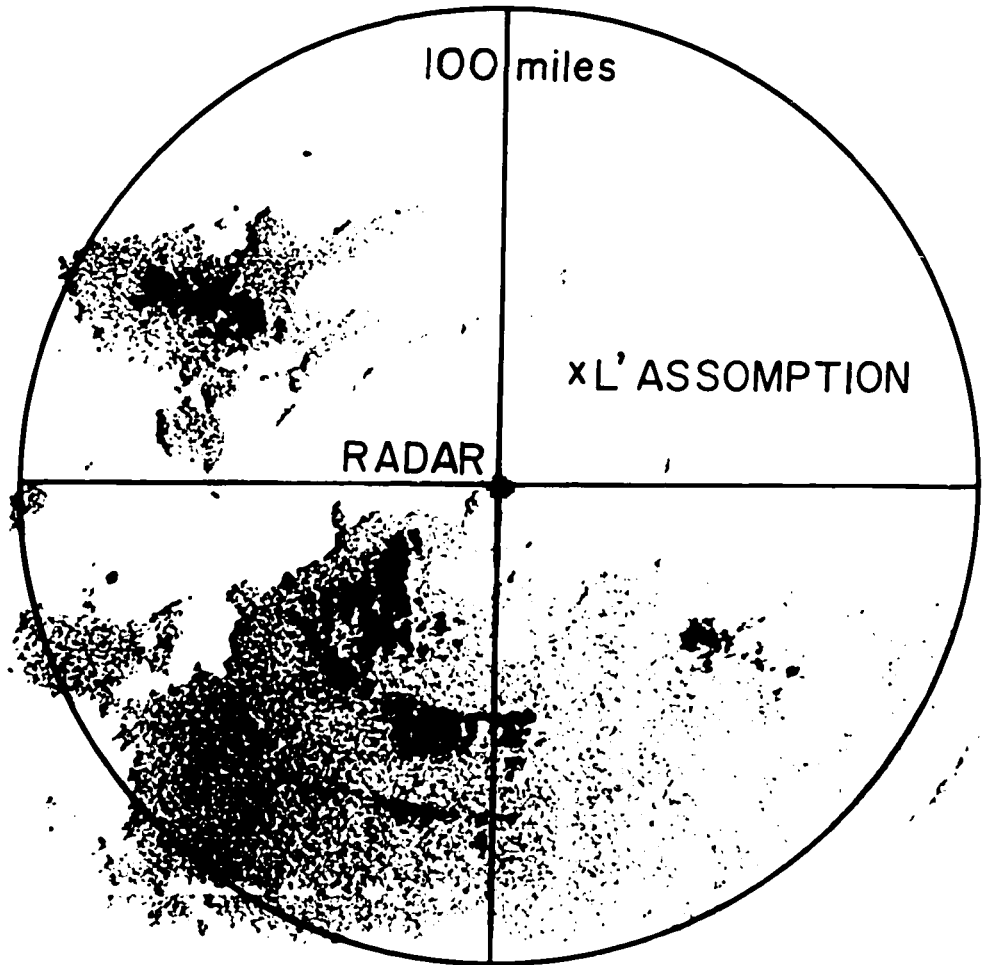


Figure 3.3. CAPPI map for height 5000 ft, thresholds 1 (light grey-shade), and 3 (medium grey-shade) appear (actual scale, for facsimile maps produced from archival film record).

and right-hand maps. Figure 3.3 shows a right-hand map on which thresholds 1 and 3 appear. The first threshold corresponds to the minimum detectable signal from a beam-filling target at 100-miles range for a given value of the calibration factor, C. Succeeding thresholds (2 to 6) are separated by a uniform factor 10 in P_r (i.e. by 10 db¹, on a logarithmic scale of P_r , or Z). The power transmitted by the radar, and the sensitivity of the receiver, are checked at regular intervals by means of a test set and standard-gain antenna mounted a short distance from the radar. The established value of the calibration factor (C) has been used, in conjunction with the radar equation (Eqn. 1.1) and the relationship $Z = 2000 R^{2.0}$ (Gunn and Marshall, 1958), to deduce snowfall rates corresponding to successive thresholds on the CAPPI maps (Table 3.1).

Table 3.1 - Snowfall rates associated with grey-shade thresholds on the CAPPI maps

Threshold		Radar Snowfall Rate	
Left Map	Right Map	(mmw h ⁻¹)	(inches of snow/22.5 minutes)
1		0.11	0.02
	2	0.33	0.05
3		1.0	0.15
	4	3.0	0.45
5		9.0	1.35
	6	27	4.0

¹The ratio of two values of P_r or Z, a/b, expressed in decibels is $10 \log_{10}(a/b)$ db.

Radar data were extracted from the 5000-ft CAPPI maps at 144 grid points, 15 miles apart in a square array. The geographical distribution of these grid points is shown in Figure 3.4. Total amount of snow was obtained at each grid point, assuming that each occurrence of a threshold or a grey shade (area between adjacent thresholds) represented the accumulation of a specified amount of snow over the 22.5-minute period between successive maps. Points immediately adjacent to a threshold, i.e. within 2 miles (0.05 inches on the scale of these maps), were assigned the snowfall amount appropriate to that threshold (Table 3.1). Points that fell in the shaded area between adjacent thresholds, were assigned snowfall amounts corresponding to the geometric mean of the upper and lower thresholds.

After total amounts of snow were obtained in the above manner, the amount at each grid point was multiplied by a factor to compensate for the non-uniformity of the display system at the time of this storm (Appendix I).

The average radar amount obtained at the twenty grid points within 42-miles range was found to be lower, by a factor 3, than the average climat amount over the same area. The averages were brought into agreement by multiplying radar amounts at all grid points by a factor 3. In effect, this represents a re-calibration of the snowfall rates associated with the thresholds on the CAPPI maps (Table 3.1) against climatological measurements over the area within 42-miles range.

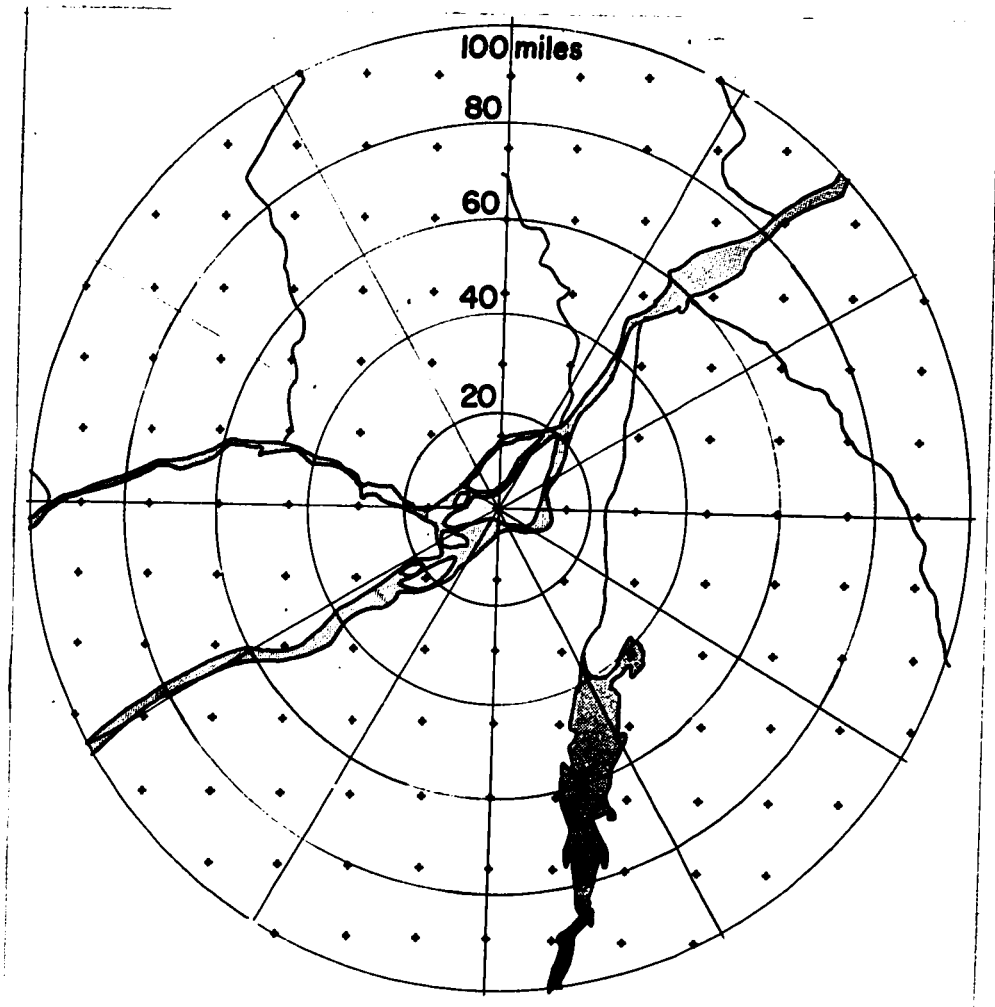


Figure 3.4. Geographical distribution of grid points at which radar data were extracted.

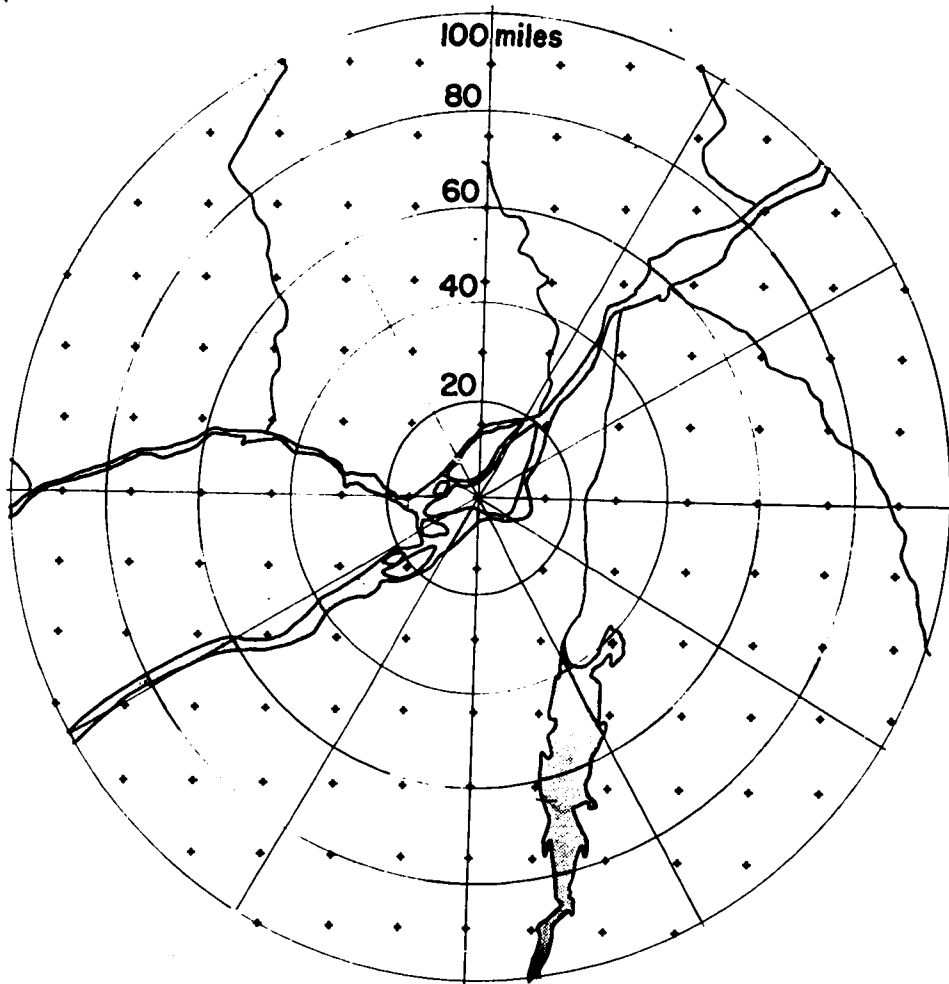


Figure 3.4. Geographical distribution of grid points at which radar data were extracted.

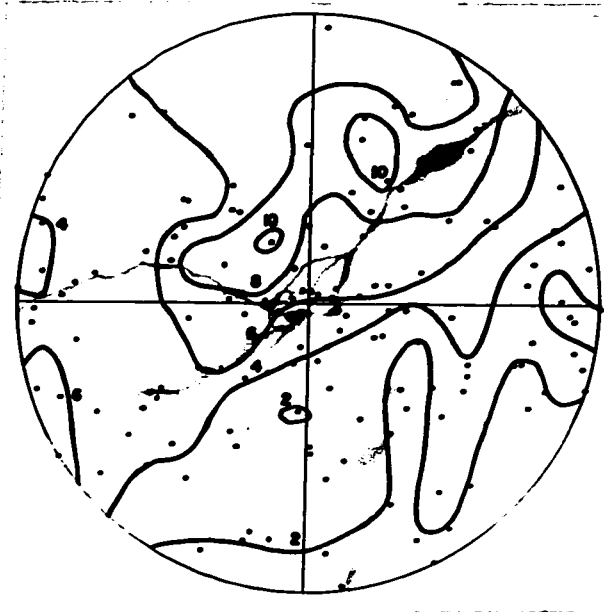


Figure 3.2 (Repeat). Climat isohyets.

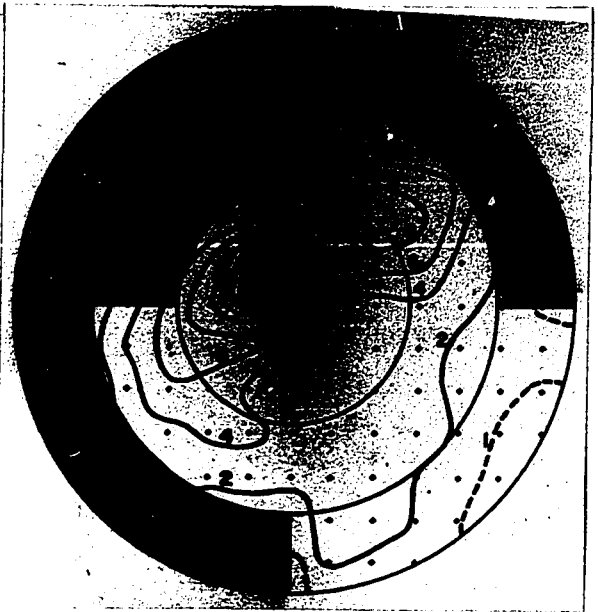


Figure 3.5. Radar isohyets (inches of snow).

Analysis of the calibration-adjusted amounts gave the radar isohyets of Figure 3.5. The pattern of isohyets on the unshaded portion of the radar map resembles that on the climat map to the extent that locations of relative maxima and minima, orientation of isohyets along the St. Lawrence River, and locations of strong gradients in amount are much the same on each map. However, radar amounts diminish rapidly with increasing range across the shaded portion of the radar maps. This "range effect" and its cause are analyzed in Chapter 4.



Figure 3.2 (Repeat). Climat isohyets.

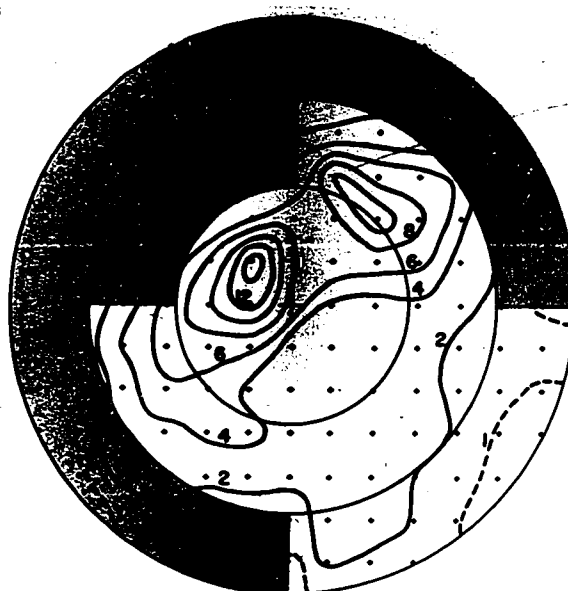


Figure 3.5. Radar isohyets (inches of snow).

Analysis of the calibration-adjusted amounts gave the radar isohyets of Figure 3.5. The pattern of isohyets on the unshaded portion of the radar map resembles that on the climat map to the extent that locations of relative maxima and minima, orientation of isohyets along the St. Lawrence River, and locations of strong gradients in amount are much the same on each map. However, radar amounts diminish rapidly with increasing range across the shaded portion of the radar maps. This "range effect" and its cause are analyzed in Chapter 4.

4. Comparison of Snowfall Amounts

4.1 Radar/climat ratio

Radar amounts at the grid points of Figure 3.5 and the corresponding climat amounts from Figure 3.2 are compared in Figure 4.1, which shows a mapping of radar/climat ratio. The median value of the ratio at grid points within 42-miles range is 1.0, as a result of the calibration adjustment described in Section 3.2. The areal variability of the radar measurements, noted in Chapter 3 and evidenced in the pattern of ratio values, led to areal grouping of the grid-point data for closer examination.

The areal groups of grid-point data, which are to be analysed in the following sections, are shown in Figure 4.2. The range boundaries at 42 and 73 miles coincide with two range gates of the 5000-ft CAPPI program (Appendix 1). The program was set up to take short-range data at a sequence of elevation angles $> 1\frac{1}{2}^{\circ}$, medium-range data at elevation $3/4^{\circ}$, and long-range data at zero-degree elevation.

Because the pattern of ratio values (Figure 4.1) varied with azimuth angle, as well as with range, the data at medium and long ranges are further sub-divided by quadrants.



Figure 4.1. Mapping of radar/climat ratio.

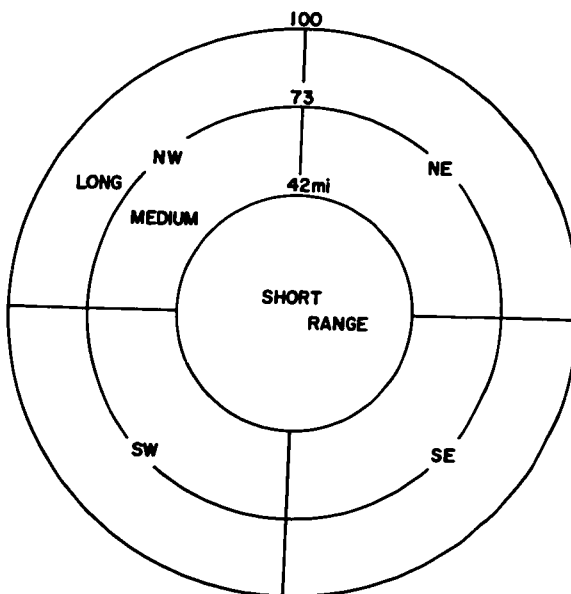


Figure 4.2. Areal groups of grid-point data.

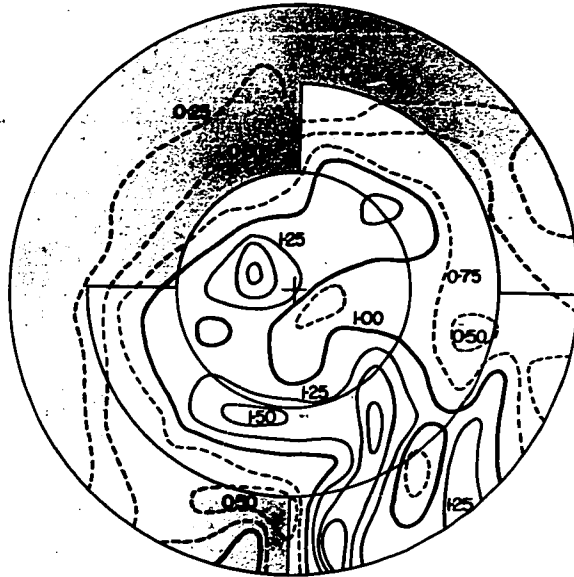


Figure 4.1. Mapping of radar/climat ratio.

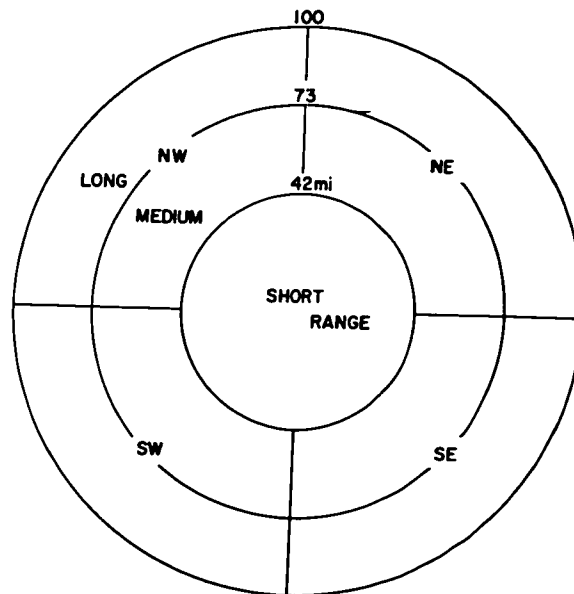


Figure 4.2. Areal groups of grid-point data.

4.2 Short-range data (range ≤ 42 miles; programmed elevations $\geq 11^\circ$)

Figure 4.3 shows a log-log plot of radar and climat amount at the 20 grid points of the short-range interval. The range of climat amounts is from 2.3 to 9.5 inches of snow, while the calibration-adjusted radar amounts range from 2.2 to 14.7 inches. Least-squares fitting of these data gave the straight-line locus with slope 1.07. The scatter of data is such that 14 of the 20 points fall within a factor 1.3 (± 1.1 dba¹) of that locus. The proximity of the slope of the locus to unity indicates that the exponent of the relationship $Z = 2000 R^{2.0}$ was applicable for this snowstorm. No conclusion can be reached about the value of the coefficient in the Z-R relationship, because of uncertainties regarding the value of the radar calibration factor (Equation 1.1) at the time of this snowstorm.

The data of Figure 4.3 show that the calibration adjustment of the original thresholds in snowfall rate (Table 3.1, Section 3.2) not only brought the average amounts into agreement, but also brought radar and ground measurements at particular points into reasonable agreement over a considerable range of snowfall amounts (2.3 to 9.5 inches). Results obtained at medium, and long range, using the calibration adjustment derived from short-range data, are analysed in the following sections.

¹In this study, the ratio of two snowfall amounts or rates, r/c expressed in decibels, is defined as $10 \log_{10}(r/c)$ dba.

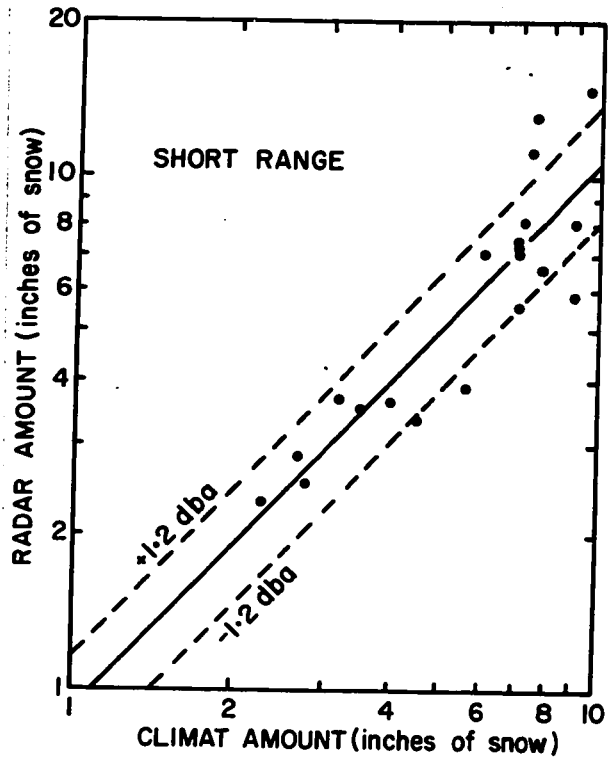


Figure 4.3. Radar versus climat amount at short-range grid points (log-log plot).

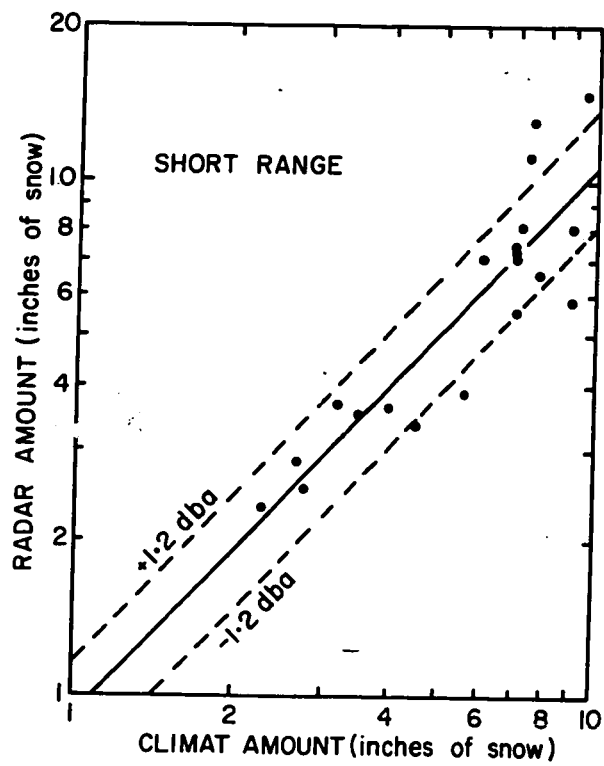


Figure 4.3. Radar versus climat amount at short-range grid points (log-log plot).

4.3 Medium-range data (range 42-73 miles; programmed elevation $3/4^\circ$)

The diameter of a conical radar beam increases linearly with range, so the spatial resolution of the basic radar data diminishes with range. In the present case, assuming beamwidth one degree, the diameter of the beam would increase from 3800 feet at 42-miles range to 6500 feet at 73 miles.

The low angle of elevation at which these data were taken resulted in partial interception of the radar beam by obstructions in certain sectors, which reduced the power available for illuminating precipitation beyond those obstructions.

Figure 4.4 shows log-log plots of radar and climat amount at the medium-range grid points. The locus obtained from the short-range data is shown on each plot, for comparison. The data of the northwest quadrant (12 grid points) fall below the short-range locus by an average factor 2.5 (-4 dba). The data of the other three quadrants (totalling 36 grid points) are scattered about the short-range locus, with 24 of the 36 points falling within a factor 1.60 (± 2 dba) of the locus. The calibration adjustment, which was based on short-range data, also brought medium-range radar measurements into reasonable agreement with ground measurements, at least in three of the four quadrants. The data of the northwest quadrant are anomalous, in that they fall below the short-range locus by an average factor 2.5 (-4 dba).

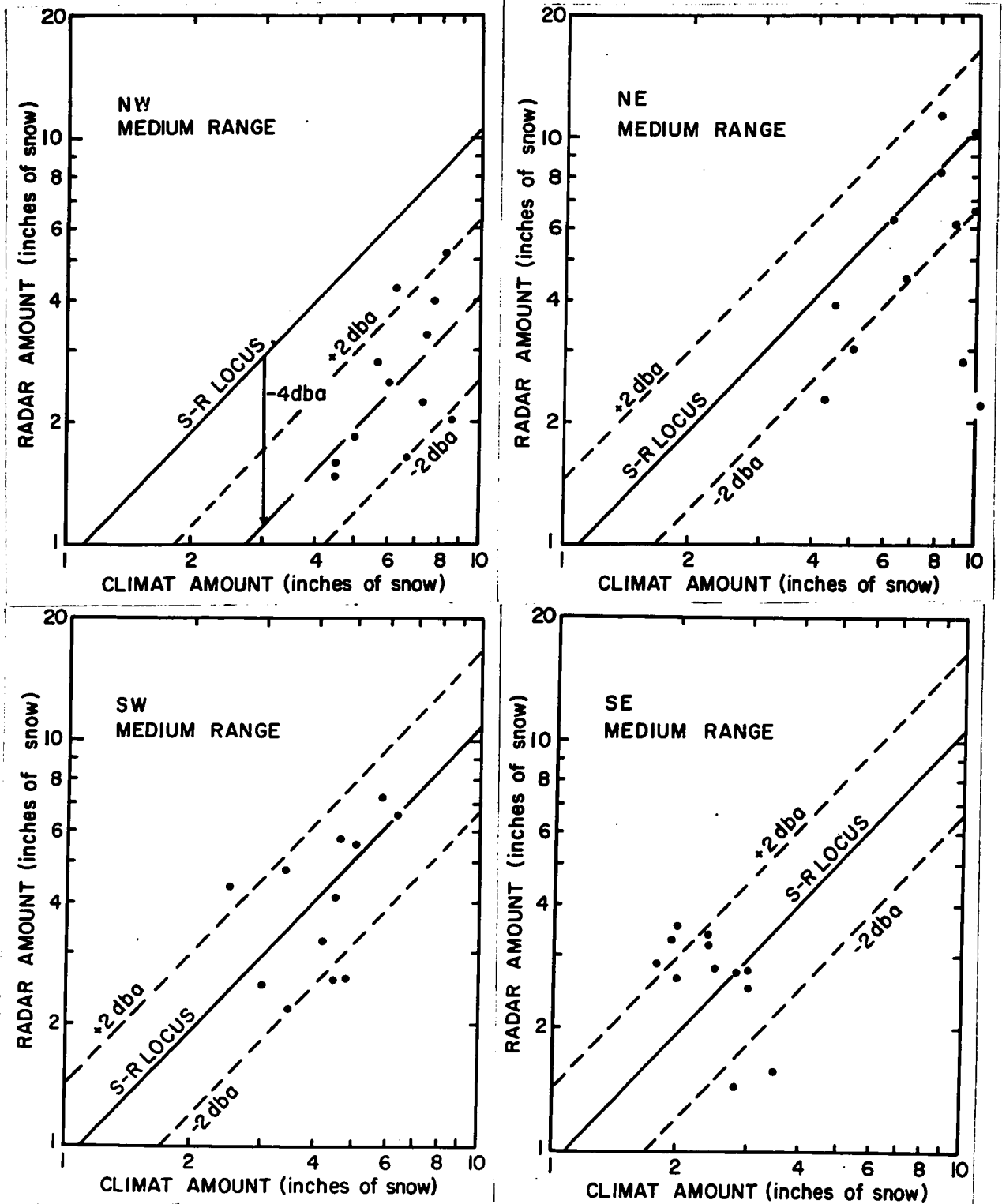


Figure 4.4. Radar versus climat amount at medium-range grid points of indicated quadrants.

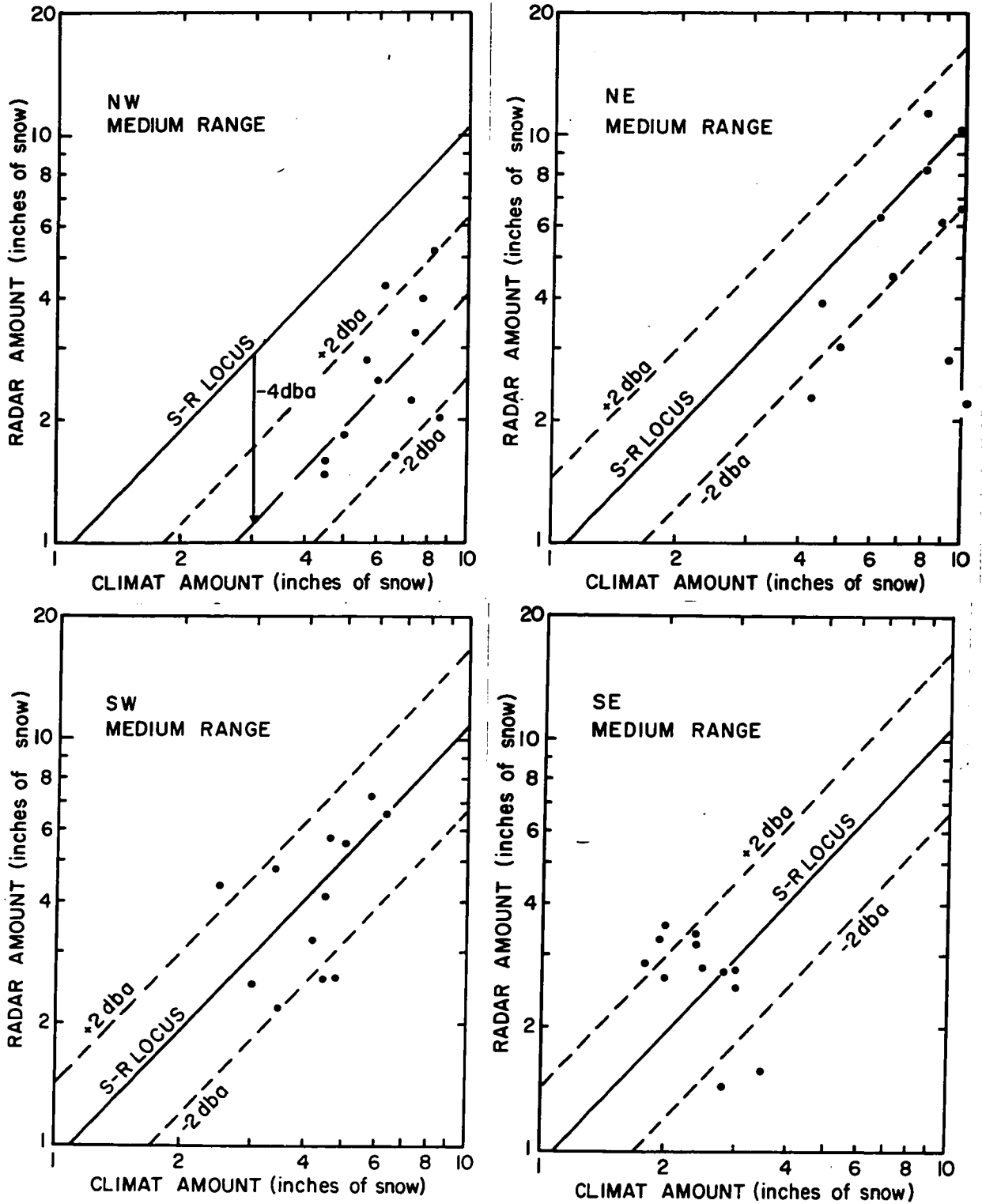


Figure 4.4. Radar versus climat amount at medium-range grid points of indicated quadrants.

4.4 Long-range data (range 73-100 miles; programmed elevation 0°)

The spatial resolution of the radar beam diminishes further in this range interval, as the diameter of the beam increases from 6500 feet at 73-miles range to 9000 feet at 100 miles.

Radar data taken at elevation zero degrees only appear on the 5000-ft CAPPI maps at ranges > 73 miles. Therefore, ground returns from many obstructions at shorter ranges do not appear, but the power available for illuminating precipitation beyond the obstructions is seriously affected.

Figure 4.5 shows log-log plots of radar and climat amount at the long-range grid points of each quadrant. As in Figure 4.4, the locus obtained from the short-range data (Fig. 4.3) is shown on each plot for comparison. The long-range data of the northwest quadrant fall below the short-range locus, by factors ranging from 4 to 20 (-6 dba to -13 dba). The long-range data points of the northeast and southwest quadrants are combined on one plot because the results obtained in those sectors were similar. The combined data points tend to be bounded on the upper side by the short-range locus, but the scatter is broad and five points fall below the locus by an approximate factor 13(-11 dba). In the southeast quadrant, two thirds of the long-range data points fall within a factor 1.6 (± 2 dba) of the short-range locus. Only in the southeast quadrant are the results obtained at long range comparable to those obtained at short range, and at medium range in three of the four principal quadrants.

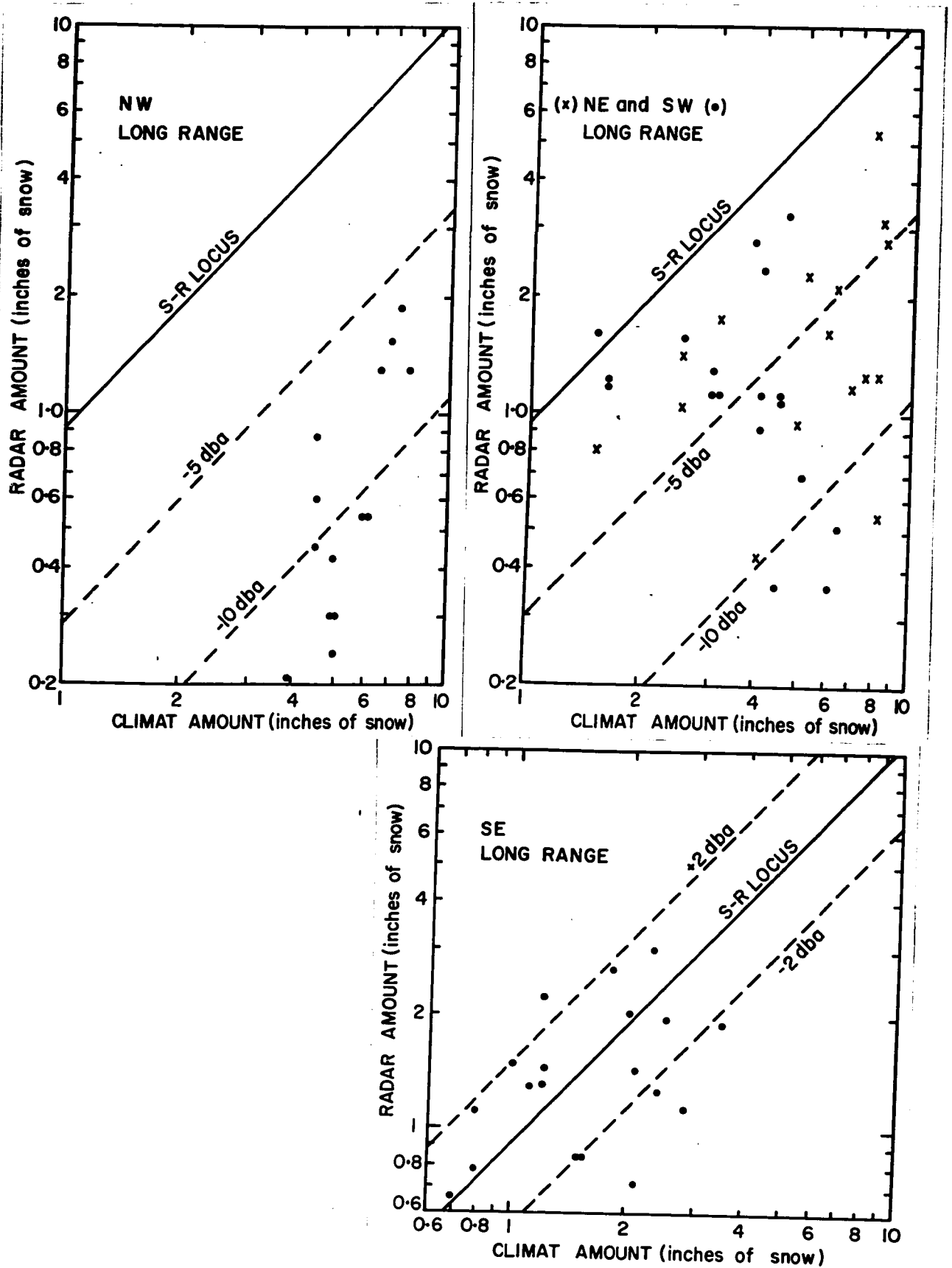


Figure 4.5. Radar versus climat amount at long-range grid points of indicated quadrants.

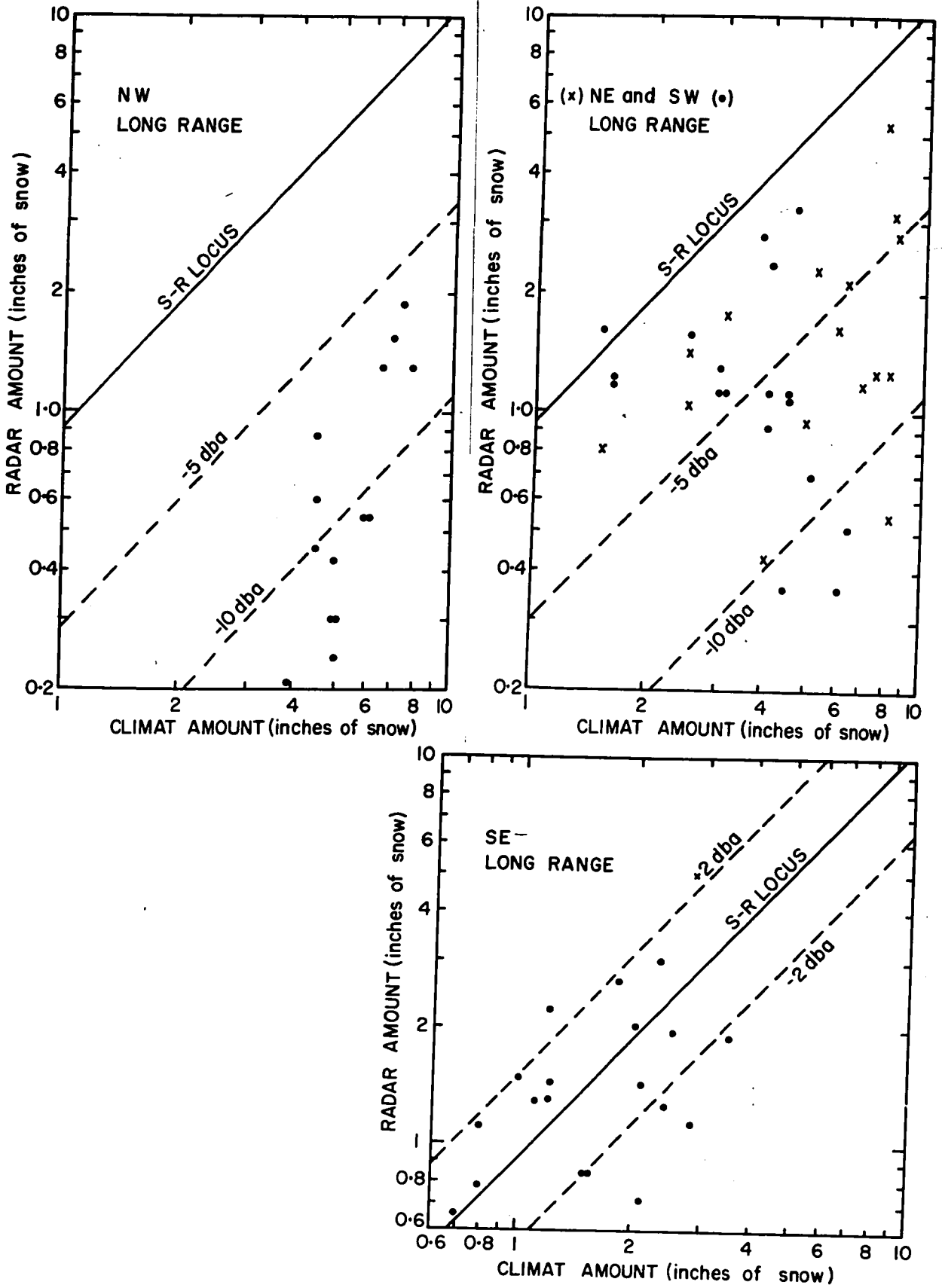


Figure 4.5. Radar versus climat amount at long-range grid points of indicated quadrants.

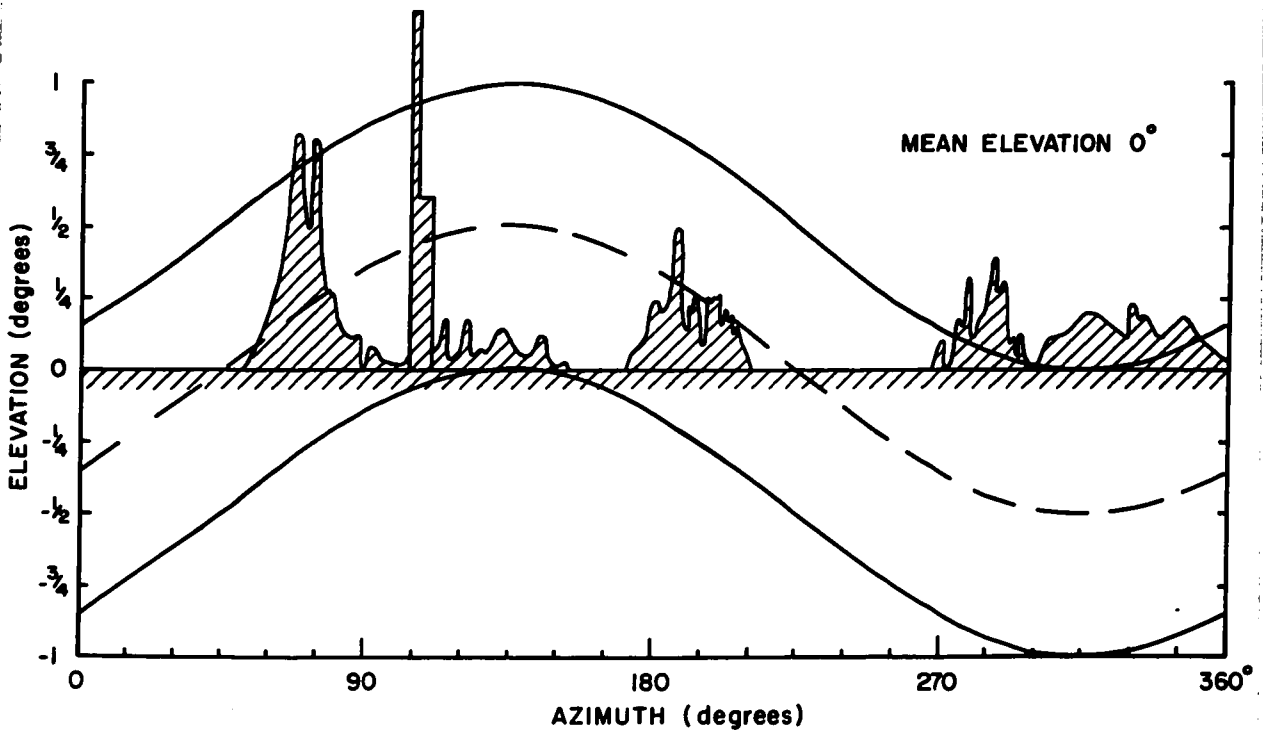
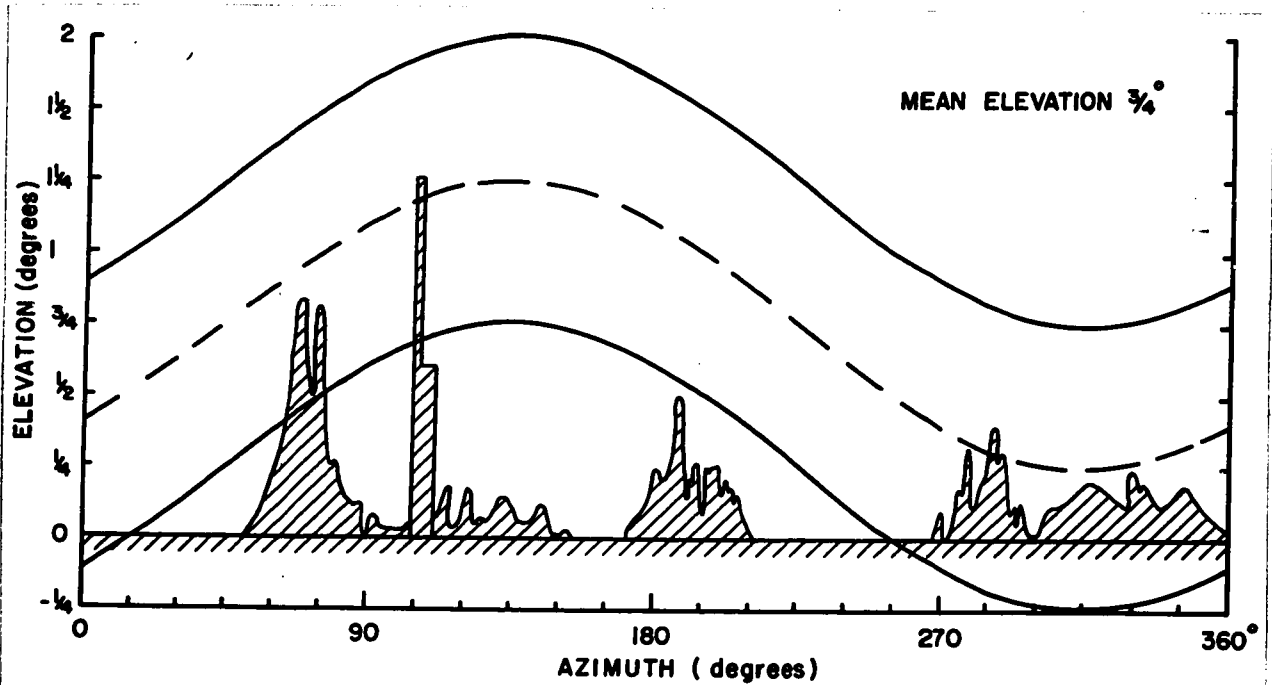
4.5 Asymmetrical pattern of radar measurements

Comparison of snowfall measurements at short, medium, and long range (Sections 4.2, 4.3, and 4.4) showed that radar amounts diminished significantly relative to the corresponding climat amounts as the radar data were taken at successively lower angles of elevation. This effect was most evident in the northwest quadrant, but was barely discernible in the southeast quadrant.

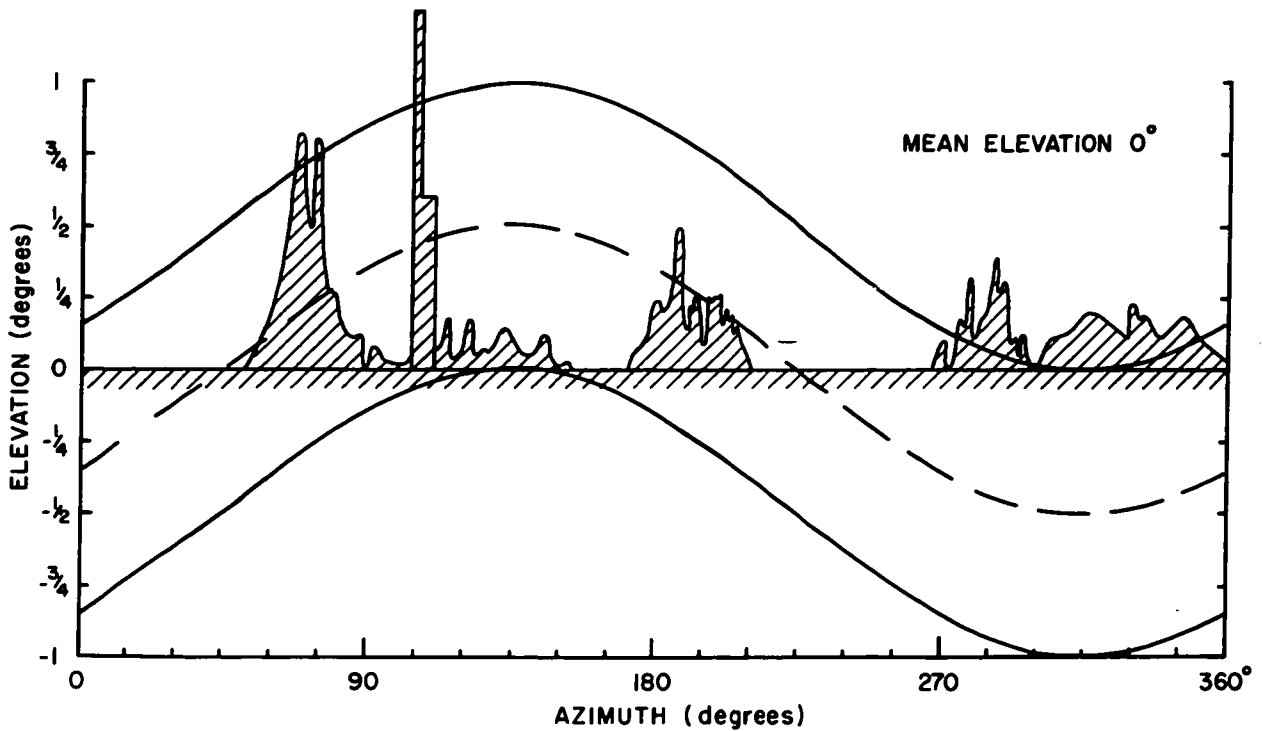
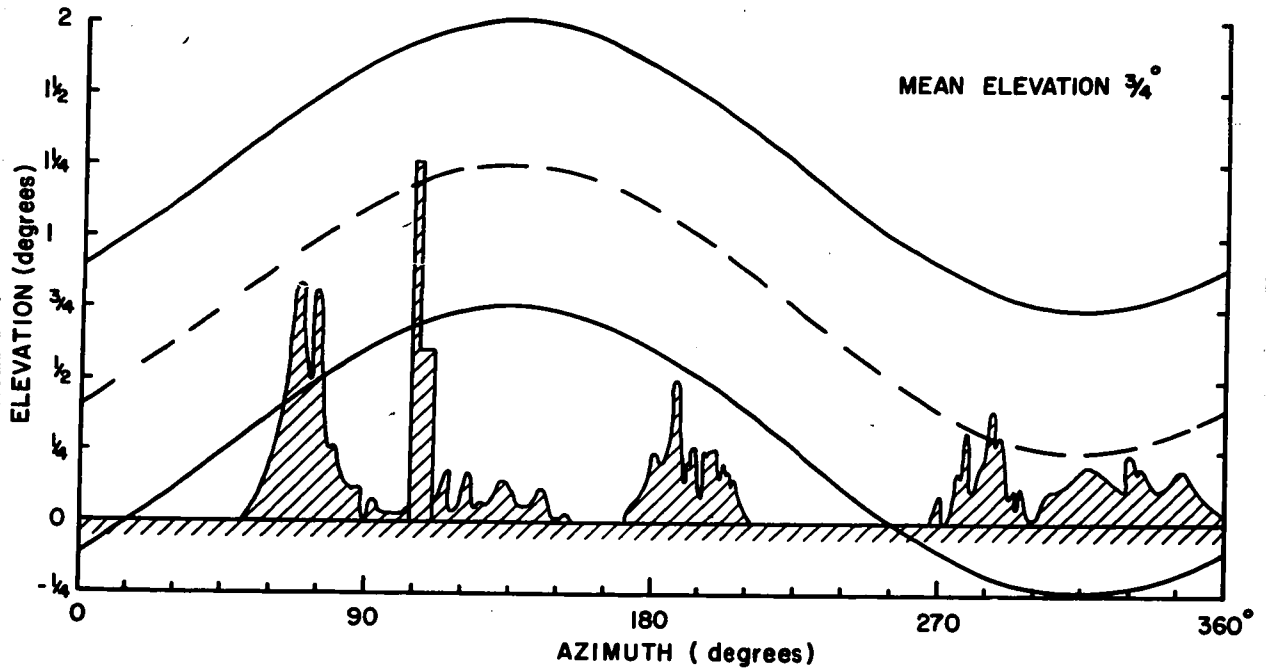
There is evidence that the asymmetrical pattern of radar measurements was caused by systematic departures from programmed elevation angles as the antenna rotated. Analysis of the heights and locations of physical obstructions around the radar site, in combination with the elevation angles and range gates of the 5000-ft CAPPI program, showed that a small tilt of the antenna's rotational axis away from the vertical, by as little as one-half degree toward the northwest, would produce an asymmetrical pattern of radar measurements similar to that obtained in this study.

The situation of an antenna rotating about an axis tilted away from the vertical by one-half degree toward 315° azimuth is illustrated in Figures 4.6 and 4.7. As a result of the tilt, the elevation angle of the antenna oscillates sinusoidally about a mean value as the antenna rotates. The lines superimposed on Figure 4.6 depict the loci of the top, centre (dashed), and bottom of a radar beam (vertical beamwidth one degree) oscillating about a mean elevation angle of $3/4^{\circ}$. Figure 4.7 shows the corresponding pattern for mean elevation angle zero degrees. In each case, the loci are superimposed on a profile of the skyline around the radar site at Montreal International Airport.

The profile was prepared from topographic data and shows the skyline in terms of radar elevation angle, with the elevation scale magnified by a factor 90 relative to the azimuth scale. Heights, bearings, and ranges



Figures 4.6 and 4.7. Elevation of top, centre (dashed), and bottom of a radar beam (vertical beamwidth 10°) from an antenna rotating about a tilted axis at indicated mean elevation angles (top, $3/4^\circ$; bottom, 0°). Loci are superimposed on a profile of the skyline around the CPS-9 radar site.



Figures 4.6 and 4.7. Elevation of top, centre (dashed), and bottom of a radar beam (vertical beamwidth 10°) from an antenna rotating about a tilted axis at indicated mean elevation angles (top, $3/4^\circ$; bottom, 0°). Loci are superimposed on a profile of the skyline around the CPS-9 radar site.

of obstructions to the radar beam were converted to radar elevation angles, taking into account the curvature of the earth and the lesser curvature of the radar beam. Thus, the profile gives for each bearing the elevation of the portion of a radar beam that would just clear all obstructions in that direction under normal propagation conditions.

The loci of Figure 4.6 (mean elevation, $3/4^\circ$) show that approximately half of the transmitted beam would be intercepted at relatively short ranges in the northwest quadrant, while no significant interception would occur in the other quadrants, except between 065° - 076° (Mount Royal) and between 104° - 107° azimuth (airport control tower). The loci of Figure 4.7 (mean elevation, zero degrees) show that almost all of the beam would be intercepted in the northwest quadrant, while only a small fraction of the beam would be intercepted in the southeast quadrant, apart from the narrow sector (104° to 111° azimuth) obstructed by the control tower and airport terminal building.

During the time the CPS-9 radar has been in operation at its present site, the zero-degree positioning of the antenna has been checked periodically. These checks were made by inserting a telescope into a slotted guide on the edge of the antenna, and sighting across to an established target on the airport terminal building, 2000 feet away. The mechanical zero-lock position (antenna locked at right angles to its axis of rotation) has remained constant, but the electronic zero-degree position, produced by electronic control of the hydraulic servo-system, has required adjustment from time-to-time to keep it in agreement with the mechanical zero-lock position.

Subsequent tests of the zero-degree positioning of the antenna, against zero-level targets established on several different bearings, showed that the rotational axis of the antenna was not vertical, but was tilted 0.4° toward 320° azimuth. Since the mechanical zero-lock position had not been altered during the intervening period, it appears likely that the orientation of the axis was much the same at the time of the snowstorm under study. Because the electronic zero-degree position has been adjusted from time-to-time, the relation between electronic and mechanical zero-degree positions at that time is not known.

The stepped-elevations of the antenna for the CAPPI program also were tested. The resulting values are given in Table 4.1 along with the programmed values, for comparison.

Table 4.1 - Stepped-elevations of radar antenna

Rotation	Elevation Angle			Elevation Steps		
	Programmed	Actual	Diff.	Programmed	Actual	Diff.
1	0°	00^1	0'	45'	39'	-6'
2	45'	39'	-6'	45'	42'	-3'
3	$1^\circ 30'$	$1^\circ 21'$	-9'	45'	47'	+2'
4	$2^\circ 15'$	$2^\circ 8'$	-7'	45'	39'	-6'
5	3°	$2^\circ 47'$	-13'	45'	49'	+4'
6	$3^\circ 45'$	$3^\circ 36'$	-9'	45'	40'	-5'
7	$4^\circ 30'$	$4^\circ 16'$	-14'	45'	41'	-4'
8	$5^\circ 15'$	$4^\circ 57'$	-18'	45'	41'	-4'
9	6°	$5^\circ 38'$	-22'	45'	42'	-3'
10	$6^\circ 45'$	$6^\circ 20'$	-25'	45'	43'	-2'
11	$7^\circ 30'$	$7^\circ 3'$	-27'	45'	40'	-5'
12	$8^\circ 15'$	$7^\circ 43'$	-32'	45'	36'	-9'
13	9°	$8^\circ 19'$	-41'	$1^\circ 30'$	$1^\circ 32'$	+2'
14	$10^\circ 30'$	$9^\circ 51'$	-39'	$1^\circ 30'$	$1^\circ 29'$	-1'
15	12°	$11^\circ 20'$	-40'	$1^\circ 30'$	$1^\circ 21'$	-9'
16	$13^\circ 30'$	$12^\circ 41'$	-49'	$1^\circ 30'$	$1^\circ 29'$	-1'
17	15	$14^\circ 10'$	-50'			
Average						-3.3'

¹Electronic zero-position assumed correct.

If the electronic zero-degree position is assumed correct, then accumulation of the successive steps in elevation angle indicates good agreement, generally within 10%, between programmed and actual elevation angles.

5. Comparison with Other Results

The present work is the first instance in which the amount of snow falling from one storm has been mapped over a substantial area from radar data. Previously-reported work in the measurement of snowfall by radar (Langille and Thain, 1951; Kodaira and Inaba, 1955; Austin, 1963) involved measurements at a few widely separated points. In the absence of other mappings of snowfall amount from radar data, the present work is compared with similar work on rain by Leber, Merritt, and Robertson (1961), Huff (1966), and Wilson (1963). These particular studies were selected from the more extensive literature describing measurements of rainfall by radar, because they are based on 10-cm radar data, which does not suffer from attenuation in rain. In the first two cases, isohyetal maps were provided which could be analyzed in the same manner as the present ones for snow. Although Wilson's results are not reported in the form of maps, they are given in a form suitable for inter-comparison. The results obtained by the above authors are analyzed in Sections 5.1, 5.2 and 5.3, for comparison with a similar analysis of the present results in Section 5.4.

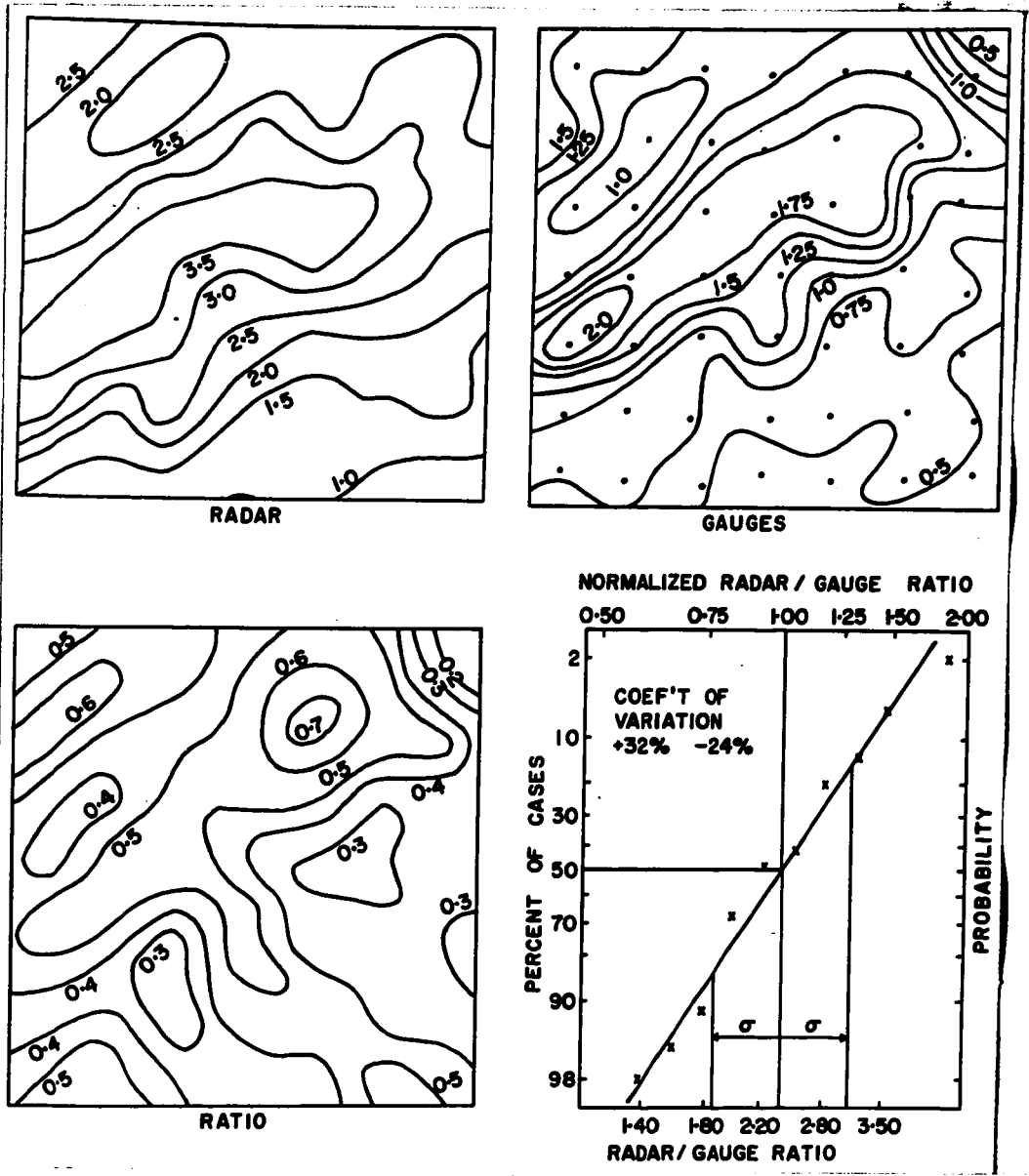
Probability plots are used to evaluate means and coefficients of variation for various groups of grid-point data. Some of the distributions are approximately Gaussian, or near-normal, while others are approximately log-normal. In the latter cases, coefficients of variation are given as factors, as well as percentages, of the respective means. The groups of data are of limited size, therefore the resulting values should be considered as approximations.

5.1 Rain in Illinois

Huff (1966) used a 9.1-cm M-33 (acquisition) radar to obtain data for 15 days on which rainshowers, or thundershowers, occurred over a dense network of raingauges in East Central Illinois. He does not state beamwidth, or elevation angle used, but Jones (1966), in describing the same radar, indicates that the antenna consists of a non-symmetrical paraboloid and that the lowest elevation angle usually was used for hydrological measurements. Technical specifications of the M-33 radar give horizontal beamwidth 1.4° , minimum vertical beamwidth 4° , and minimum elevation 2° (i.e. bottom of 4° beamwidth at zero-degrees elevation). Measurements were made out to a maximum range of 40 miles.

Using $Z = 200 R^{1.6}$, Huff mapped rate of rainfall every 5 minutes from gain-step photographs of the PPI-display, i.e. sets of "black and white" or "on-off" photographs taken at specific settings of threshold signal. Figure 5.1 shows his isohyetal mapping of total rainfall amount over 400 mi^2 , for a case in which the mean ground-measured rainfall was 1.38 inches. This was the only case in which the mean rainfall was greater than 0.4 inches.

Figure 5.2 shows Huff's mapping of total rainfall from data recorded at the 49 gauges in the East Central Illinois Network. The gauges are spaced approximately 3 miles apart in an area 20 x 20 miles. Figure 5.3 shows his mapping of the gauge/radar ratio.

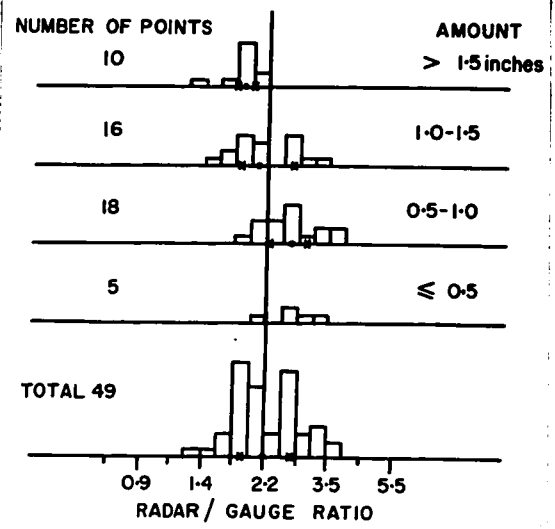


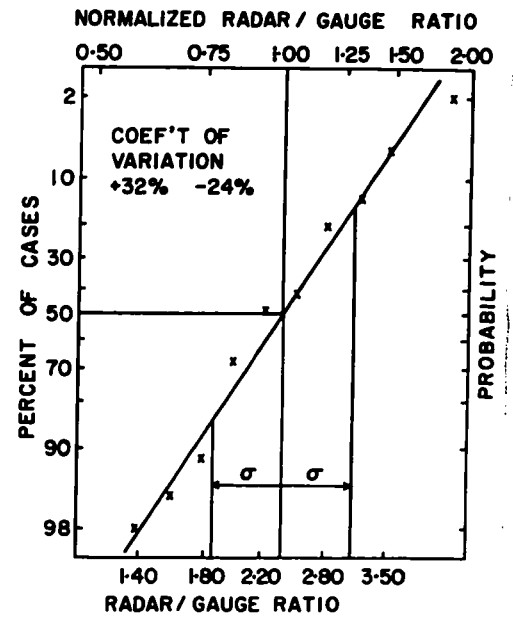
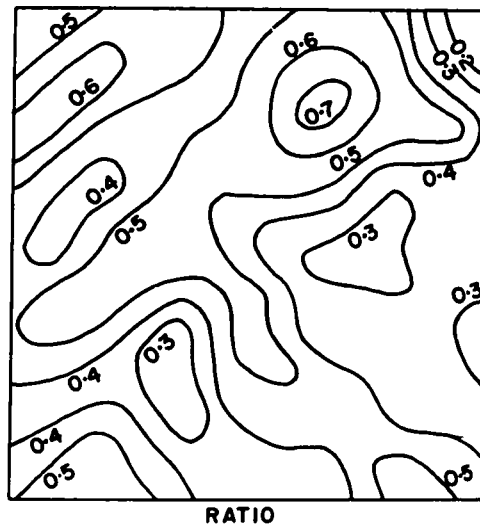
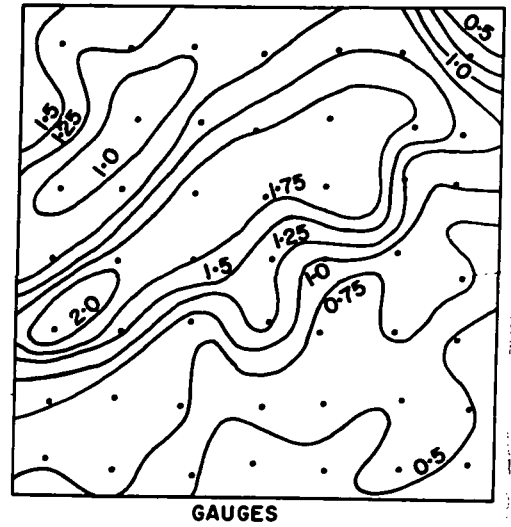
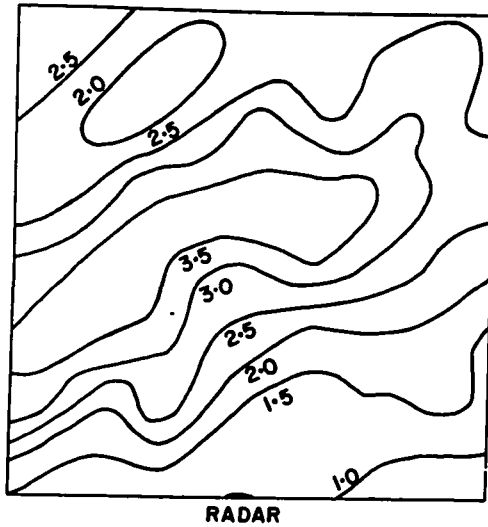
Figs. 5.1 and 5.2 (top). Radar and gauge isohyets, inches of rain (after Huff, 1966).

Figure 5.3 (centre left). Map of gauge/radar ratio (after Huff, 1966).

Figure 5.4 (centre right). Probability plot of radar/gauge ratio values (inverse of Huff's).

Figure 5.5 (bottom). Grid points distributed with radar/gauge ratio and amount of rainfall.



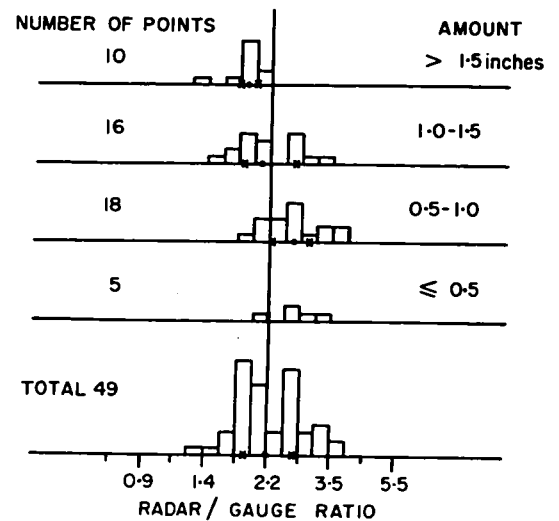


Figs. 5.1 and 5.2 (top). Radar and gauge isohyets, inches of rain (after Huff, 1966).

Figure 5.3 (centre left). Map of gauge/radar ratio (after Huff, 1966).

Figure 5.4 (centre right). Probability plot of radar/gauge ratio values (inverse of Huff's).

Figure 5.5 (bottom). Grid points distributed with radar/gauge ratio and amount of rainfall.



Huff's results have been analysed in the following way, for comparison with other results. The distribution of grid points (i.e. locations of gauges, Figure 5.2) with radar/gauge ratio, the inverse of the ratio mapped by Huff, were plotted on probability paper. This was first done on a linear scale of ratio, and the distribution was reasonably Gaussian. It was more nearly so when a logarithmic scale of ratio was used, as in Figure 5.4. Thus the distribution is better described as log-Gaussian, or log-normal, with standard deviation $\sigma = 0.12$, which is the logarithm of 1.3. That is the basis for giving a coefficient of variation as a factor 1.3 (+30% or -23%) stated in that form by comparison with other cases.

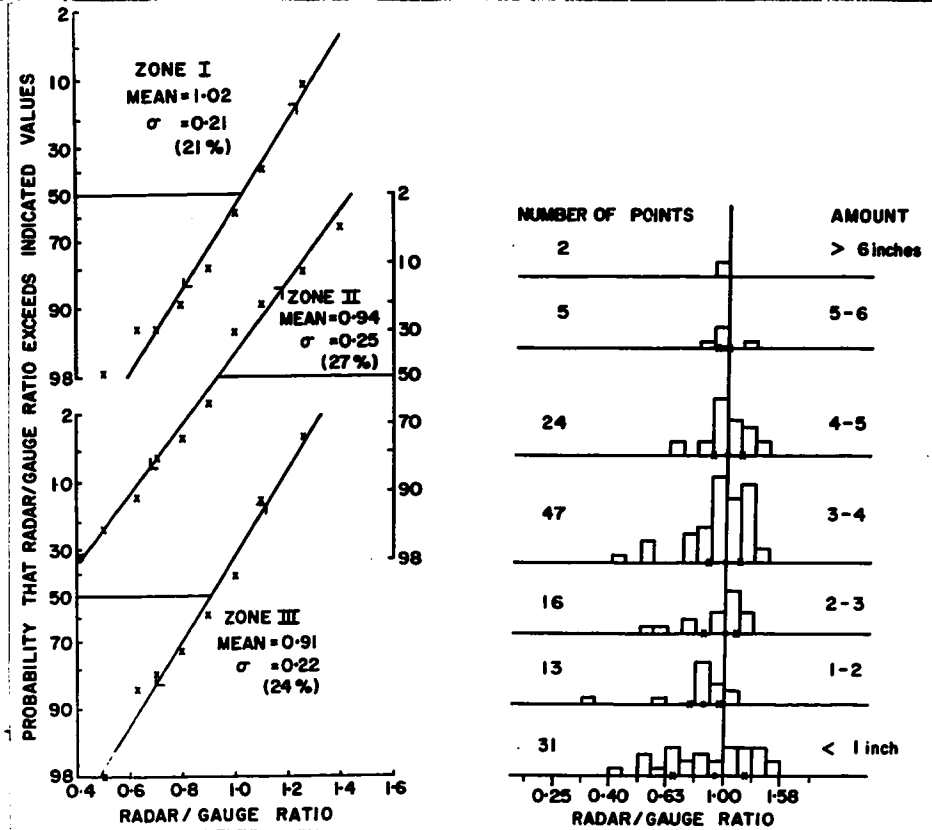
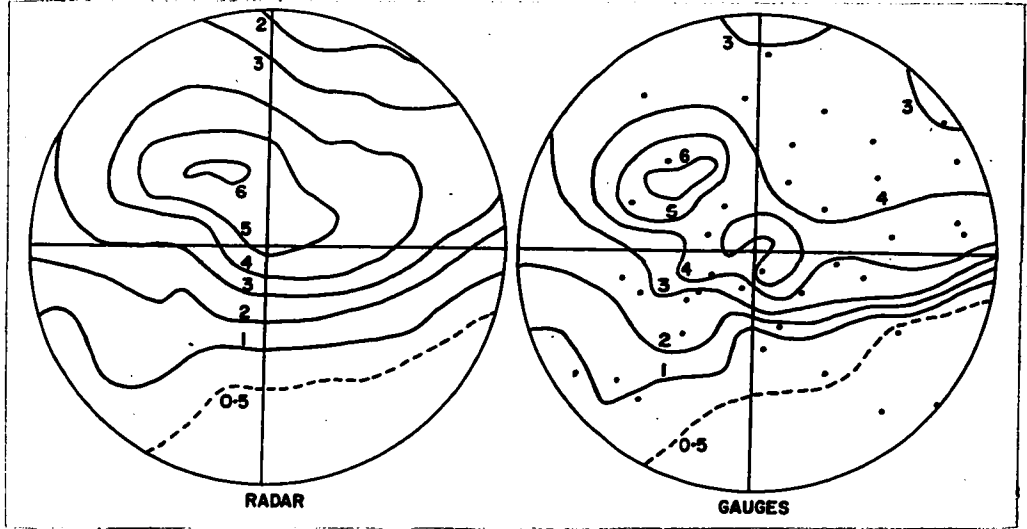
The distribution of grid points with radar/gauge ratio is shown in Figure 5.5, separately for 4 intervals of rainfall amount, and again for all of the grid points. The trend of decreasing ratio value with increasing amount is significant. Since larger amounts of rain must surely be attributable to higher rainfall rates, this trend suggests that the exponent of the relationship that was used, $Z = 200 R^{1.6}$, was too large for this particular case. Distributions of rainfall amount with rainfall rate would be required in order to say how much too large. The tendency for bimodal distribution of the whole group of grid points (bottom of figure) appears to be a result of grouping data having the above-noted trend.

5.2 Rain in Indiana

Leber, Merritt and Robertson (1961) used a 10-cm WSR-57 radar, an operational station of the U.S. Weather Bureau, to obtain data for a 24-hour segment of a record-breaking four days of storms. The WSR-57 has a two-degree conical beam and the antenna was maintained at elevation 1° . Hourly multiple-exposure photographs of the PPI-display scope (optimally 10 to 12 sampling exposures per hour) gave hourly maps of rainfall amount, assuming $Z = 200 R^{1.6}$. The result of summing these in turn is shown in the radar map of Figure 5.6, which extends to a range of 100 nmi (nautical miles). The 24-hour rainfall amounts range from 0.2 inches to 6 inches. A remarkably similar pattern appears in the isohyetal map of Figure 5.7, which is based on rainfall data recorded by 40 gauges at indicated locations.

The maps given by Leber et al were analyzed in the following way, for comparison with Huff's rainfall measurements and with the present snowfall measurements. A rectangular grid with modular spacing 15 nmi was used to take data from their radar and gauge maps (Figures 5.6 and 5.7) and the ratio of radar to gauge amount (radar/gauge ratio) was calculated for each grid point. Probability plots (Figure 5.8) show the distribution of grid points with radar/gauge ratio on a linear scale, separately for each of the following range-intervals:

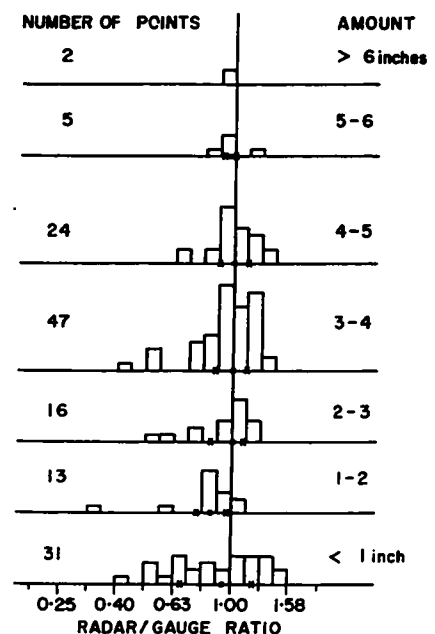
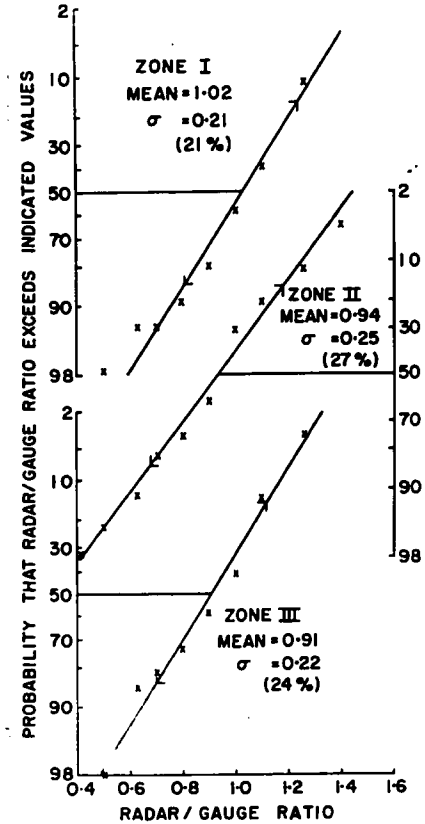
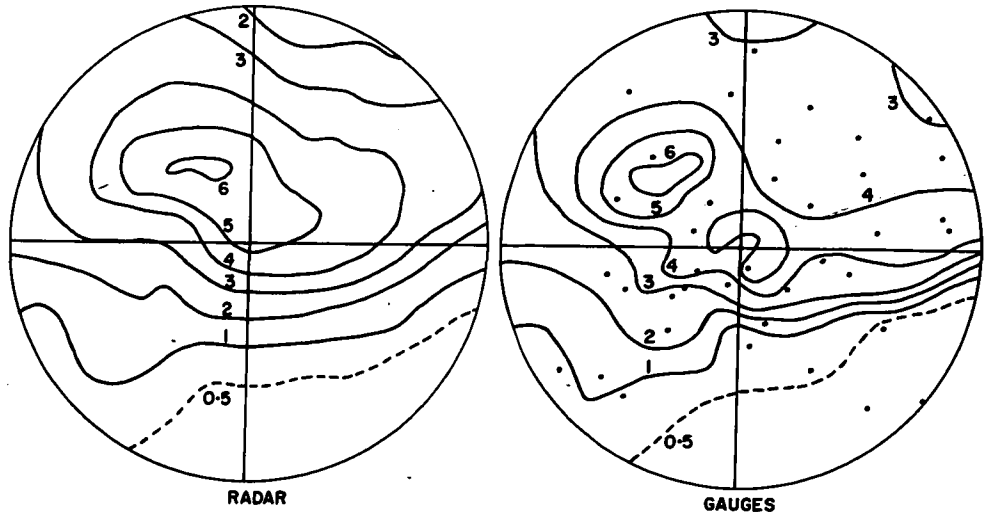
Zone I	0- 58 nmi	45 points
Zone II	58- 78 nmi	44 points
Zone III	78-100 nmi	49 points.



Figures 5.6 and 5.7 (top). Radar and gauge isohyets, inches of rain (after Leber et al, 1961).

Figure 5.8 (bottom left). Probability plots of radar/gauge ratio values at grid points of indicated zones.

Figure 5.9 (bottom right). Grid points distributed with radar/gauge ratio and amount of rainfall.



Figures 5.6 and 5.7 (top). Radar and gauge isohyets, inches of rain (after Leber et al, 1961).

Figure 5.8 (bottom left). Probability plots of radar/gauge ratio values at grid points of indicated zones.

Figure 5.9 (bottom right). Grid points distributed with radar/gauge ratio and amount of rainfall.

There is a startling consistency among the three zones in values of mean and coefficient of variation. Atlas (1964) has commented that Leber et al must have observed nicely cylindrical showers, in which the radar-observed precipitation was practically invariant to height 30 000 ft. This is the approximate height of the top of the beam at 100 nmi range. The proximity of the mean ratio values to unity must not be taken too seriously, since the difficulty of calibrating the radar is great, and of calibrating the photographic integrator still greater. The near-Gaussian distribution of random errors is satisfactory; it too lacks significant variation with range.

The distribution of grid points with radar/gauge ratio, on a logarithmic scale, is shown in Figure 5.9, separately for 7 intervals of amount rather than range intervals. The distributions become narrower with increasing amount, but there is no discernible trend in the median value of the ratio. Since the larger rainfall amounts must surely be attributable to higher rainfall rates, the lack of discernible trend supports the validity, in this case, of the exponent 1.6 in the relationship $Z = 200 R^{1.6}$ that was used.

5.3 Rain in New Jersey

Wilson (1963) used data from another WSR-57 radar located at Atlantic City, N.J., to investigate the relationship between radar-echo intensity and rainfall rate. In this case, the antenna was maintained at zero-degrees elevation and a set of stepped-gain photographs of the PPI-display scope was taken 3 or 4 times each hour for a number of storms. After each storm, the minimum detectable signal for each step in receiver gain (sensitivity) was measured in order to calibrate the photographic data, which were then manually digitized in grid squares 2.5 x 2.5 nmi. Instead of using fixed values of a and b, in a relationship of the form $Z = aR^b$, Wilson combined that generalized Z-R relationship with a simplified form of the radar equation, $\bar{P}_r = \frac{C}{r^2} Z$, to obtain the following equation:

$$R = \left(\frac{r^2 \bar{P}_r}{aC} \right)^{1/b} \quad (5.1)$$

For each of three storms reported, constant values were chosen for the product aC and for b. The resulting radar-measured hourly rainfall amounts, for all grid squares containing a recording raingauge, were compared with corresponding hourly amounts recorded by the gauges. For each storm, the values of the constants aC and b were adjusted to obtain best-fit agreement between radar and gauge measurements. Such comparisons of hourly amounts were made for a maximum of 60 recording gauges, located from 19 to 100 nmi range.

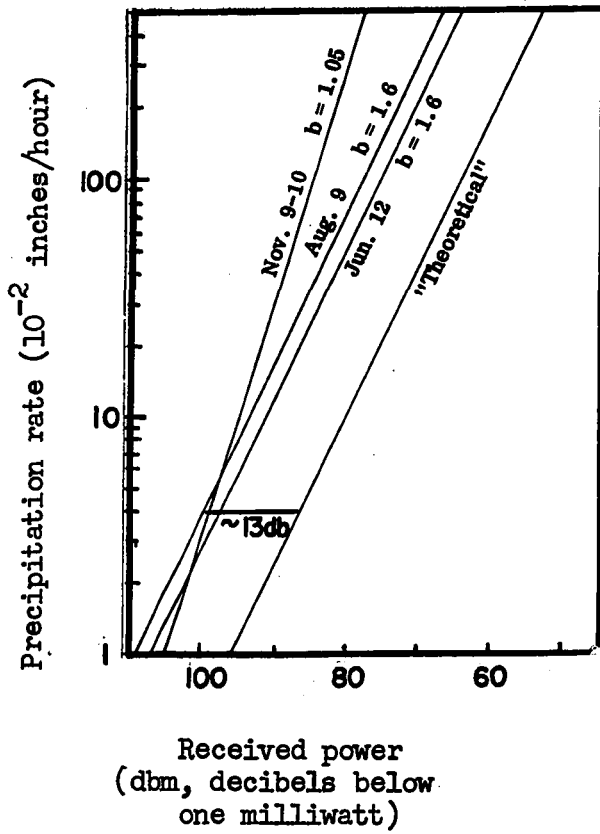


Figure 5.10. Precipitation rate vs echo intensity normalized to 100 nmi (after Wilson, 1963).

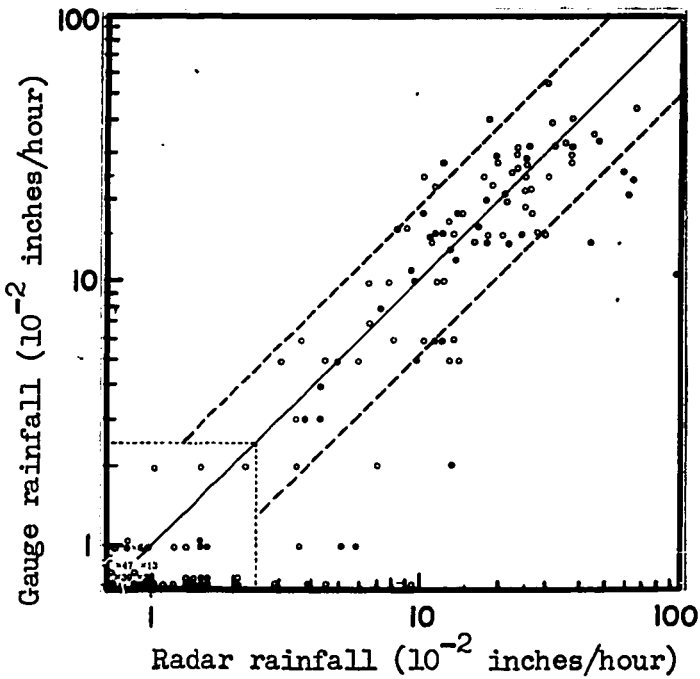


Figure 5.11. Hourly radar rainfall vs gauge values (after Wilson, 1963)

- 19-40 nmi
- 14-60 nmi

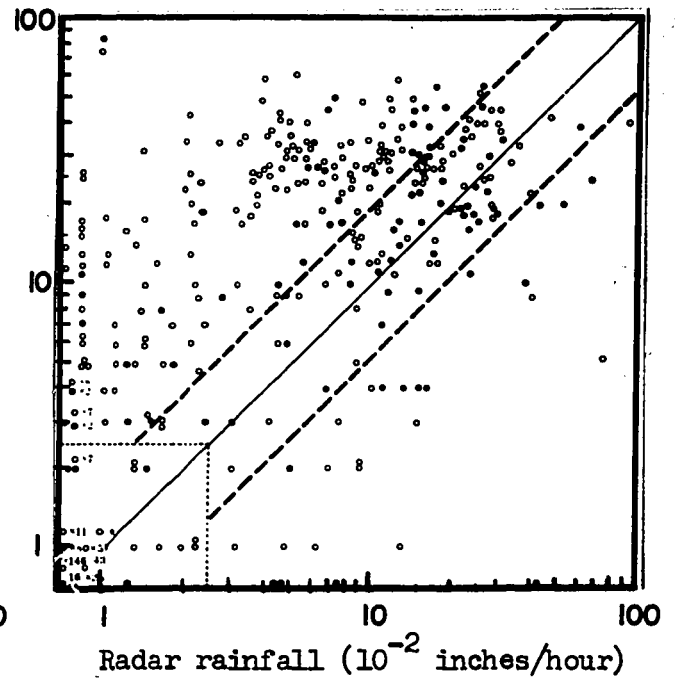


Figure 5.12. Hourly radar rainfall vs gauge values (after Wilson, 1963)

- 60-80 nmi
- 80-100 nmi

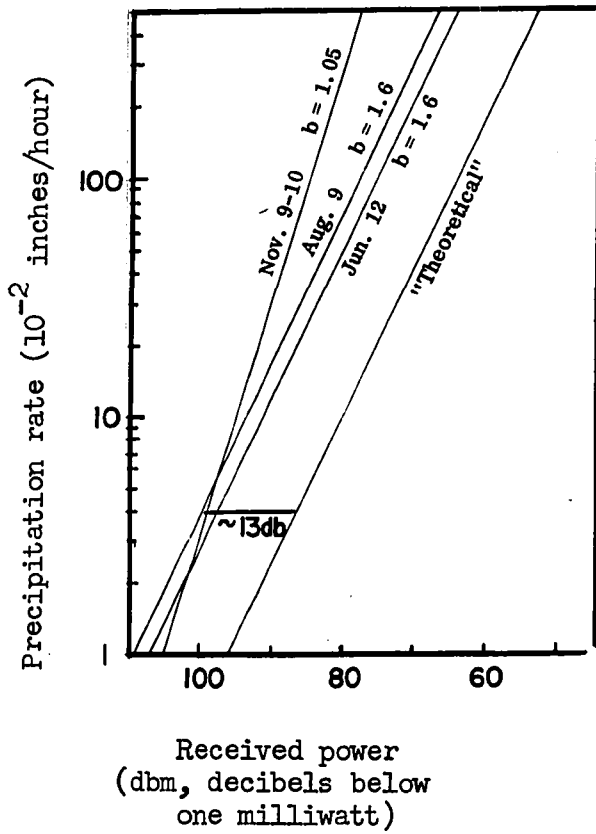


Figure 5.10. Precipitation rate vs echo intensity normalized to 100 nmi (after Wilson, 1963).

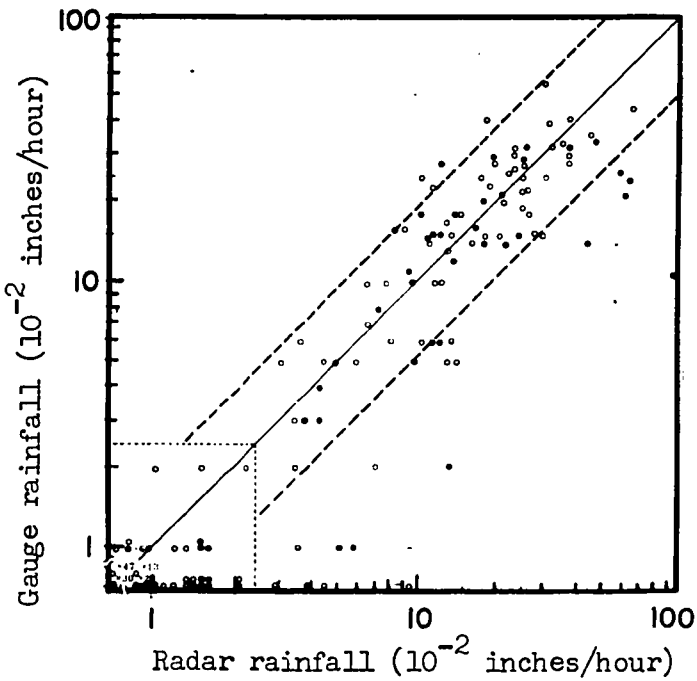


Figure 5.11. Hourly radar rainfall vs gauge values (after Wilson, 1963)

- 19-40 nmi
- 14-60 nmi

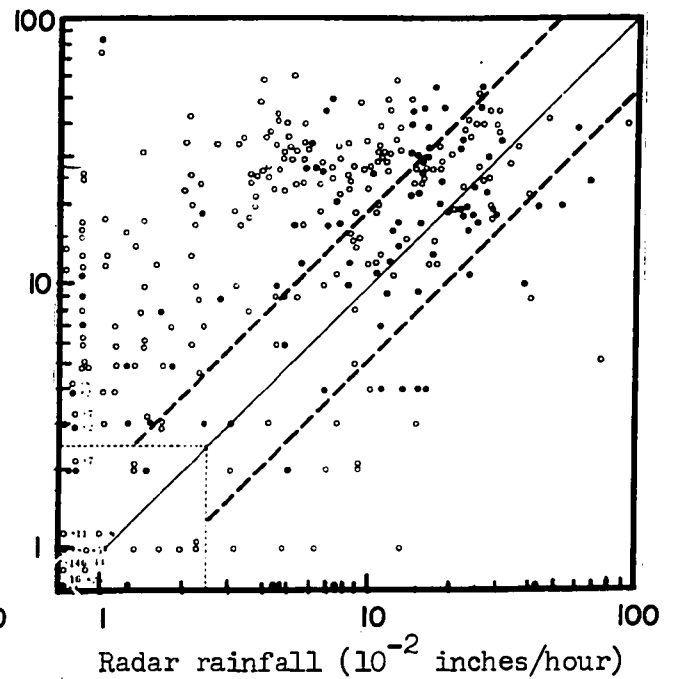


Figure 5.12. Hourly radar rainfall vs gauge values (after Wilson, 1963)

- 60-80 nmi
- 80-100 nmi

Figure 5.10 shows that the values of aC , obtained in the foregoing manner for each of three storms, were reasonably consistent. In terms of received power, they fall about 13 db (approximate factor 20) below the theoretical $P_r - R$ curve at $R = 1 \text{ mm h}^{-1}$ (i.e. $4 \times 10^{-2} \text{ in/hr}$). As Wilson explained, the discrepancy between theoretical and empirical curves is probably due to the radar calibration factor, C . The implication is that the actual sensitivity of the radar was approximately 13 db (factor 20) below its rated value. Figure 5.10 also shows that the best value of b was 1.6 for the storms of 12 June and 9 August, but was 1.05 for the storm of 9-10 November.

Wilson found that the quality of the radar measurements diminished markedly at ranges beyond 60 nmi. This is shown by the scatter diagrams of Figure 5.11 and 5.12, in which hourly radar-derived amounts for the storm of 9-10 November are plotted against actual gauge values. Figure 5.11 is for gauges located between 19 and 60 nmi range, and Figure 5.12 is for those from 60 to 100 nmi. Disregarding data points within the small box at the lower left of each figure, because gauge measurements become unreliable at those rates, the scatters of data show that radar and gauge values are in reasonable agreement out to 60-nmi range, but that many of the radar-measured amounts fall below the gauge-measured amounts at longer ranges. Wilson tabulated the number of data points on each figure for which radar-measured amounts were within a factor 2.0 ($\pm 3 \text{ db}$ in P_r) of the corresponding gauge amounts, i.e. between the dashed loci on each figure. In the range interval 19 to 60 nmi, 72 of 101 measurements fell within those limits, while only 97 of 324 measurements (30%) were that accurate at ranges between 60 and 100 nmi.

5.4 Snow at Montreal

The relationship $Z = 2000 R^{2.0}$, for aggregate snow, was used to obtain total snowfall amounts for a 48-hour period from 3-cm radar data taken at an average height of 5000 ft (Section 3.2). The original radar amounts, rather than the calibration-adjusted amounts of Figure 3.5, are used for the present comparison with the results obtained by Huff (Section 5.1) and Leber et al (Section 5.2).

The probability plots of Figure 5.13 show the distribution of grid points with radar/climat (amount) ratio, separately for three groups of grid points at short, medium, and long ranges (< 42 miles, 42-73 miles, and 73-100 miles, respectively). Each group of grid points refers to an area in which the effects of beam interception were minimal (Section 4.5). The mean value of radar/climat ratio does not vary appreciably with range (0.33 at short range, 0.3 at medium and long range), but the degree of scatter about the mean does increase with range. The coefficient of variation of the approximately log-normal distributions increases from a factor 1.3 at short range, to 1.8 at long range.

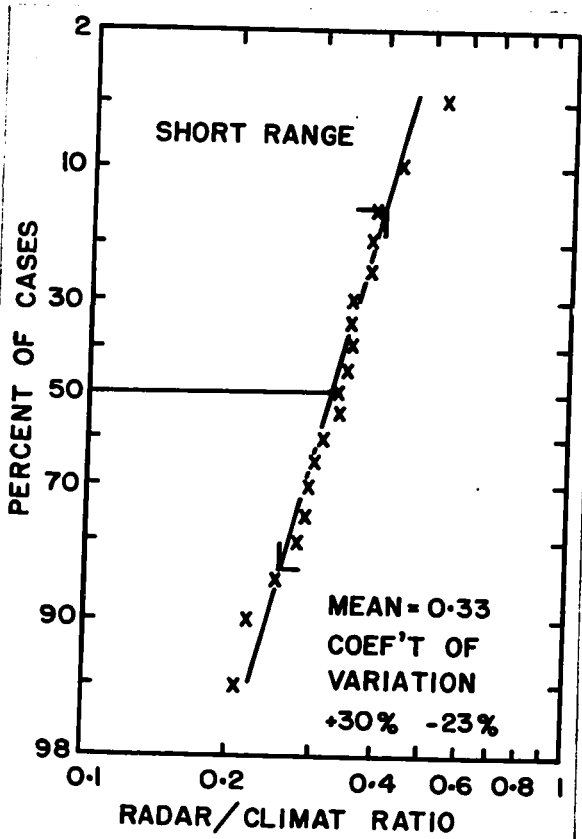
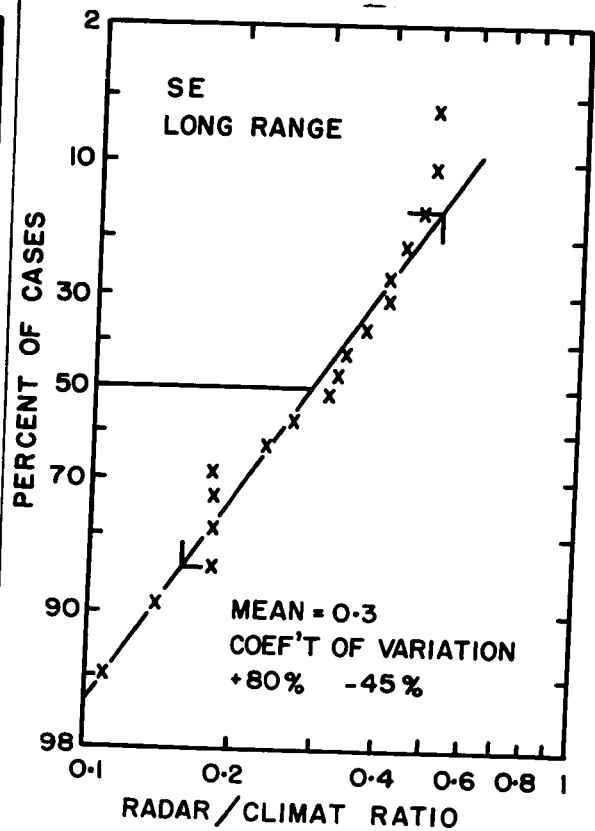
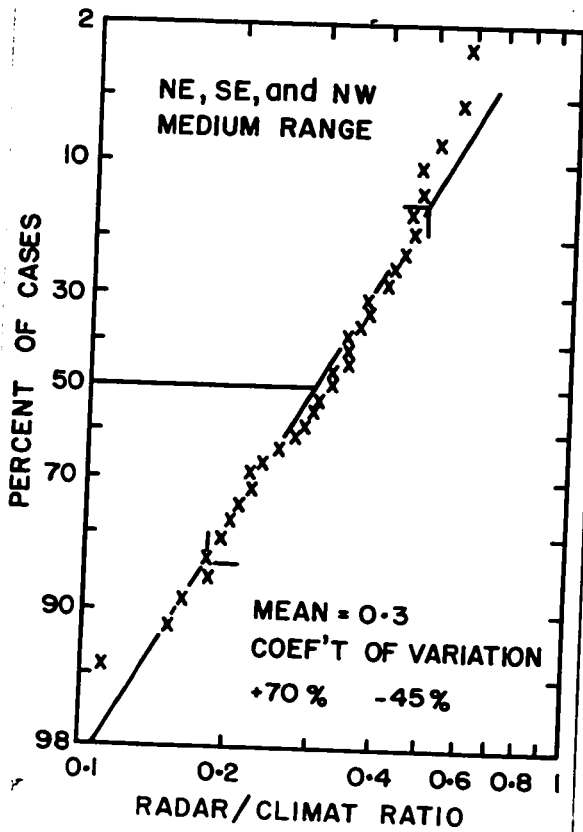


Figure 5.13. Probability plots of radar/climat ratio values at grid points of indicated areas.



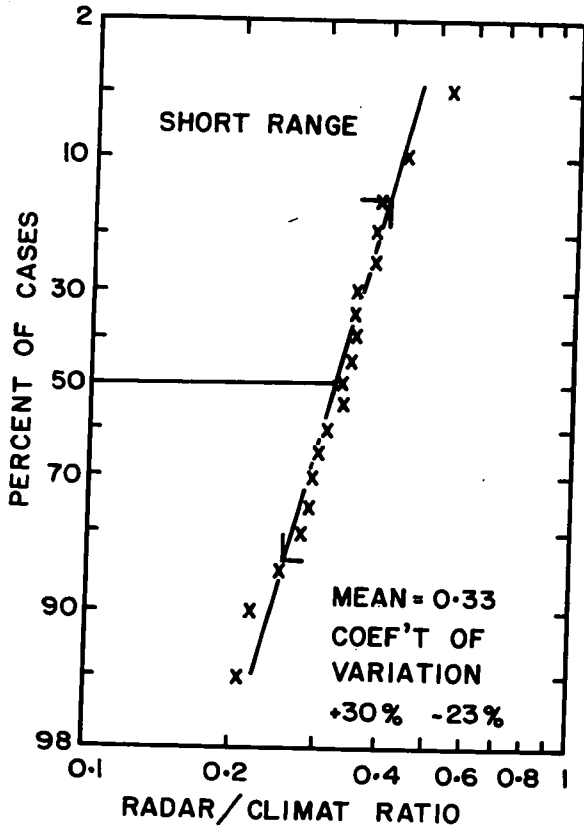
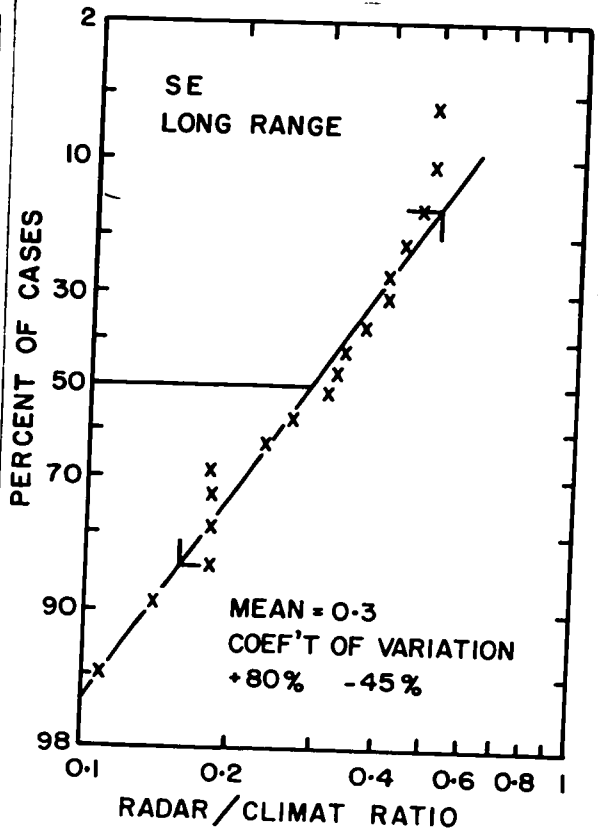
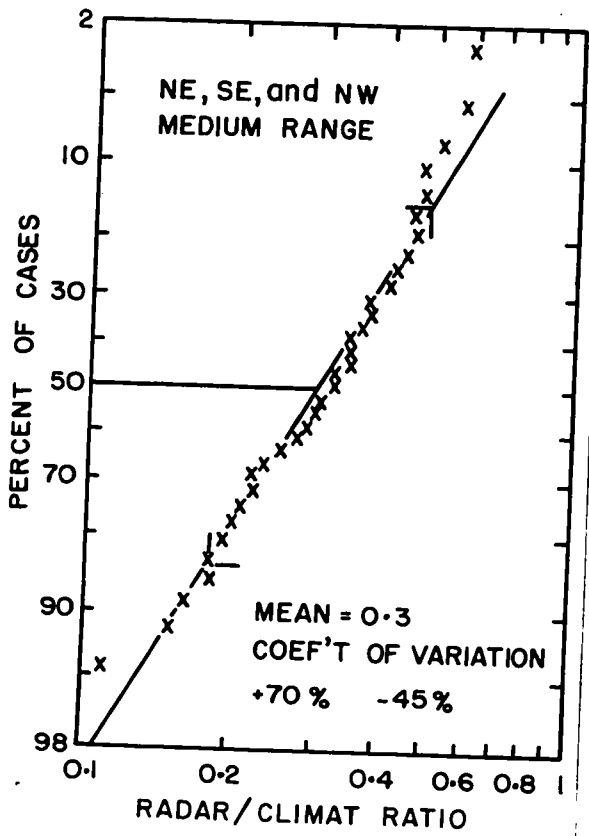


Figure 5.13. Probability plots of radar/climat ratio values at grid points of indicated areas.



5.5 Accuracy of radar measurements

The relative accuracy of radar-measured amounts of precipitation for one storm, or one day, can be assessed from the data of Table 5.1, which gives results obtained in three of the four case studies.

Table 5.1 - Summary of results

		Number of <u>grid points</u>	Radar/gauge ratio Coefficient of Variation				
			<u>Mean</u>	<u>Factor</u>	<u>Percentages</u>		
Rain in Illinois (Huff)	400 mi ²	49	2.2	1.3	+30%	-23%	
Rain in Indiana (Leber et al)	30,000 nmi ²						
			Zone				
		45	I	1.0	(1.2)	+20%	-20%
		44	II	0.9	(1.3)	+27%	-27%
		49	III	0.9	(1.25)	+24%	-24%
Snow at Montreal	15,000 mi ²						
		20	S-R	0.33	1.3	+30%	-23%
		36	M-R	0.3	1.7	+70%	-41%
		19	L-R	0.3	1.8	+80%	-45%

The range of mean values, from 2.2 for rain in Illinois to 0.3 for snow at Montreal, can be explained primarily in terms of radar calibration problems, and secondarily in terms of values of the coefficients in the Z-R relationships that were used.

Accurate calibrations and uniformity of performance are difficult to achieve in weather radar operations, partly because the systems must be capable of handling a large range of signal strengths (60 to 70 db, or factors 10^6 to 10^7), and partly because of the fluctuating character of signal returns from precipitation. Additional problems are encountered when the complexity of the overall system is increased by adding ancillary display, or recording equipment. (Appendix 1).

In the present case of snow at Montreal, uncertainties regarding radar calibration and performance of the display system suggest that a mean value of 0.3 is reasonable agreement in the circumstance. The situation is not known in similar detail for the other cases, but Huff's mean value of 2.2 also indicates reasonable agreement in the circumstance. In the case of Leber et al, mean values ranging from 1.0 to 0.9 should not be taken as evidence that measurements of similar accuracy can be made consistently. This is borne out by Wilson's results (Figure 6.10), which suggest that the actual radar calibration was about 13 db (factor 20) below its rated value. However, it is to the credit of the operators that the sensitivity apparently did not vary by more than 2 db in P_r , for the three storms that are documented. This is indicated by the consistency of the average power received for $R = 1 \text{ mm h}^{-1}$ ($4 \times 10^{-2} \text{ in/hr}$, Figure 5.10).

While doubting the significance of the ratio-values close to unity, there is a notable consistency within each storm, as indicated by values between 20 and 40% for the coefficient of variation. With that limited scatter it should be possible to use a radar, in combination with a small number of gauges for calibration purposes, to obtain amount of precipitation at any point within reasonable range to within 30% of the correct value. By summing radar-measured amounts at a point over several storms, or by integrating amount over an area within one storm, it should be possible to evaluate total amounts more accurately.

6. Variation of Snowfall Rates at a Point

6.1 Gauge-measured rates

Having found that the CPS-9 radar could be used to map snowfall amounts with reasonable accuracy over a substantial area, there was a need to determine how well it could measure snowfall rates at a point. This was done by comparing 5000-ft radar data with snowfall rates recorded by a gauge at L'Assomption, 28 miles north-northeast of the radar site.

The tipping-bucket raingauge at L'Assomption is heated in winter to melt snow as it accumulates and thereby measure the rate of accumulation of water. Snowfall rates are determined, in terms of water content, from the time interval between successive tips. Rate resolution at low snowfall rates is limited, since the times between tips are long. For example, tips occurring one hour apart correspond to a mean precipitation rate of 0.25 mmw h^{-1} , but give no information about variations in rate.

Since the gauge is heated, evaporation losses are probably significant, particularly at low snowfall rates. In measuring snowfall rates by the optical attenuation of a light beam, Warner and Gunn (1967) obtained considerable improvement of the correlation between optical and heated-gauge measurements when evaporation losses were assumed to be 0.3 mmw h^{-1} . Although a different gauge was used at L'Assomption, similar evaporation losses have been assumed to obtain evaporation-corrected snowfall rates from the gauge data. These are represented by the rectangles in Figures 6.1 and 6.2. Times of bucket tips are indicated by solid vertical lines and the correction for evaporation is given by the hatched portion at the top of each rectangle. Continuous curves have been drawn through these rectangles in such a way that the area under the curve, which is a measure of snowfall amount, from the onset of snow to each tip-time equals the sum of the

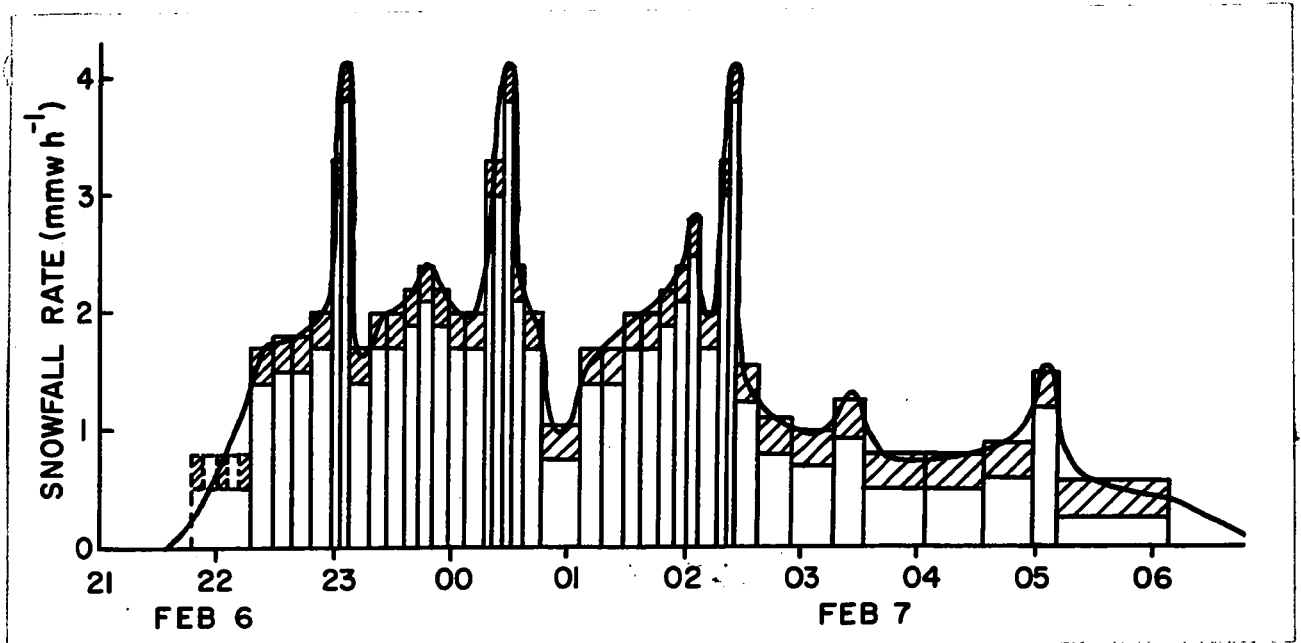


Figure 6.1. Snowfall rates from recording gauge at L'Assomption (hatched portion at the top of each rectangle indicates evaporation correction of 0.3 mmw h^{-1}).

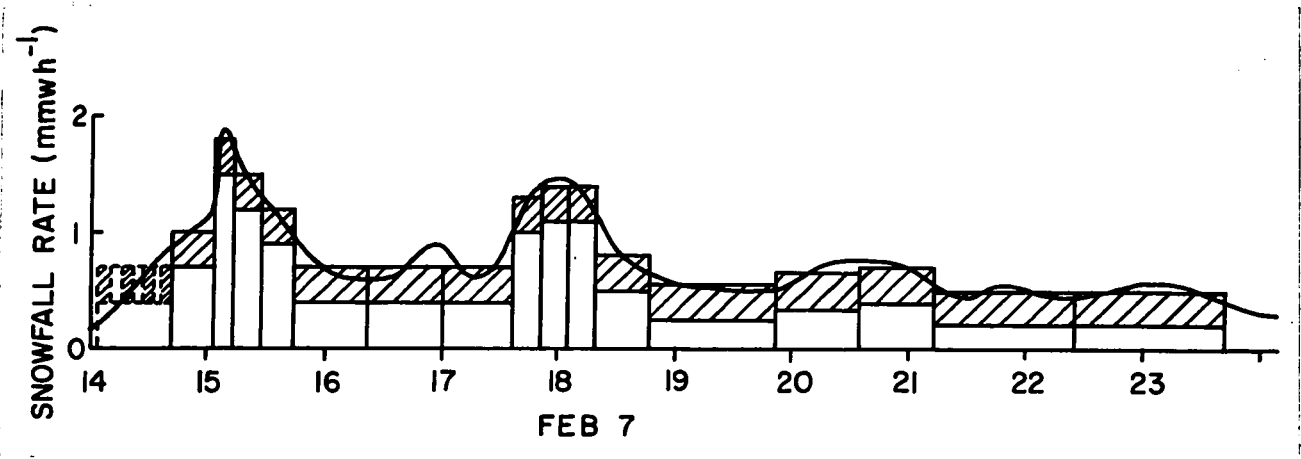


Figure 6.2. Snowfall rates from recording gauge at L'Assomption (hatched portion at the top of each rectangle indicates evaporation correction of 0.3 mmw h^{-1}).

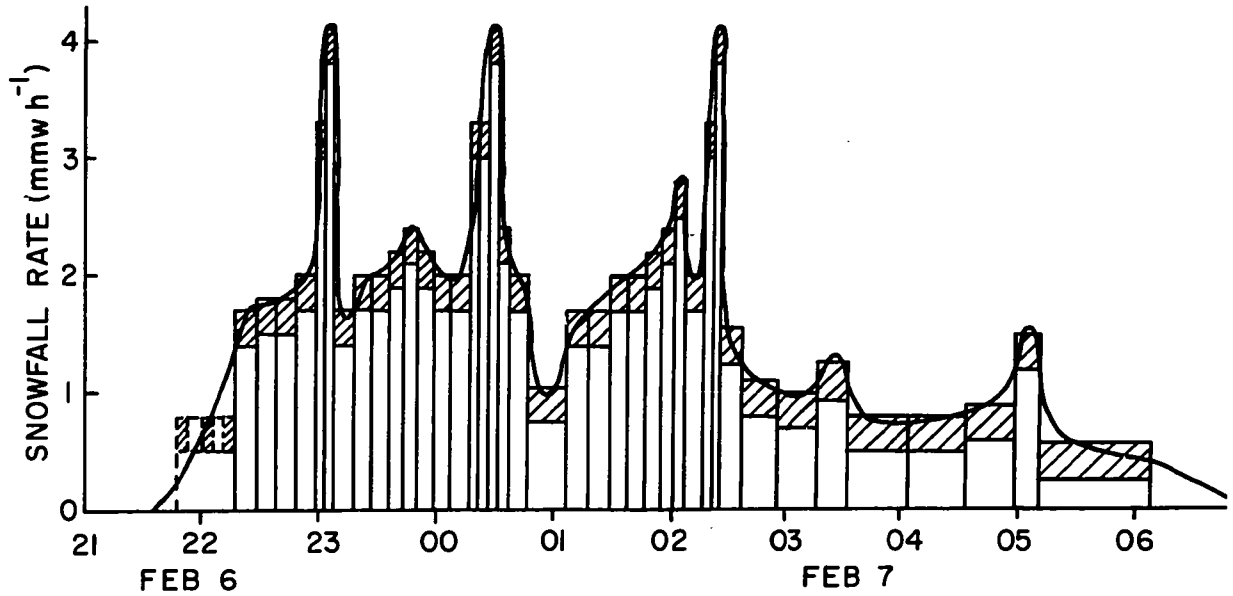


Figure 6.1. Snowfall rates from recording gauge at L'Assomption (hatched portion at the top of each rectangle indicates evaporation correction of 0.3 mmw h^{-1}).

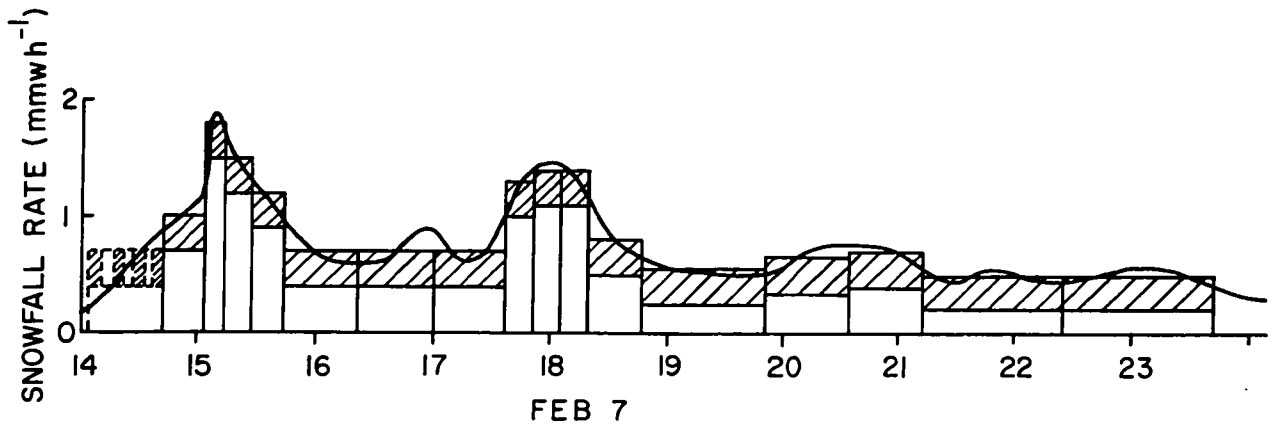


Figure 6.2. Snowfall rates from recording gauge at L'Assomption (hatched portion at the top of each rectangle indicates evaporation correction of 0.3 mmw h^{-1}).

rectangular areas up to that time. This was done to obtain a realistic representation of the variations in snowfall rate for comparison with the corresponding 5000-ft radar data.

6.2 Snow trails and trajectories

Before comparing gauge and radar data, or while making the comparison, one must decide what map location at 5000 ft will have radar data best related to the gauge. The decision, in effect, involves a correction for horizontal displacement of the falling snow, which is determined by the wind profile in the vertical and the snow's fall speed. A mean fall speed of 1 m sec^{-1} may be reasonably assumed, but the variation of wind with height may be complex as both wind speed and direction may change with height, and with time.

First consider a simple case, in which wind direction is constant and the wind speed increases linearly with height. Figure 6.3 shows that under these conditions snow reaching the ground at a given point P can be related to conditions aloft by two lines, marked "trail" and "trajectory" (Marshall, 1953). In this case, a point source (G) is generating snow at a steady rate as it moves with the wind (V_G) at the generating height. Under these conditions, the trail and trajectory are in the same plane and both are parabolic. The trail remains attached to the generator, and moves with it. Figure 6.3 shows the trail at time t, when it intersects the ground at P. The snowfall rate at P, at time t, should be closely correlated to the rate measured at the same time at M(t), on the trail at the radar-map height. The trail as drawn shows where all the snow is at time t, between the generator and the ground. It also shows the path followed by a single snowflake, but only if drawn relative to axes moving with the snow generator.

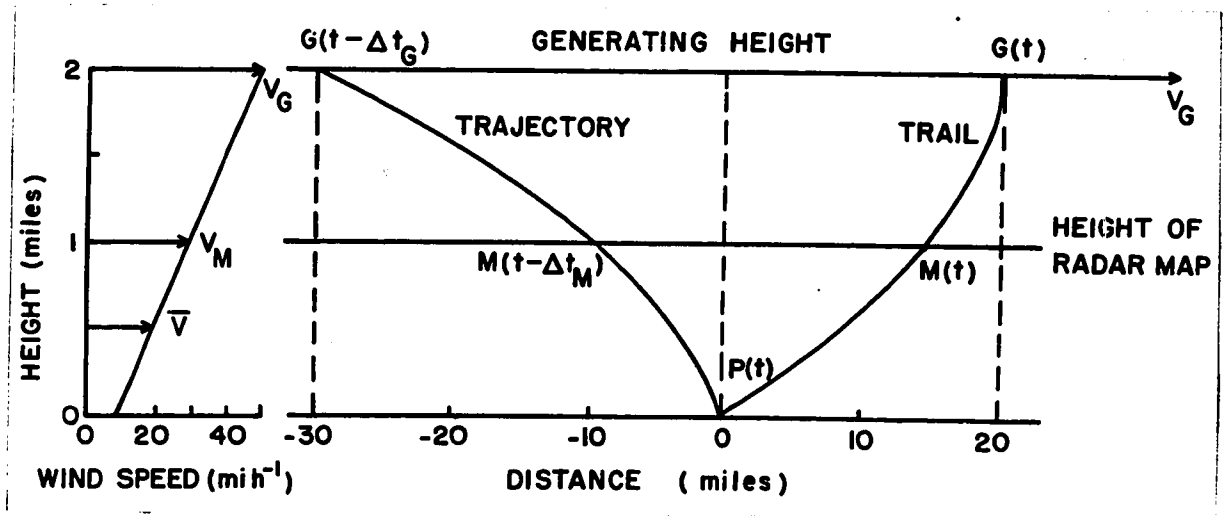


Figure 6.3. Trail and trajectory of snow falling from a point-source moving at a constant speed (V_G) at the generating height.

(left) Wind profile - direction constant and speed increasing linearly with height.

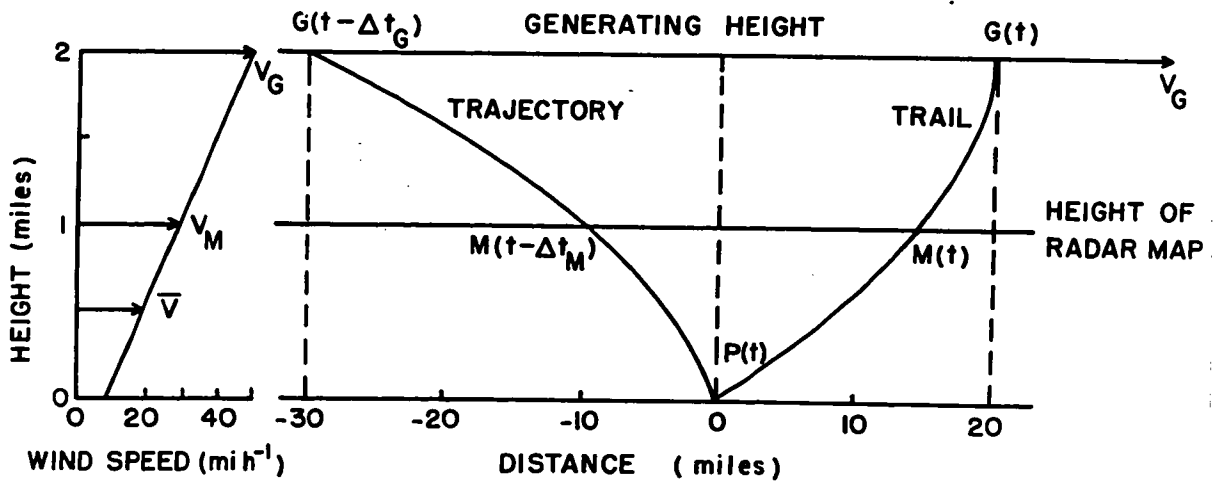


Figure 6.3. Trail and trajectory of snow falling from a point-source moving at a constant speed (V_G) at the generating height.

(left) Wind profile - direction constant and speed increasing linearly with height.

For axes fixed to the ground, the path followed by snowflakes arriving at P is the parabolic curve labelled "trajectory". Snow arriving at P, at time t , originated at the top of the trajectory at an earlier time. In falling toward P, the snow passed through the radar-map height at $M(t - \Delta t_M)$, where Δt_M is the snow's fall-time from that height to the ground. There should then be a good correlation between the snowfall rate at P, and the rates measured earlier on the trajectory. Thus, radar data on the trajectory can provide short-term forecasts of snowfall rates at P which do not involve assumptions about the generation rate. For forecasts with a greater lead-time, one could go on upward along the trajectory, to utilize radar data from the generating height, and then proceed horizontally upstream in the precipitation pattern: or one could stay at the height of the lowest reliable radar map, and proceed horizontally upstream at that height. In either case, upstream refers to the motion of the radar-observed precipitation pattern at the selected height.

Now consider a case in which wind direction and speed both vary with height. If the average (vector) wind in a layer is \bar{V} , the horizontal displacement of snow falling through the layer is $-\bar{V}(\Delta t)$, where Δt is the time the snow takes to traverse the layer. Applying this to the earlier, more intense part of this storm, the average wind in the lowest 5000-ft layer was $060^\circ/22$ (east-northeast/22 mi h^{-1}). This average wind and a fall-time of 25 minutes define a point at 5000 ft 9 miles east-northeast of L'Assomption (bearing 060°). Uncertainty was felt, more with regard to the average wind than to the assumed fall speed of 1 m sec^{-1} for snow, therefore radar data taken at several nearby points were compared with the gauge data. Figure 6.4 shows the locations of the points that were tested, and indicates the one at which the radar data best fitted the gauge-measured rates. It corresponds to a point at 5000-ft $078^\circ/7$ miles from L'Assomption.

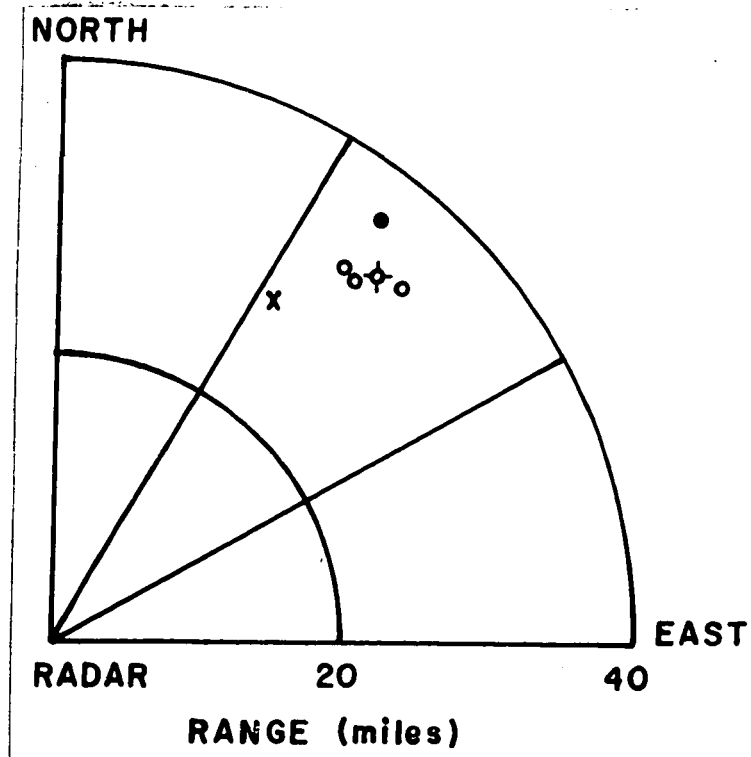


Figure 6.4. Location of 1'Assomption gauge (x) and 5000-ft point on trajectory (●) for V of $060^\circ/22 \text{ mi h}^{-1}$. Other points tested are indicated by circles (o). The point that gave the best fit between radar and gauge data is indicated (\oplus).

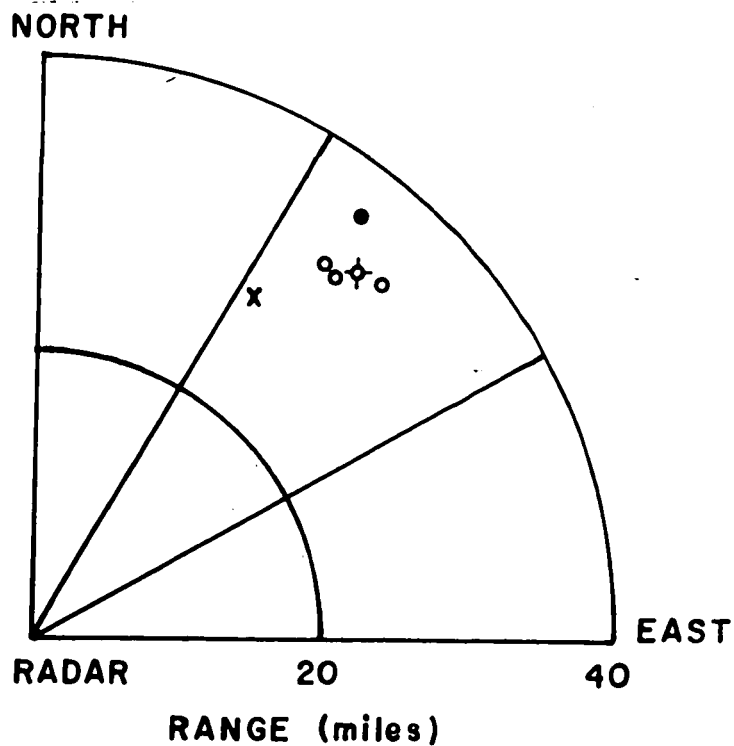


Figure 6.4. Location of l'Assomption gauge (x) and 5000-ft point on trajectory (●) for V of $060^\circ/22 \text{ mi h}^{-1}$. Other points tested are indicated by circles (○). The point that gave the best fit between radar and gauge data is indicated (⊕).

6.3 Radar-derived rates

Radar information about snowfall rates at the selected 5000-ft point ($078^{\circ}/7$ miles from L'Assomption) is given in Figure 6.5. The vertical lines indicate the intervals of snowfall rate between thresholds of the grey-shade appearing at that point at each map-time¹. By assuming a steady motion of the precipitation patterns between successive maps, estimated times of threshold-crossing were obtained. These times, obtained by the straightforward technique based on the foregoing assumption, are indicated by the vertical sides of the shaded rectangles in Figure 6.5. There was no more than one threshold crossing inferred between successive maps but the areal resolution of the radar system is considered adequate to indicate more than one, if this were to occur.

The radar-derived information of Figure 6.5 were fitted by a number of continuous curves, one of which is shown in Figure 6.6. These curves varied in amplitude, but successive threshold-crossing times were the same, in each case, as those indicated by the sides of the shaded rectangles. Measurement of areas under the respective curves showed that snowfall amounts obtained in this manner would differ by less than 15%, in spite of the fact that maximum and minimum snowfall rates permitted at each map-time were separated by a factor 2.5.

¹The relationship between reflectivity factor and rainfall rate used with the particular radar maps on which this work was done was $Z = 1000 R^{2.67}$. While this relationship is useful for these particular maps, which were produced by scanning the rapid-access film record for this storm (Appendix 1), it is not generally acceptable.

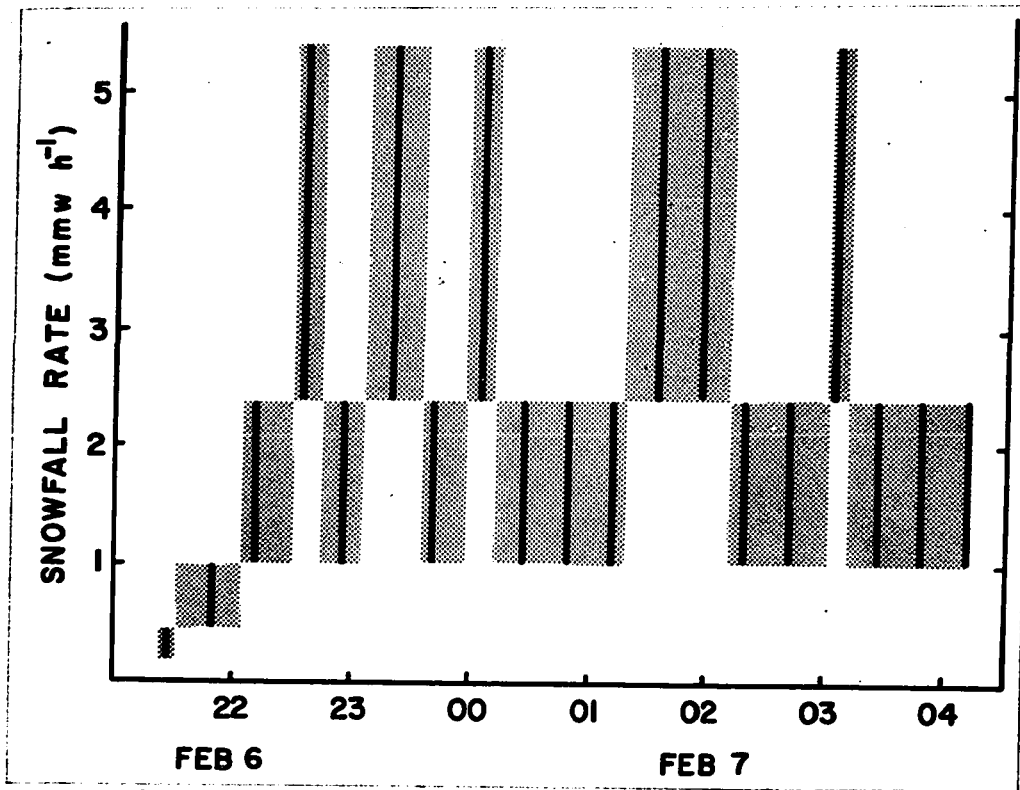


Figure 6.5. Radar data for 5000-ft point 078°/7 miles from 1' Assumption (vertical lines give the allowable range of snowfall rates for each map time, and sides of shaded rectangles indicate times of threshold crossing deduced from radar data).

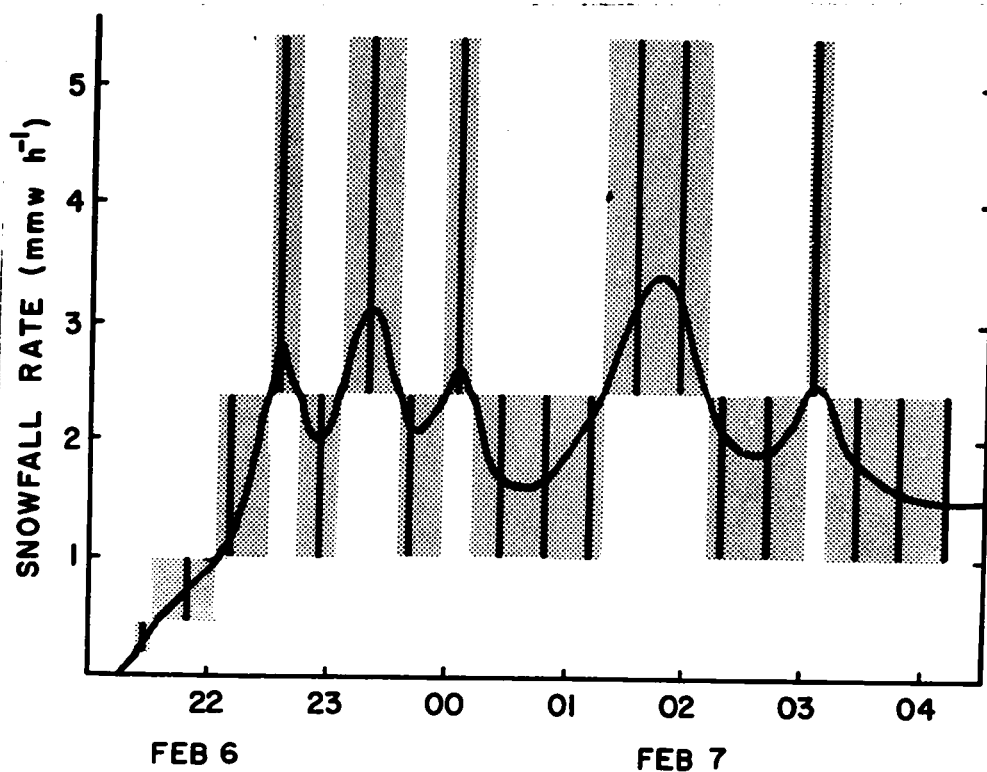


Figure 6.6. Continuous curve fitted to radar data of Figure 6.5.

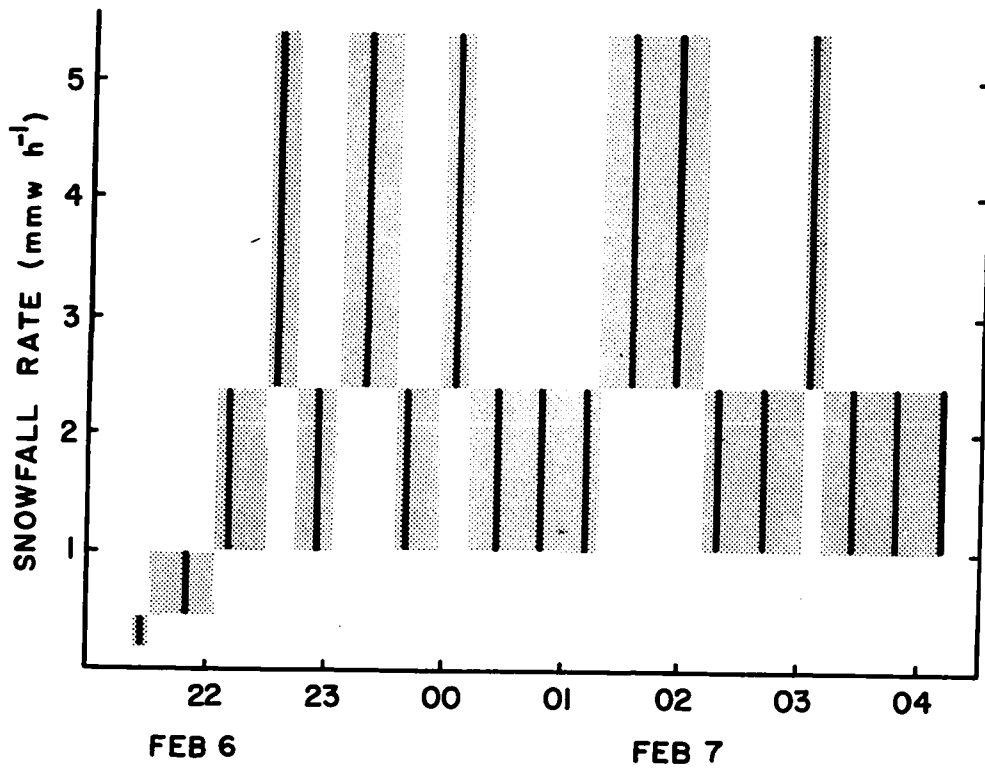


Figure 6.5. Radar data for 5000-ft point 078°/7 miles from l'Assomption (vertical lines give the allowable range of snowfall rates for each map time, and sides of shaded rectangles indicate times of threshold crossing deduced from radar data).

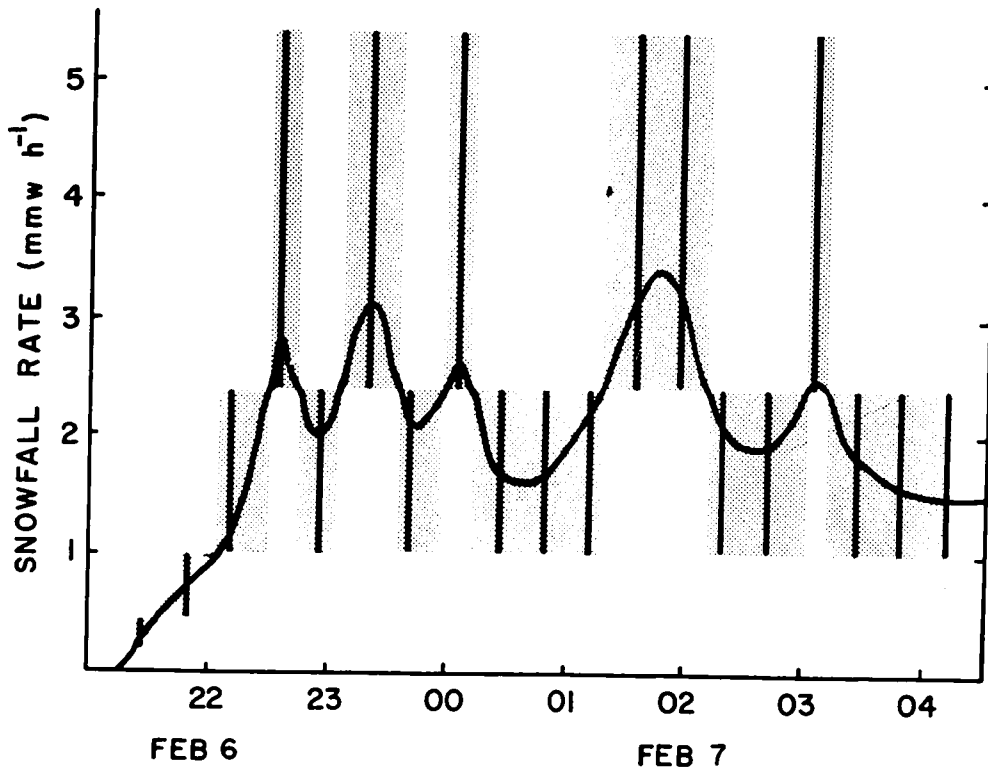


Figure 6.6. Continuous curve fitted to radar data of Figure 6.5.

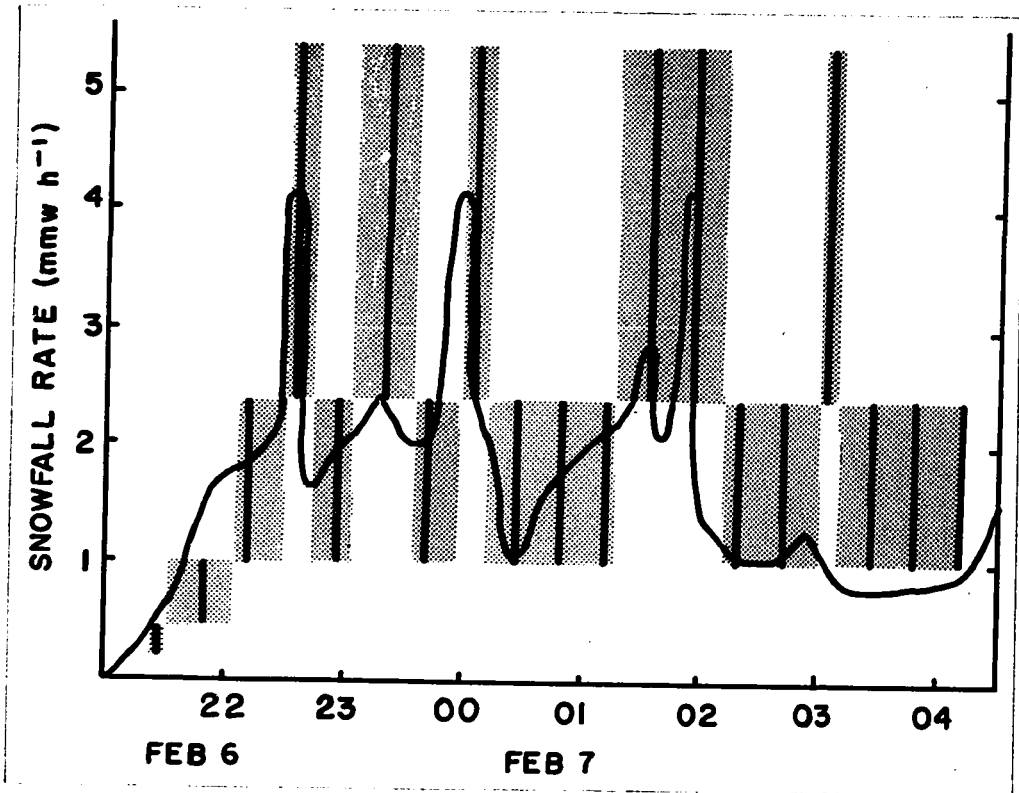


Figure 6.7. Gauge-derived snowfall rate curve (Fig. 6.1) displaced 22 minutes earlier and superimposed on radar data for 5000-ft point 078°/7 miles from l'Assomption (Fig. 6.5).

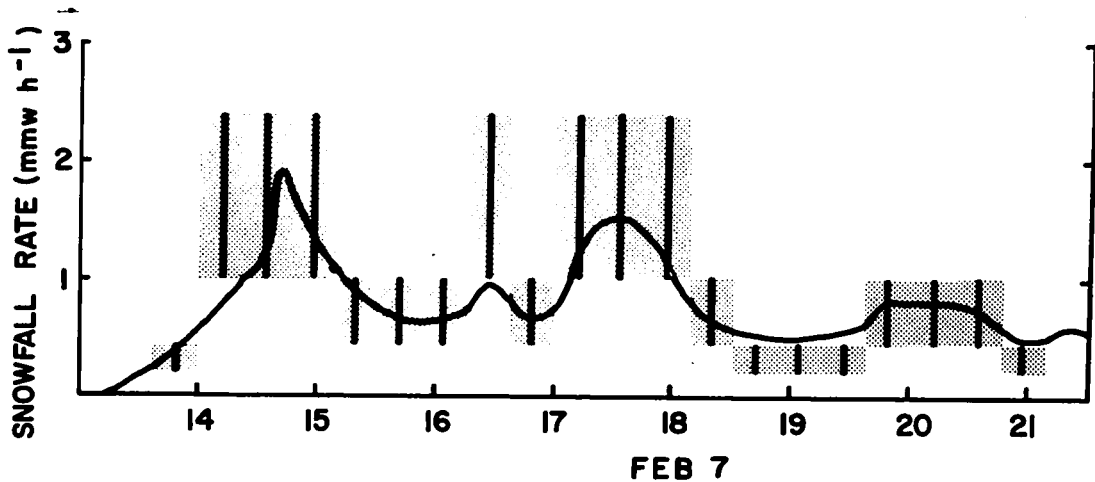


Figure 6.8. Gauge-derived snowfall rate curve (Fig. 6.2) displaced 22 minutes earlier and superimposed on radar data for 5000-ft point over l'Assomption.

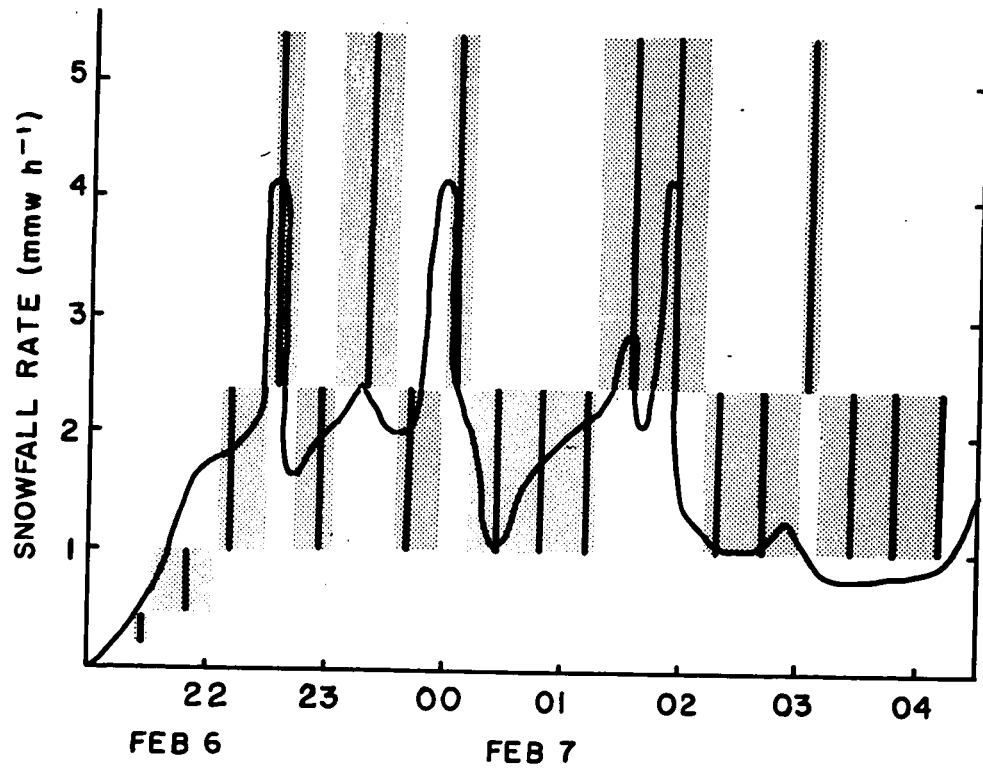


Figure 6.7. Gauge-derived snowfall rate curve (Fig. 6.1) displaced 22 minutes earlier and superimposed on radar data for 5000-ft point 078°/7 miles from l'Assomption (Fig. 6.5).

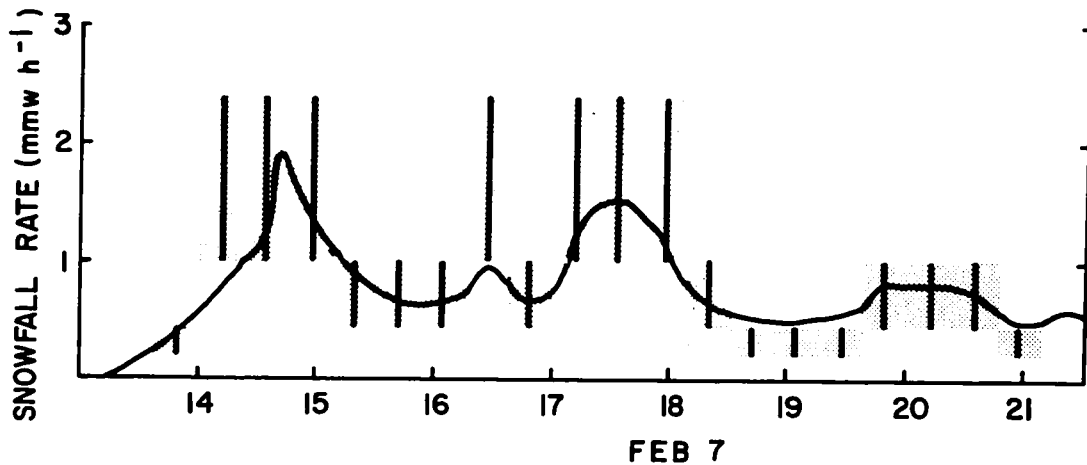


Figure 6.8. Gauge-derived snowfall rate curve (Fig. 6.2) displaced 22 minutes earlier and superimposed on radar data for 5000-ft point over l'Assomption.

6.4 Comparison of gauge-measured and radar-derived rates

The gauge data for the earlier, more intense part of this storm were shown in Figure 6.1, and the radar data for the best-related 5000-ft point were given in Figure 6.5. These are brought together in Figure 6.7, with a time difference adjusted for best fit. Taking this difference of 22 minutes, as the time required for the snow to fall 5000 ft, a fall-speed of 1.1 m/sec is obtained, as compared to the 1.0 m/sec that had been assumed.

A similar comparison of radar and gauge data for the later, less intense part of the storm appears in Figure 6.8. In this case, the radar data were taken at the point on the maps corresponding to the location of the gauge, because light winds prevailed in the snow-generating volume of the system which produced this snow. In effect, the 5000-ft point (Figure 6.3) was directly over the gauge because the horizontal displacement of the falling snow was small.

Although the agreement between radar and gauge data for both parts of this storm is encouraging, the analysis does suggest that smaller intervals between snowfall-rate thresholds are needed, particularly at high rates, to improve the rate resolution of the radar system. Arithmetic spacing of the snowfall-rate thresholds should be considered, as an alternative to the present geometric spacing.

7. Variation of Radar-derived Snow Parameters with Height

Preceding chapters dealt exclusively with radar data taken from 5000-ft CAPPI maps, and snowfall measurements at the ground. Comparison of these observations effectively calibrated the radar data against climatological measurements. This chapter deals with radar data taken at CAPPI heights 5, 10, 15, and 20 thousand feet to bring out information about the growth of snow with distance fallen. No snow was detected at CAPPI heights 25 and 30 thousand feet.

7.1 Grid-point values of snowfall amount

Figure 7.1 gives grid-point values of snowfall amount derived from radar observations at four CAPPI heights (5, 10, 15, and 20 thousand feet), and from measurements at the ground. It was assumed that the relationship $Z = 2000 R^{2.0}$ was applicable at all heights. This assumption is without great justification; fresh insights become available when variations with time are studied (Section 7.4). Bracketted values for CAPPI heights 5 and 10 thousand feet (Figure 7.1) are unreliable because of the tilted axis of the antenna, which made the beam lower than intended in the northwestern quadrant (Section 4.5).

Ninety-eight percent of the snow that reached the ground within 100 miles of the radar site was generated at heights below 20 000 ft. In the southeast quadrant it appears that most of the snow was generated in the layer from 20 000 to 10 000 ft, and subsequently fell to the ground with little further growth. The pattern in the northwest quadrant is quite different. There, more than 90% of the snow was produced below 15 000 ft, and much of the growth took place below 10 000 ft.

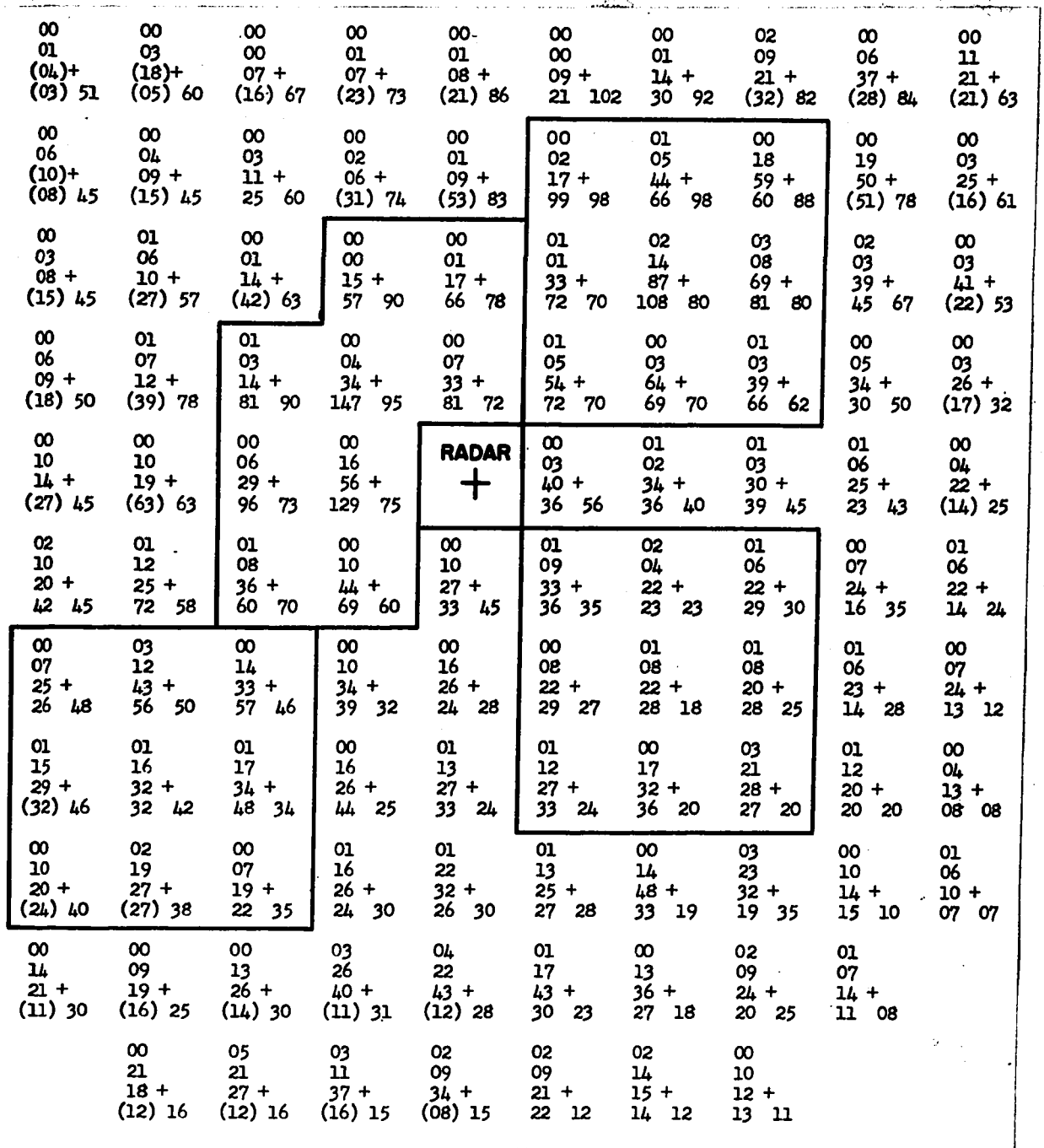


Figure 7.1. Grid-point values of snowfall amount derived from radar observations at four CAPPI heights, and from measurements at the ground (units: 10^{-1} inches of snow). Grid points (+'s) are located 15 miles apart in a square array (as in Figure 3.4).

	<u>Amount</u>	<u>Height (10^3 ft)</u>
	dd	20
	cc	15
Plotting model	bb +	10 +
	aa gg	5 ground

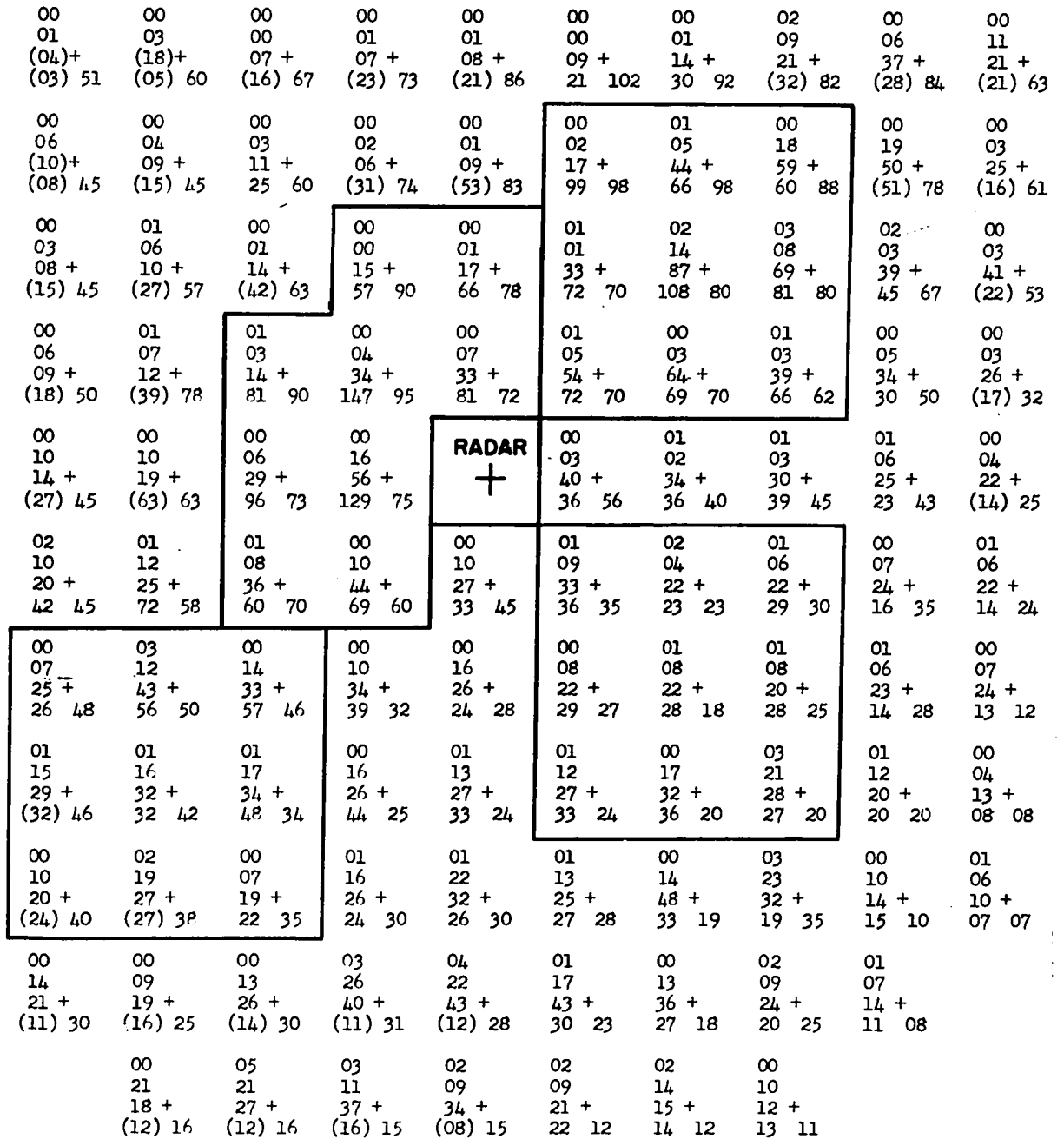


Figure 7.1. Grid-point values of snowfall amount derived from radar observations at four CAPPI heights, and from measurements at the ground (units: 10^{-1} inches of snow). Grid points (+'s) are located 15 miles apart in a square array (as in Figure 3.4).

	<u>Amount</u>	<u>Height (10^3 ft)</u>
	dd	20
	cc	15
Plotting model	bb +	10 +
	aa gg	5 ground

7.2 Variation of radar amount with height

Variations of radar amount with height were determined for four separate areas on the radar maps. Four separate blocks of 9 grid points each (Figure 7.1) were selected. Within each of these blocks, climat (ground-measured) amounts of snow were relatively uniform. At each CAPPI height, amounts were averaged over the 9 grid points of each block to obtain the values given in Table 7.1. In the northern areas, less than 10% of the snow

Table 7.1 - Average amount of snow observed at indicated heights

HEIGHT (10 ³ ft)	NW (inches of snow)	NE	SE	SW	- BLOCK -	NW (% of 5000-ft value)	NE	SE	SW
20	0.03	0.1	0.1	0.1		~ 0.5	~ 1	~ 4	~ 3
15	0.6	0.6	1.0	1.3		8	8	35	35
10	3.1	5.2	2.5	2.9		35	70	90	80
5	8.7	7.7	2.8	3.6		100	100	100	100
Ground	7.7	8.0	2.5	4.3		90	105	90	120

that reached 5000 ft was generated above 15 000 ft, 30 to 60% was produced in the layer from 15 to 10 thousand feet, and the balance (60% to 30%) below 10 000 ft. In the south, 35% of the snow that reached 5000 ft was generated above 15 000 ft, 50% was produced in the layer from 15 000 to 10 000 ft, and there was little further growth below 10 000 ft.

Horizontal displacement of the snow by the variable wind field through which it fell undoubtedly contributed to the above-noted differences in growth pattern. Wind speed and wind direction both varied with height, and with time, during the 48-hour period under study; as a result, the falling snow was displaced horizontally in a complex and variable pattern (Chapter 6 and Appendix 2). These effects are not taken into account, either in Figure 7.1 or in Table 7.1.

7.3 Duration of snow exceeding given rates

Figure 7.2 shows the average duration of snow exceeding given threshold rates at each CAPPI height, separately for each block (Figure 7.1) and averaged over 9 grid points in each case. The loci show the duration of snow exceeding any rate at each height. In situations where the next higher threshold was not attained, extensions of the loci are indicated by dashed lines. Since threshold 4 ($R = 9 \text{ mmw h}^{-1}$, using $Z = 2000 R^{2.0}$) was not exceeded during this snowstorm, several of the extensions curve downward sharply between thresholds 3 and 4 (3 and 9 mmw h^{-1} , respectively).

Observations taken over a period of years at McGill Observatory (located in downtown Montreal) suggest an upper limit to snowfall rates in this area: rates in excess of 10 mmw h^{-1} have not been observed (Gunn, 1965). Recording-gauge data taken at McGill Observatory during the period under study show that the duration of snowfall rates exceeding 5 mmw h^{-1} was 0.3 hours. The gauge at L'Assomption recorded rates exceeding 4 mmw h^{-1} for 0.2 hours. The lack of echo exceeding threshold 4 in this storm is surely attributable to physical characteristics of the snowstorm, rather than the radar system.

In the northern blocks (Figure 7.2), the loci for 5 and 10 thousand feet show a relatively slow exponential decrease in duration with increasing threshold. Beyond threshold 3 (and in one case between thresholds 2 and 3), the rate of decay increases. The available data for height 15 000 ft (NE-block) also suggest an exponential decrease in duration, but at a more rapid rate than at the lower heights. In the southern blocks, the loci for 5 and 10 thousand feet show that duration decays relatively slowly between thresholds 1 and 2, but the rate of decay increases beyond threshold 2 (1 mmw h^{-1}). The available data for height 15 000 ft (SE-block) also suggest an exponential decrease in duration, similar to that obtained in the NE-block.

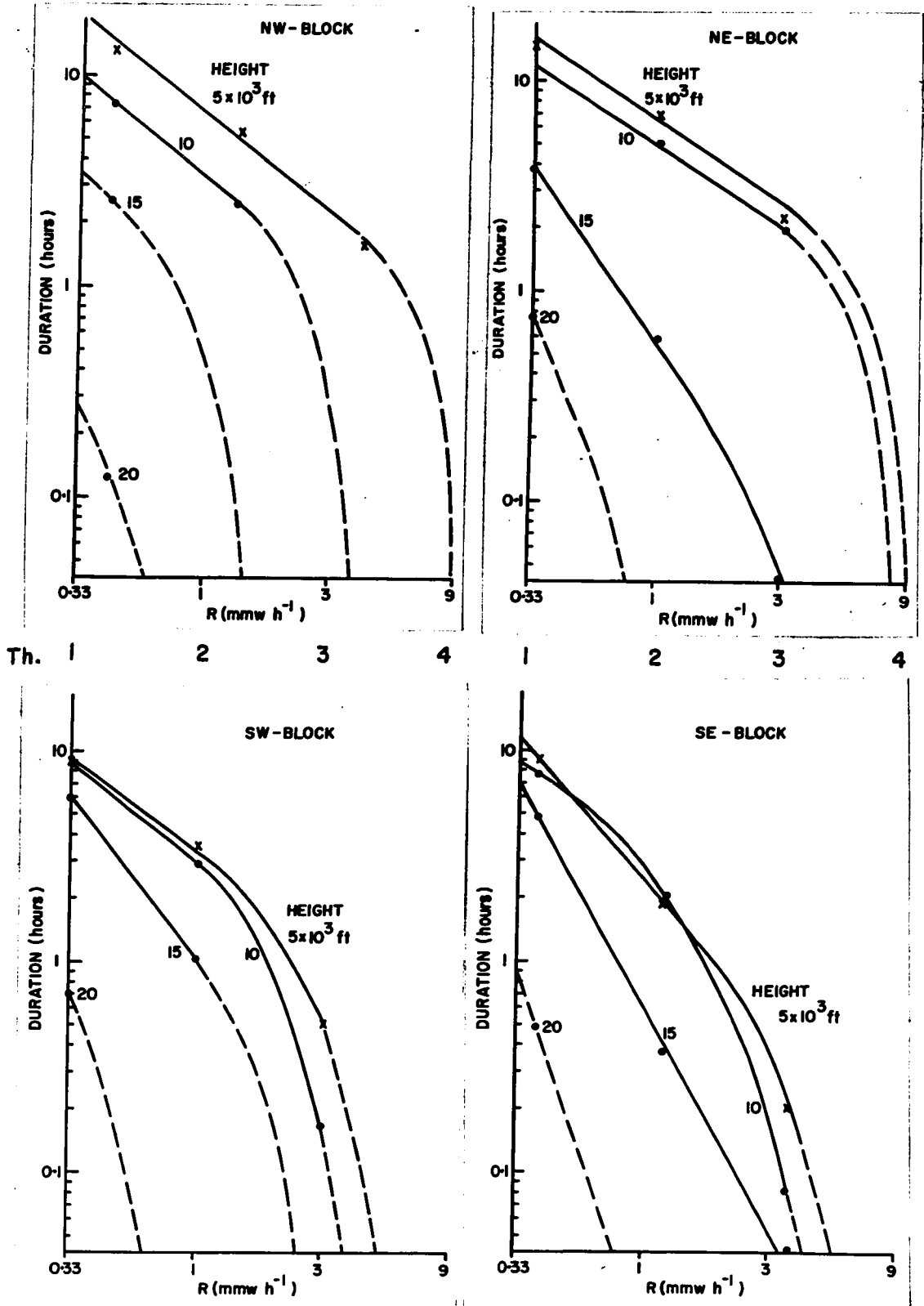


Figure 7.2. Duration of snow exceeding given threshold rates at indicated CAPPI heights.

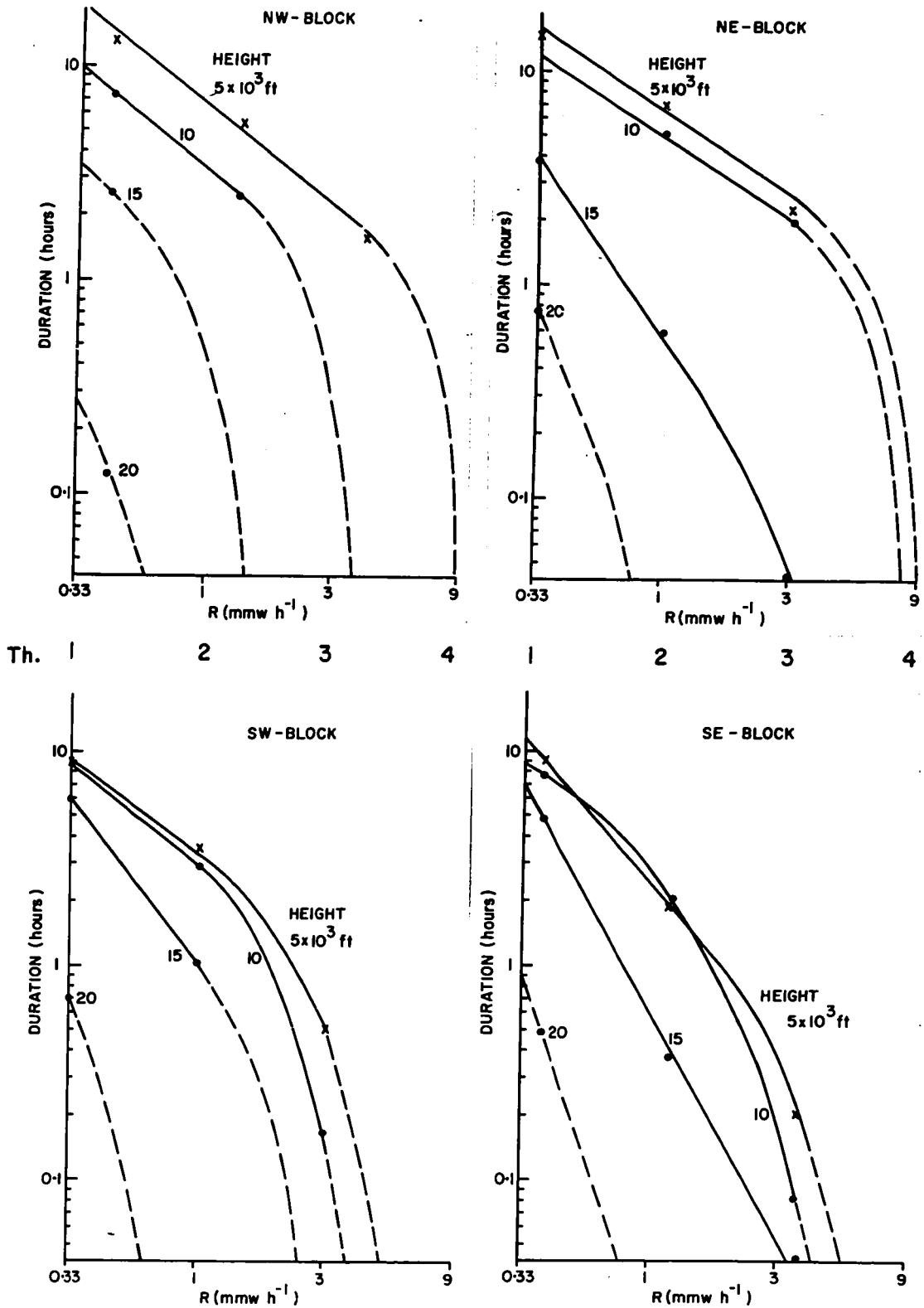


Figure 7.2. Duration of snow exceeding given threshold rates at indicated CAPPI heights.

7.4 Variation with time of averaged snowfall parameters

Figure 7.3 shows the variation of \bar{Z} , radar reflectivity averaged over 45 grid points at each CAPPI height, during the first snowfall associated with this storm. The 45 grid points (9 each from the four blocks outlined on Figure 7.1, and 9 grid points intermediate to those blocks) are representative of an area of 10 000 square miles. The curves of Figure 7.3 are based on smoothed values of \bar{Z} , which were obtained by taking a running average over three consecutive values (22.5 minutes apart) at each height.

Figure 7.4 shows the variation of $\sqrt{\bar{Z}}$, square root of radar reflectivity averaged over the same set of 45 grid points at each CAPPI height. This parameter is proportional to R, snowfall rate averaged over the same set of grid points, if Z is proportional to $R^{2.0}$ at all heights as was assumed. The curves of Figure 7.4 are based on smoothed values of $\sqrt{\bar{Z}}$, as in Figure 7.3.

The period from 1500 to 1900EST was a transitional phase, during which a widespread pattern of falling snow spread northward across the area under consideration. The overhanging character of the advancing pattern of snow is evidenced on Figures 7.3 and 7.4; snow was first detected, more or less simultaneously, at heights 15 and 20 thousand feet, half an hour later at 10 000 ft, and another half hour later at 5000 ft. The respective \bar{Z} and $\sqrt{\bar{Z}}$ curves show corresponding lags during this transitional phase. The overhanging pattern of falling snow appears to be related to shearing wind conditions. At the time, winds veered and increased in speed with height, from $050^\circ/15 \text{ mi h}^{-1}$ near the ground to $170^\circ/40 \text{ mi h}^{-1}$ near 20 000 ft.

From 1900EST 6 February to 0300EST 7 February, the pattern of falling snow covered the area under consideration at the lower CAPPI heights; the coverage was more variable at 15 and 20 thousand feet as distinct bands of snow moved into the area from the south, and out of the area in a northerly

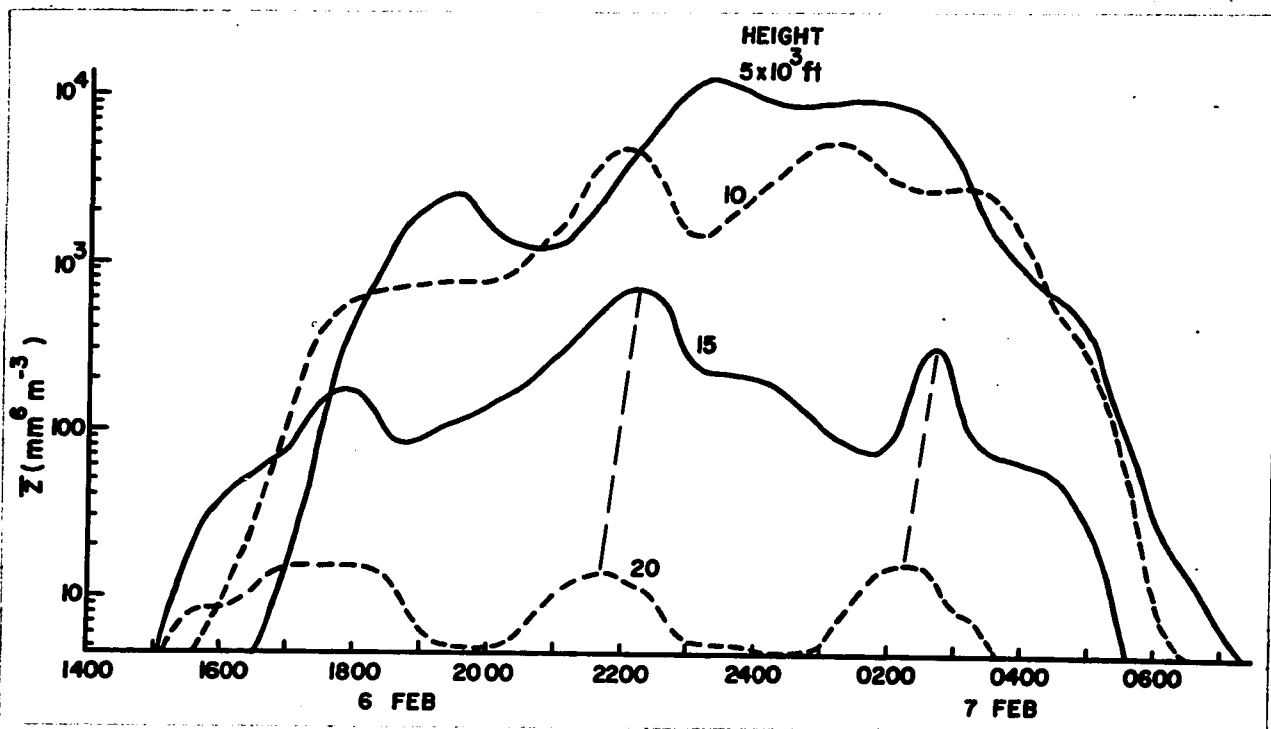


Figure 7.3. Variation of \bar{Z} with time at indicated CAPPI heights.

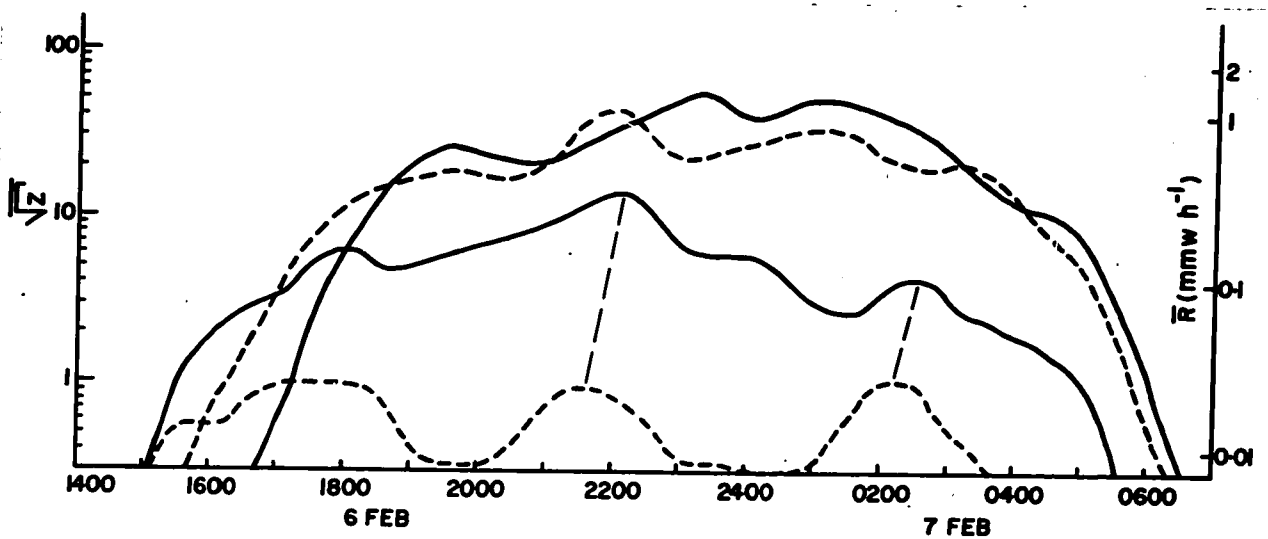


Figure 7.4. Variation of $\sqrt{\bar{Z}}$ with time at indicated CAPPI heights.

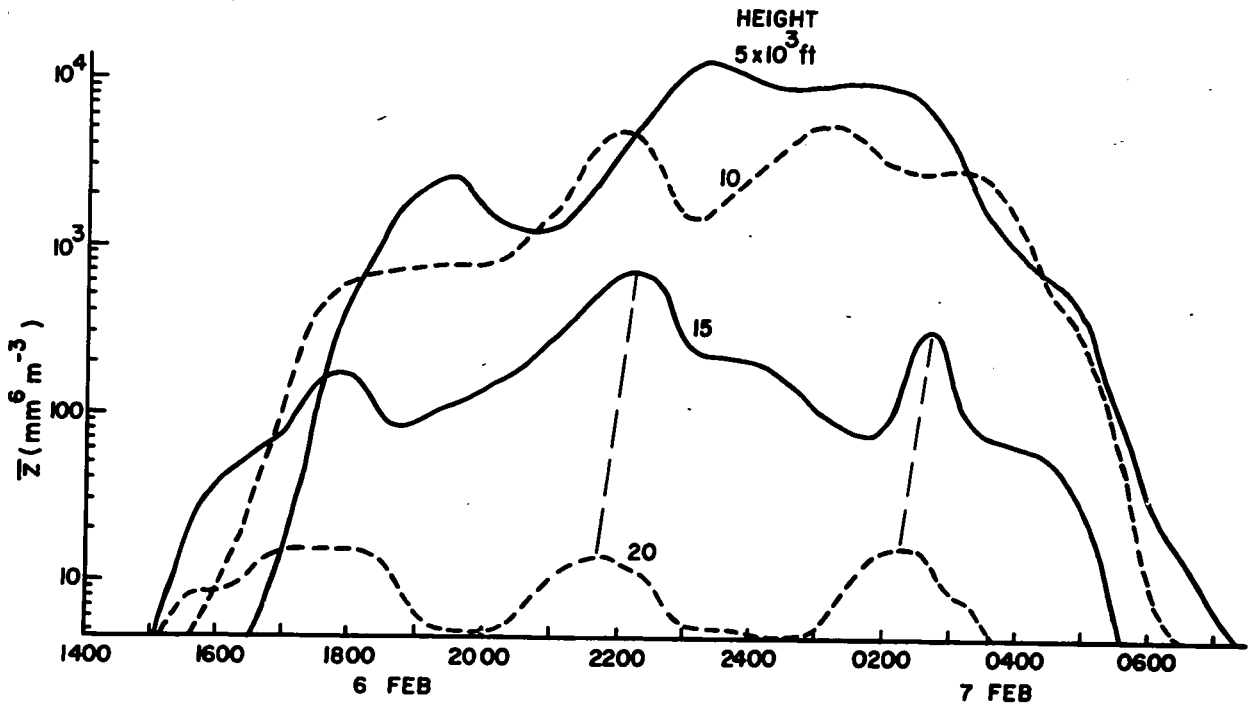


Figure 7.3. Variation of \bar{Z} with time at indicated CAPPI heights.

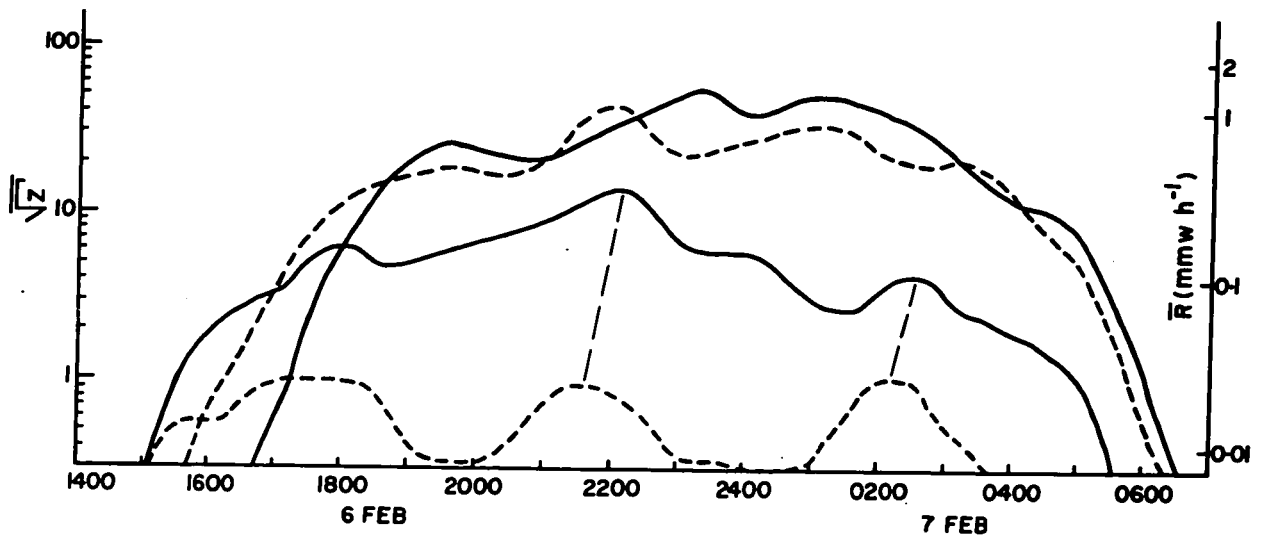


Figure 7.4. Variation of $\sqrt{\bar{Z}}$ with time at indicated CAPPI heights.

direction. Maxima at height 15 000 ft (Figures 7.3 and 7.4) tend to lag the maxima at 20 000 ft by about half an hour. However, the same can't be said for 15 versus 10, or 10 versus 5 thousand feet. During this period, values of \bar{Z} and $\sqrt{\bar{Z}}$ increased as the snow grew during its fall. Values of \bar{Z} generally increased by factors that ranged from 30 to 15 between 20 and 15 thousand feet, further factors 5 to 15 between 15 and 10 thousand feet, and smaller factors of 2 or 3 between 10 and 5 thousand feet. The corresponding values for $\sqrt{\bar{Z}}$ range from 12 to 6 between 20 and 15 thousand feet, 3 to 9 between 15 and 10 thousand feet, and 1.0 to 1.5 between 10 and 5 thousand feet. At height 5 and 10 thousand feet, mean snowfall rates based on $\sqrt{\bar{Z}}$ (Figure 7.4) are in closer agreement than corresponding rates based on \bar{Z} (Figure 7.3). This does not apply at heights above 10 000 feet.

The period 0300 to 0700EST was another transitional phase, during which the pattern of falling snow moved northward out the area under consideration, first at 20 000 ft and then at successively lower CAPPI heights.

Figures 7.5 and 7.6 show the variation of \bar{Z} and $\sqrt{\bar{Z}}$ at each CAPPI height during the second snowfall. The curves were obtained in the same manner as those of Figures 7.3 and 7.4.

The period 0900 to 1200EST 7 February was a transitional phase, during which an elongated pattern of falling snow gradually moved into the area under consideration from the southwest. The snow was associated with a pressure trough, the axis of which was oriented from northwest to southeast across the St. Lawrence Valley (Figure 2.3). Winds were light at all heights, generally less than 15 mi h^{-1} , in the vicinity of this trough. Although wind directions were easterly northeast of the trough and westerly to the southwest, there was no appreciable wind shear in the vertical. This lack of shear is evidenced on the curves of Figures 7.5 and 7.6; snow was first detected, more

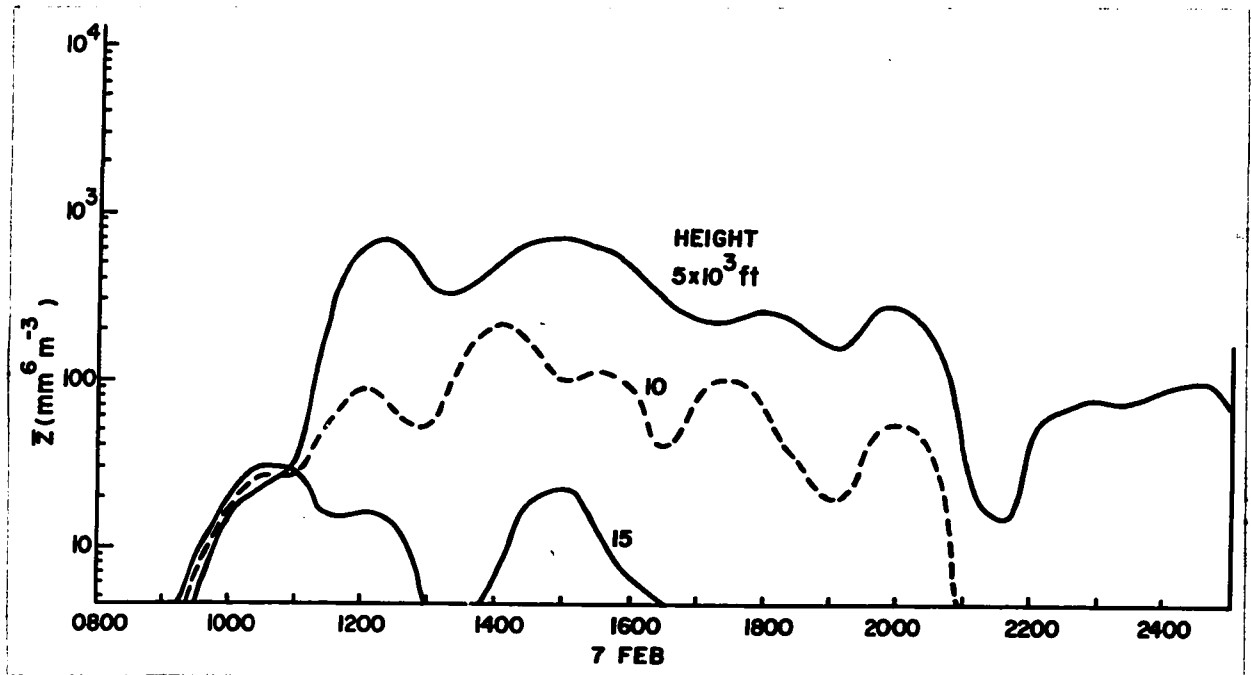


Figure 7.5. Variation of \bar{Z} with time at indicated CAPPI heights.

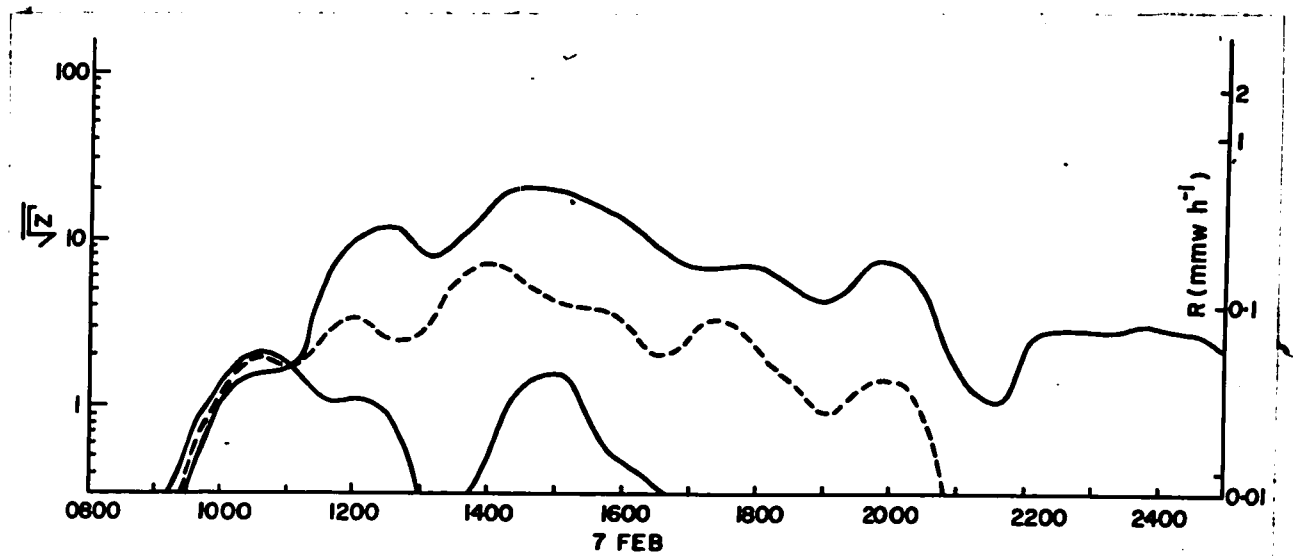


Figure 7.6. Variation of \sqrt{Z} with time at indicated CAPPI heights.

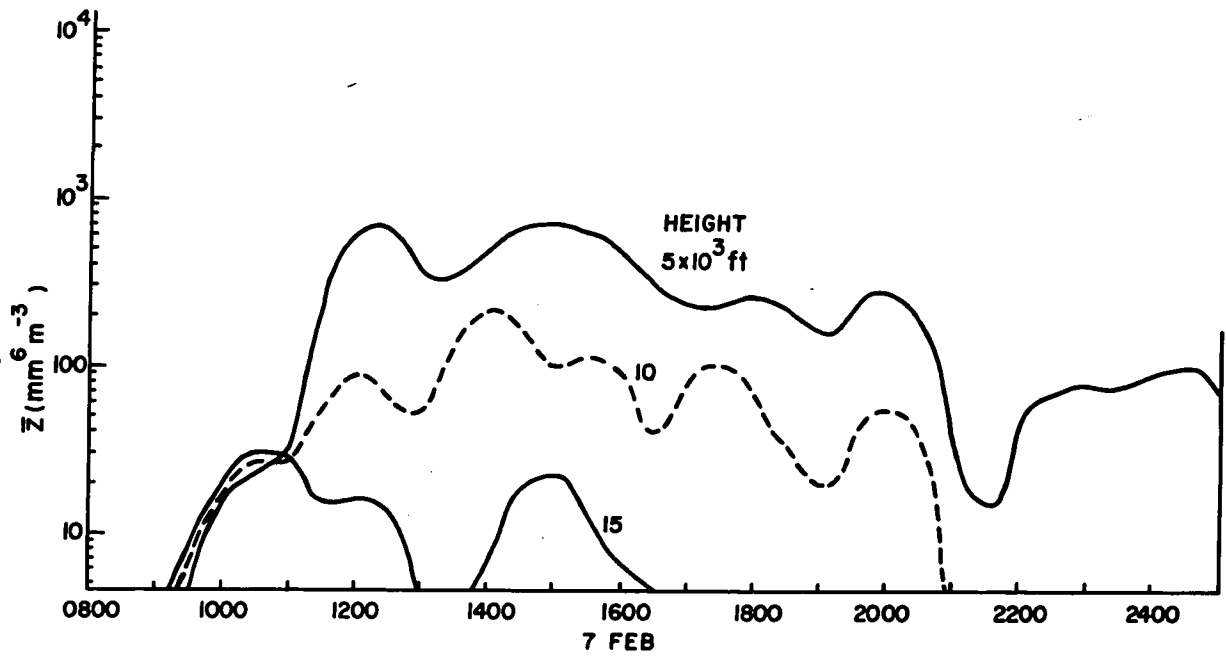


Figure 7.5. Variation of \bar{Z} with time at indicated CAPPI heights.

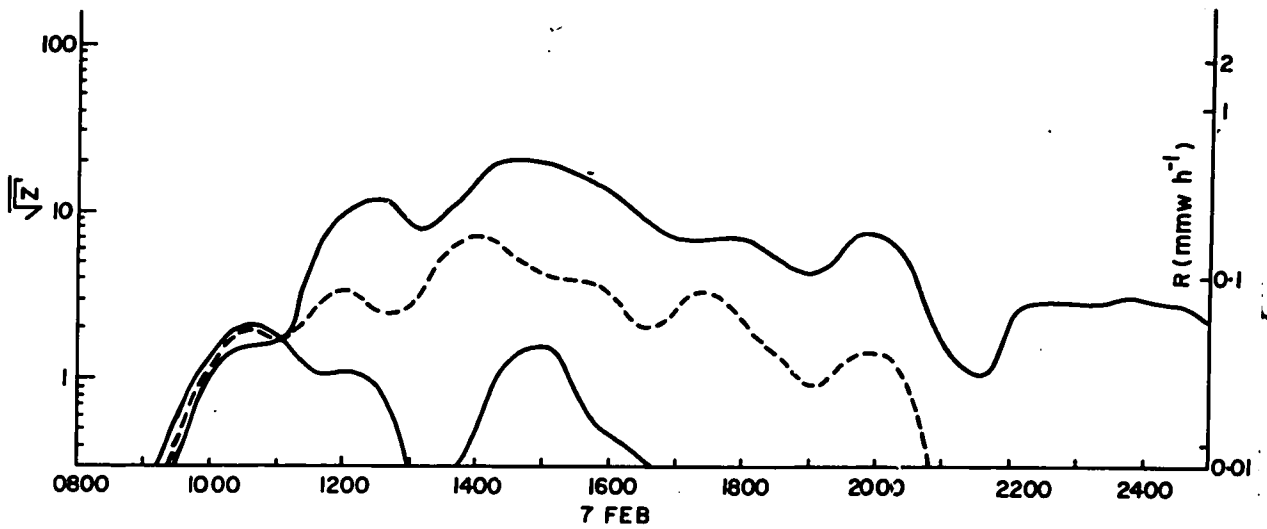


Figure 7.6. Variation of \sqrt{Z} with time at indicated CAPPI heights.

or less simultaneously, at 5, 10, and 15 thousand feet, and there was no significant lag in developments between these heights.

From 1200 to 2400EST, the pressure trough (and its associated pattern of falling snow) moved slowly northeastward along the St. Lawrence Valley to the area between Montreal and Quebec City. The relative lack of wind shear also is indicated by the zero-phase shift between the pattern features at 5, 10 and 15 thousand feet (Figures 7.5 and 7.6). No snow was detected at 20 000 ft, during this period. Values of \bar{Z} generally increased by factors that ranged from 5 to 10 between 15 and 10 thousand feet, and by a further factor 5 between 10 and 5 thousand feet. The corresponding factors for $\sqrt{\bar{Z}}$ range from 5 to 8 between 15 and 10 thousand feet, and 3 to 4 between 10 and 5 thousand feet. Averaging over $\sqrt{\bar{Z}}$, rather than \bar{Z} , does not appear to afford any particular advantage in this situation.

8. Summary and Conclusions

This study provides evidence that useful measurements of snowfall at the ground can be derived from 3-cm radar observations at an average height of 5000 ft. An isohyetal mapping of snowfall during one 48-hour period (one storm) was obtained from radar data using the relationship $Z = 2000 R^{2.0}$, which had been derived from measurements of the size distribution of aggregate snowflakes in samples collected near the ground. For comparison, an isohyetal mapping was prepared from ruler-measurements of new-fallen snow taken daily at 140 climatological stations.

The best agreement between radar-measured and ground-measured amounts was obtained at short range (<42 miles). The distribution of short-range grid points with radar/climat (amount) ratio was found to be approximately log-normal. Two-thirds of the ratio values fell within a factor 1.3 (+30% -25%) of the mean value. The systematic error implied by the initial value of the mean (0.33) was attributed to uncertainties regarding calibration of the radar data, and was reduced to negligible proportions by means of a calibration adjustment. The same adjustment, based on short-range data, also was applied to medium- and long-range data.

The exponent of the relationship $Z = 2000 R^{2.0}$ was correct for the 5000-ft data taken during this snowstorm. This was evidenced by the lack of bias toward underestimation, or overestimation, of small amounts of snow (~2 inches), all of which had accumulated at rates less than one mmw h⁻¹, relative to large amounts (~10 inches), most of which had accumulated at higher rates. No conclusion could be reached about the value of the coefficient in the above Z-R relationship, because of the above-mentioned uncertainties regarding calibration. If the value of the coefficient is taken to be correct, the results obtained at short range indicate that the minimum

detectable reflectivity (snowfall rate) at the output of the radar system was $2 \times 10^2 \text{ mm}^6 \text{ m}^{-3}$ (0.33 mmw h^{-1}), rather than $20 \text{ mm}^6 \text{ m}^{-3}$ (0.11 mmw h^{-1}) as had been assumed.

In certain sectors, at medium and long range (42 to 100 miles), the quality of the radar measurements was similar to that at short range: the mean value of radar/climat ratio was $\approx 10\%$ lower, and two-thirds of the ratio values fell within a factor 1.6 (+60% -40%) of that mean. In the other sectors, mean values fell off rapidly with range, and the scatter of ratio values increased more markedly with range. The pattern of deterioration was found to be related to the distribution of topographic obstructions around the radar site, and to systematic deviations from programmed angles of elevation of the radar antenna, caused by a non-vertical axis of rotation. Measurements, comparable in quality to those at short range, were obtained in sectors where the elevation of the radar beam was one-half beamwidth ($\frac{1}{2}^\circ$, in this case), or more, above the elevation of topographic obstructions. Progressive deterioration in the quality of the measurements occurred at lower elevation angles.

The variation with time of gauge-measured snowfall rates at a point can be determined from radar observations along the trajectory of the snow falling toward that point. Comparison of radar and gauge measurements, with a lag corresponding to the fall-time of the snow from the height of radar observation to the ground, showed this. The results obtained in the above comparison suggest that smaller intervals between snowfall-rate thresholds (factor 3 in R, or 10 db in radar-signal power, in this case) are needed to improve the resolution of higher snowfall rates. Arithmetic, rather than geometric spacing of thresholds should be considered for radar observations of snow.

Under the assumption that the relationship $Z = 2000 R^{2.0}$ was applicable at greater heights, amounts of snow that fell through successive 5000-ft layers were calculated in order to bring out information about the growth of snow with distance fallen. Ninety-eight percent of the snow that reached 5000 ft was produced below 20 000 ft, 90 to 65% below 15 000 ft, and 10 to 35% in the layer from 10 to 5 thousand feet.

The duration of snow exceeding each radar threshold (or related snowfall-rate threshold) tended to decay exponentially with increasing threshold value at heights 5 and 10 thousand feet. Durations of snow exceeding a given threshold decreased markedly with height, especially at heights above 10 000 ft. Snowfall rates exceeding 9 mmw h^{-1} were not observed during this storm.

Further studies of other snowstorms are required: (a) to determine the consistency of the correlation between radar measurements at low heights and measurements at the ground, (b) to examine the spatial and temporal pattern of snow growth in relation to other meteorological parameters.

REFERENCES

- Atlas, D., 1964: Advances in Radar Meteorology. Advances in Geophysics 10 317-478. Academic Press, Inc., New York.
- Atlas, D., and V.G. Plank, 1953: Drop size history in a shower. J. Meteorol. 10, 291-295.
- Austin, P.M., 1963: Radar Measurements of the Distribution of Precipitation in New England Storms. Proc. 10th Conf. on Radar Meteorol. American Meteorological Society, Boston, Mass.
- Battan, L.J., 1959: Radar Meteorology. Univ. of Chicago Press, Chicago, Illinois.
- Carlson, P.E., 1968: Measurement of Snowfall by Radar. Proc. 13th Conf. on Radar Meteorol., 384-387, American Meteorological Society, Boston, Mass.
- East, T.W.R., 1958: Electronic Constant Altitude Plan Position Indicator for Weather Radar. Scientific Report MW-28, Stormy Weather Group, McGill University, Montreal, Canada.
- Gunn, K.L.S., 1965: Measurements on New-fallen Snow. Scientific Report MW-44, Stormy Weather Group, McGill University, Montreal, Canada.
- Gunn, K.L.S., P.E. Carlson and L. Feldman, 1966: Distribution of Snow with Intensity as a Function of Height. Proc. 12th Conf. on Radar Meteorol., 241-244. American Meteorological Society, Boston, Mass.
- Gunn, K.L.S. and T.W.R. East, 1954: The Microwave Properties of Precipitation Particles. Quart. J. Roy. Meteorol. Soc. 80, 522-545.
- Gunn, K.L.S. and J.S. Marshall, 1955: The Effect of Wind Shear on Falling Precipitation. J. Meteorol. 12 (4), 339-349.
- Gunn, K.L.S. and J.S. Marshall, 1958: The Distribution with Size of Aggregate Snowflakes. J. Meteorol. 15 (5), 452-461.

- Gunn, R. and G.D. Kinzer, 1949: The Terminal Velocity of Fall for Water Droplets in Stagnant Air. *J. Meteorol.* 6, 243-248.
- Huff, F.A., 1966: The Adjustment of Radar Estimates of Storm Mean Rainfall with Raingauge Data. *Proc. 12th Conf. on Radar Meteorol.*, 198-203. American Meteorological Society, Boston, Mass.
- Imai, I., M. Fujiwara, I. Ichimura, and Y. Toyama, 1955: Radar Reflectivity of Falling Snow. *Pap. in Meteor. and Geophys. (Japan)* 6 (2), 130-139.
- Jones, D.M.A., 1966: The Correlation of Raingauge-Network and Radar-Detected Rainfall. *Proc. 12th Conf. on Radar Meteorol.*, 204-207, American Meteorological Society, Boston, Mass.
- Kodaira, N. and M. Inaba, 1955: Measurement of Snowfall Intensity by Radar. *Pap. in Meteorol. and Geophys. (Japan)* 6 (2), 126-129.
- Langille, R.C. and R.S. Thain, 1951: Some Quantitative Measurements of Three Centimeter Radar Echoes from Falling Snow. *Canadian J. Phys.* 29, 482.
- Langleben, M.P., 1954: The Terminal Velocity of Snow Aggregates. *Quart. J. Roy. Meteorol. Soc.* 80, 174-181.
- Leber, G.W., C.J. Merritt, and J.P. Robertson, 1961: WSR-57 Analysis of Heavy Rains. *Proc. 9th Weather Radar Conf.*, 397-402. American Meteorological Society, Boston, Mass.
- Legg, T.H., 1960: The Quantitative Display of Radar Weather Patterns on a Scale of Grey. *Scientific Report MW-31*, Stormy Weather Group, McGill University, Montreal, Canada.
- Marshall, J.S., 1953: Precipitation trajectories and patterns. *J. Meteorol.* 10 (1), 25-29.

- Marshall, J.S. and W.M.K. Palmer, 1948: The Distribution of Raindrops with Size. *J. Meteorol.* 5 (4), 165-166.
- Ohtake, T., 1968: Change of Size Distribution of Hydrometeors through a Melting Layer. *Proc. 13th Conf. on Radar Meteorol.*, 148-153. American Meteorological Society, Boston, Mass.
- Warner, C., and K.L.S. Gunn, 1967: Measurement of Snowfall by Optical Attenuation. Research Report MW-51, Stormy Weather Group, McGill University, Montreal, Canada.
- Wein, M., 1965: Facsimile and Areal Integration for Weather Radar. Scientific Report MW-40, Stormy Weather Group, McGill University, Montreal, Canada.
- Wilson, J.W., 1963: Relationship between gage-measured precipitation rates and radar-echo intensities. *Proc. 10th Conf. on Radar Meteorol.*, 241-246, American Meteorological Society, Boston, Mass.

Appendix 1 - CPS-9 radar and CAPPI display system¹

The radar and display system operate in the following manner (Fig. A1). As the radar scans in azimuth, it proceeds through a 3 3/4-minute cycle of stepped elevations. Thresholded radar-signal returns are written radially on a cathode-ray tube (CRT) in a succession of range-gated annular rings. Each ring gives the distribution of detectable precipitation target at one angle of elevation (PPI), over a range interval in which the radar beam is within a pre-selected height interval (CAPPI). Figure A2 shows how CAPPI maps for heights 5, and 15 thousand feet, are built up from such rings, in separate cycles. The actual synthesis of each CAPPI map is made on a frame of film in the camera, which is exposed for 3 3/4 minutes during one cycle. Six CAPPI maps at six heights (5, 10, 15, 20, 25, and 30 thousand feet) are produced every 22.5 minutes (6 x 3 3/4 minutes).

At the end of each 3 3/4-minute cycle, the exposed frame advances into a rapid-access processor and is processed while radar returns for the next CAPPI frame are written on the CRT and photographed. At the end of that cycle the just-developed frame advances to the gate of a scanner. For the next 3 3/4 minutes a flying spot of uniform brightness, generated in a

¹The present work, which is based on the output of this radar system, analyses two aspects of one major snowstorm, i.e. correlation of low-level radar returns with snowfall measurements at the ground, and variation of radar returns with height. Both aspects were completed some time ago (Gunn, Carlson, and Feldman, 1966; Carlson, 1968). There were unsatisfactory aspects, however: (a) an unnatural decrease of sensitivity with range, (b) an unreasonably large exponent, b , in the relation $Z = ar^b$. These led the author late in 1968 to reconsider the data and the radar system from which they came. Two specific faults were uncovered in the system (Appendix 1, and Section 4.5), and have been avoided in a complete re-analysis of the data. Happily, the value of b (in $Z = ar^b$) has come back to 2.0 and the behaviour with range has been rationalized.

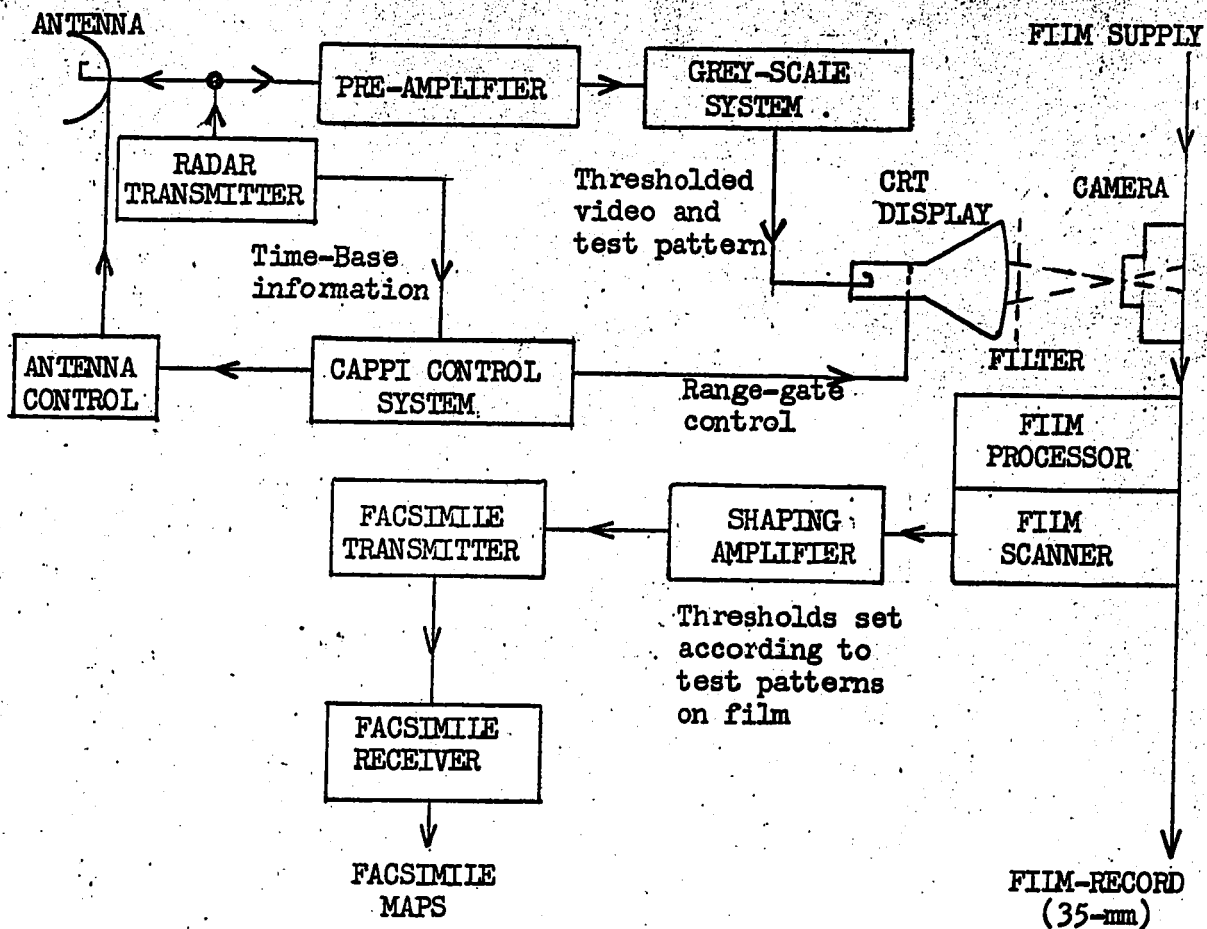


Figure A1. Block diagram of radar and CAPPI display system.

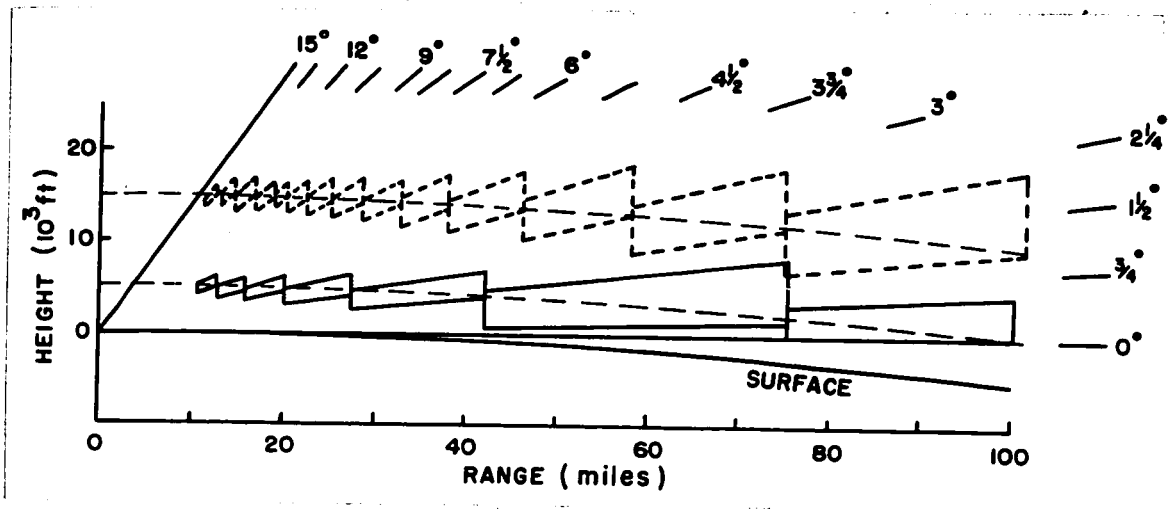


Figure A2. Programmed elevation angles, and range gates for 5000-ft (solid) and 15 000-ft (dashed) CAPPI maps.

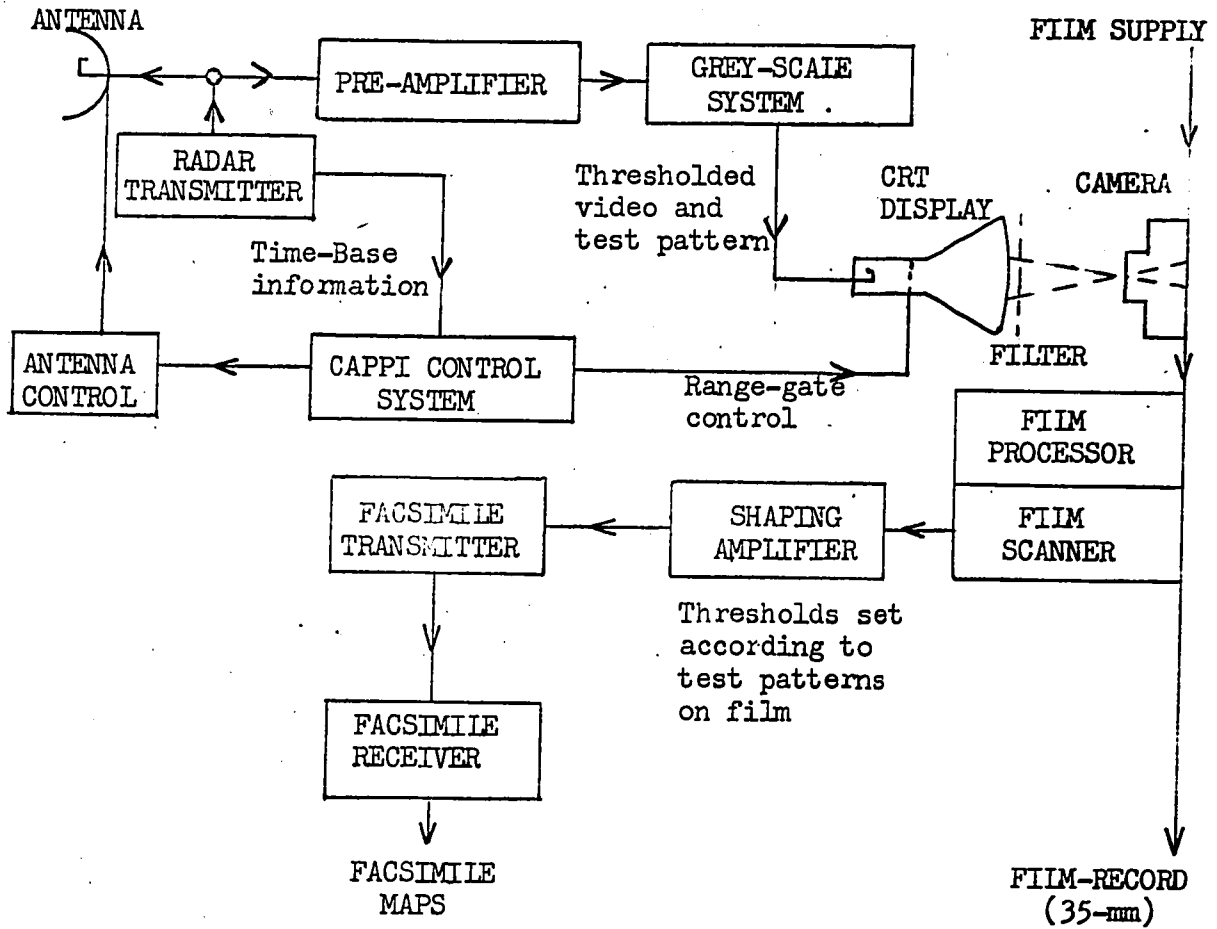


Figure A1. Block diagram of radar and CAPPI display system.

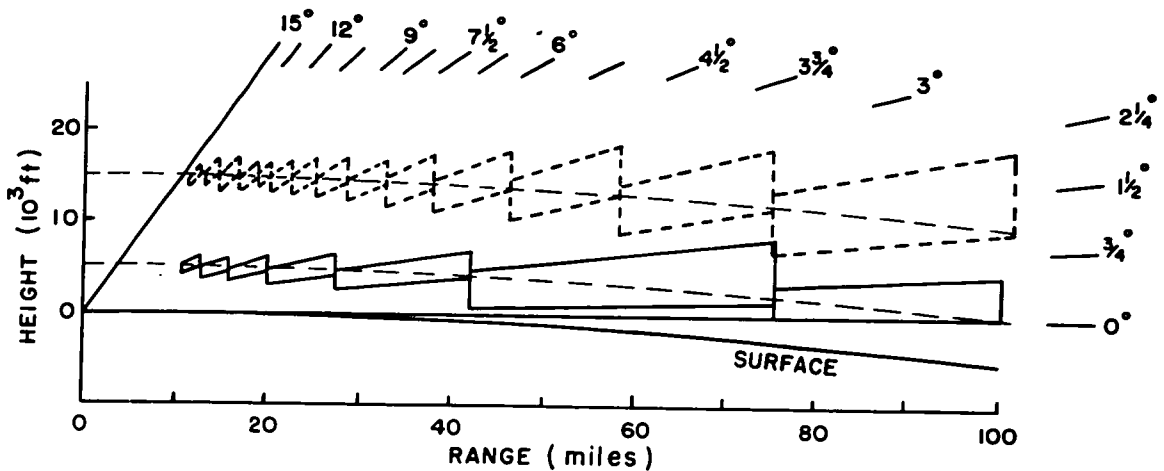


Figure A2. Programmed elevation angles, and range gates for 5000-ft (solid) and 15 000-ft (dashed) CAPPI maps.

rectangular raster on another CRT, makes one slow scan of the frame. The variable amount of light transmitted through the image on the film is focussed onto a photomultiplier. The modulated output of the photomultiplier passes through a shaping amplifier, after which the thresholded output is converted to a signal suitable for facsimile transmission. Each facsimile map is received over a $3\frac{3}{4}$ -minute period in synchronism with the slow scan of the CAPPI frame.

Facsimile maps are available for operational purposes during the event, with a lag of $7\frac{1}{2}$ minutes between completion of observations at a given CAPPI height and completion of the corresponding facsimile map. Available for research after the event are (a) the facsimile maps, and (b) the rapid-access film record from which the facsimile maps were derived.

Radial-writing lines of uniform brightness on the CRT actually produce density on the film that varies with radial distance (range), because luminance (lumens per unit area) decreases with radial distance as the overlap of writing lines decreases. A variable-density filter, on which the fraction of light transmitted increases linearly with radial distance, is mounted on the face of the display CRT to compensate for this effect; the objective being that uniform signal (written radially) should produce uniform density on the film at all ranges.

Uniform response of the display system to a uniform input signal is essential for quantitative interpretation of the thresholded data on CAPPI maps; especially as 6 thresholds, at intervals of 10 db in radar-signal power, are recorded as 6 grey shades, at intervals of 1.0 to 1.5 db in film density. Relatively small variations in film density will, after scanning, result in relatively large variations of apparent radar-signal power on the facsimile maps. Further, small variations in the performance of the scanner also will produce relatively large variations of apparent radar-signal power on the facsimile maps.

Recent tests of the rapid-access display system

The response of the rapid-access display system to uniform test signals was checked in 1968 by R.W. Shaw (meteorologist), M. Claassen (radar technician), and the present author.

Uniform signals corresponding to several levels of radar-signal power were simulated and written radially out to a distance corresponding to 140-miles range. A variable-density filter was mounted on the face of the CRT, as in normal operations, because the patterns were written radially. The uniform test-signals that were used correspond to four levels of radar signal ranging from thresholds 1 to 3 in the normal operation of the display system.

Measurements of density were made on the resulting frames of film at 1-mm intervals (equivalent to 20-mile range intervals) along bearings corresponding to north, south, east, and west in normal operations. Values of film density are plotted on Figure A3 for each of the test-signals. Disregarding the anomalies within 20-miles range for a moment, the data from 20 to 140 miles are fitted by straight lines with slopes that range from 1.1 db (film density) per 100 miles, for the test-signal corresponding to threshold 1, to 1.8 db per 100 miles, for that corresponding to threshold 3. Deviations of data points from the fitted lines are small, therefore the lines may be considered as radial profiles of film density on two-dimensional mappings. Considering that each 1-db step in film density usually corresponds to a 10-db step in radar-signal power in normal operations, the above slopes would indicate 11 db and 18 db reductions in apparent radar-signal power between 20 and 120 miles range on the facsimile maps.

At short range, film density drops sharply from range 20 miles, to a minimum at approximately 10 miles, then rises to a maximum at zero range. These variations probably are attributable to the combined effects of a

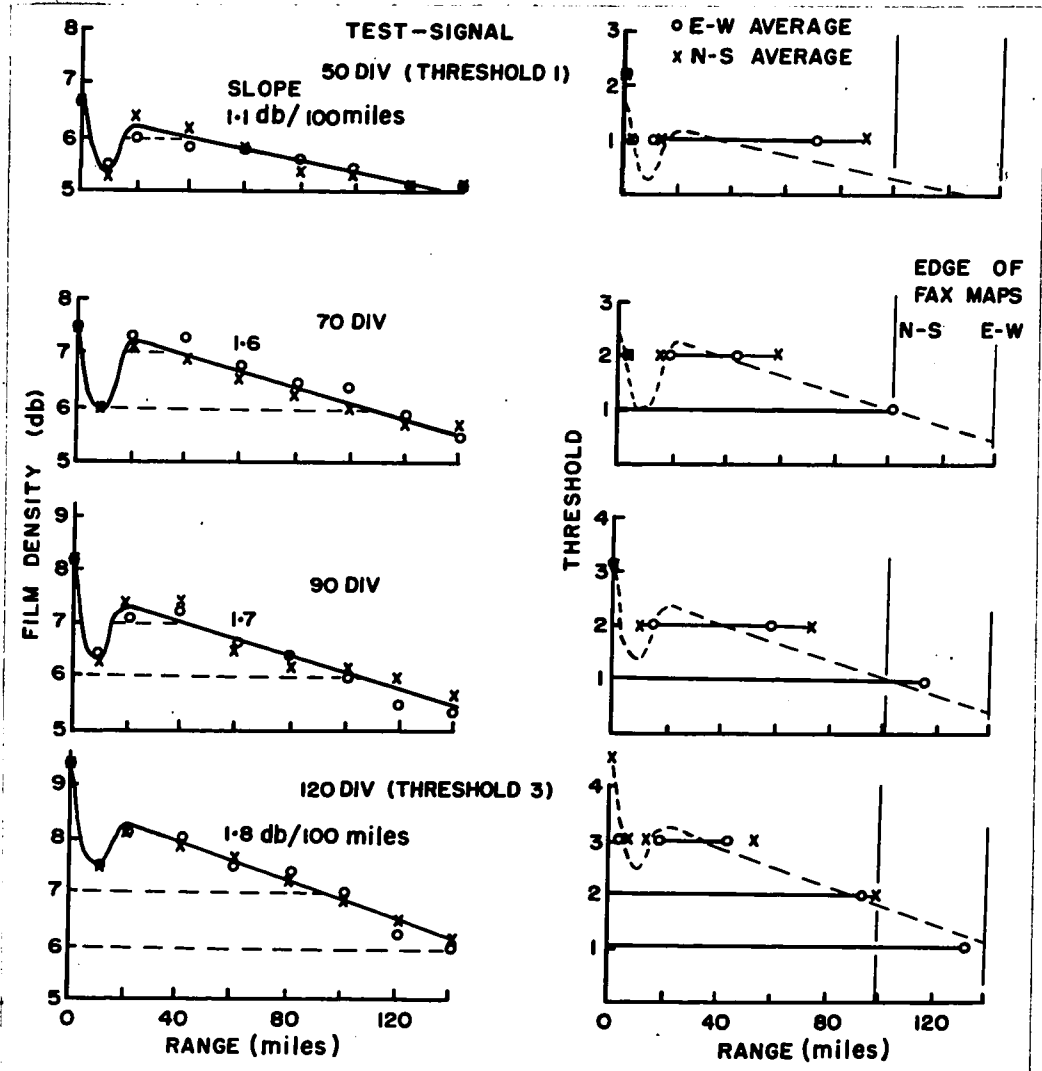


Fig. A3. Variation of film density with range on frames resulting from uniform-signal tests.

Fig. A4. Radial distance (range) to indicated thresholds on facsimile maps, produced by scanning test-frames of Fig. A3.

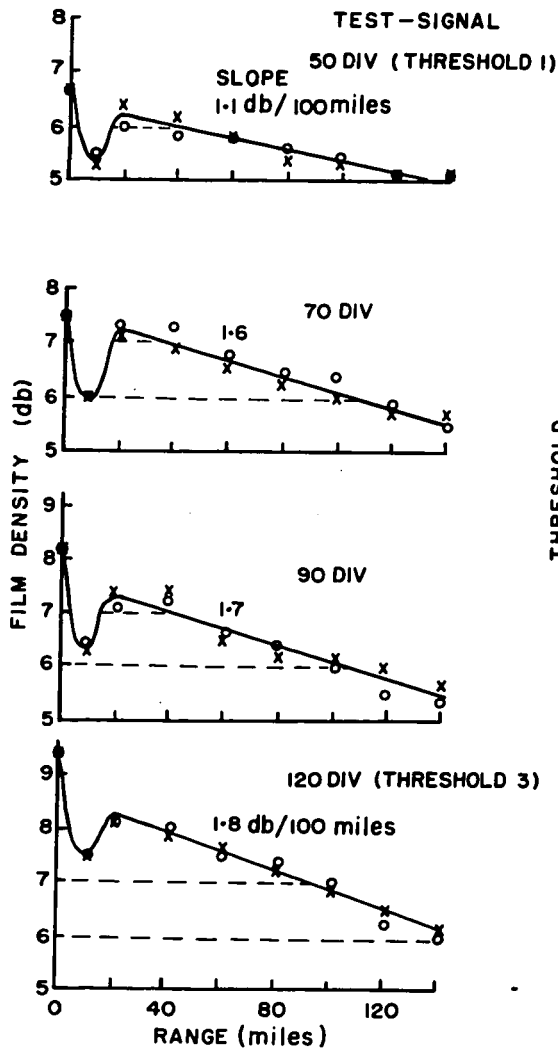


Fig. A3. Variation of film density with range on frames resulting from uniform-signal tests.

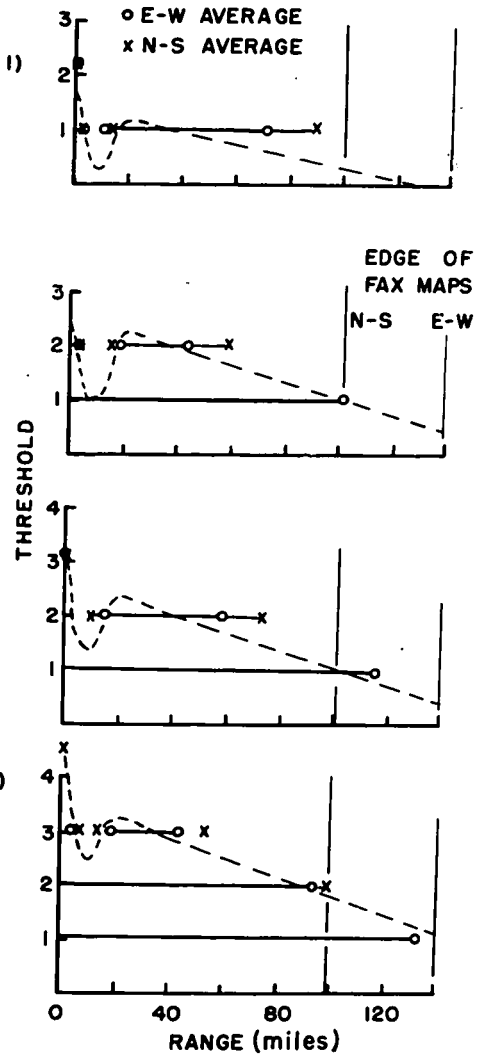


Fig. A4. Radial distance (range) to indicated thresholds on facsimile maps, produced by scanning test-frames of Fig. A3.

burned and weakened phosphor near the centre of the CRT, and a low-density hole in the dense central portion of the compensating filter.

The above test-frames were scanned to produce facsimile "maps". Because of the variation of density with range on the film, the resulting "maps" contained 1, 2, or 3 thresholds in radially-symmetric patterns. The distance (range) to each threshold was measured on these maps along the same bearings as were the film densities of Figure A3. These ranges are plotted on Figure A4. Ordinate scales of Figures A3 and A4 have been matched as closely as possible and the profiles of film density are repeated on Figure A4. Positions of thresholds on the facsimile maps are sufficiently close to positions of threshold values of density on the film profiles to suggest that the scanner was performing satisfactorily.

Non-uniformities in the response of the display system have the effect of systematically altering the sensitivity of the combined radar and display system. Minimum-detectable signal, and therefore minimum-detectable precipitation rate, become functions of range or position on the film and facsimile output of the display system.

Archival and rapid-access film records

Operation of another CRT display and another camera during 1963-64 had provided an archival film record, which involved normal rather than rapid-access processing, complementary to that produced by the rapid-access display system. As reported in Chapter 3, the present work is based on facsimile maps which were produced by scanning the archival film record for this snowstorm, although early work had been based on CAPPI maps produced from the rapid-access film record.

At intervals during 1963-64, a uniform signal of known amplitude had been fed into the display system for one CAPPI frame. During these tests the cathode currents of the respective CRT's were measured and, if required, small adjustments were made to restore the cathode current to a specified value for each CRT. Although the resulting test frames in the film records were not produced for this specific purpose, they do provide a way of assessing the performance of each CRT, in combination with its variable-density filter and camera, at the time each test was made.

Patterns on facsimile maps that resulted from a series of cathode-current tests showed that there had been a sudden change in the performance of the rapid-access display system in January 1964, about a month before the snowstorm under study. Prior to that time the test-maps showed that the non-uniformities in the rapid-access display tended to be radially symmetric, much the same as those depicted in Figure A3 and A4. After that time the test-maps showed consistent asymmetries, which apparently resulted from a displacement of the variable-density filter in such a way that the dense central portion of the filter was no longer centred on the radial-writing pattern of the CRT. The range of variation across the asymmetrical pattern was approximately 3 db in film density, which produced a variation of 30 db in apparent radar-signal power on the resulting facsimile maps.

The response of the display system (CRT, variable-density filter, and camera) which had produced the archival film record was more uniform than that of the rapid-access system. The sudden change in January to an asymmetric condition did not apply to the archival system. Test-frames from cathode-current tests showed this. In addition, successive thresholds in the test patterns were separated by 1.3 to 1.5 db in film density, as compared to one db on the rapid-access film record. Accordingly, the archival film record of this snowstorm was scanned to produce a set of facsimile maps for this study.

Correction for non-uniform response of the display

Figure A5 shows a mapping of the correction field that was applied to the radar data of this study to compensate for non-uniformities in the response of the display system. Because the facsimile maps were produced by scanning the archival film record five years after the event, non-uniformities at two different stages and times were involved. Two frames that resulted from cathode-current tests on 6 February 1964 provided a record of the response of the display (CRT, filter, and camera) at that time, in the form of density variations across the test-frames. The performance of the scanner at the later date was also taken into account by scanning these test-frames to produce facsimile "maps", which were used to generate the correction field of Figure A5. In order to obtain better resolution of the combined pattern of non-uniformities, the voltage-steps between thresholds (in the output of the scanner) were reduced by a factor 5. Thus successive thresholds on the resulting facsimile "maps" were separated by 2 db in apparent radar-signal power, rather than 10 db, as was the case in scanning the remainder of the archival film record. Figure A6 shows a facsimile map that was obtained from a high-resolution scan (i.e. with closely-spaced thresholds) of one of the test-frames. Three of the high-resolution thresholds (1', 3', and 5') appear, while thresholds 2', 4', and 6' appear on a partner map. Grid-point data extracted from these maps were converted to correction factors for application to CAPPI data at individual grid points. The correction factor, expressed in radar-signal power, ranged from +4 db at a few points near the centre of the map to -6 db at long range in the northwest quadrant.

The closely-spaced thresholds, described above, were also used to test the performance of the scanner by scanning a "clear" gate, i.e. by operating the scanner with no film in the gate. The resulting pair of facsimile "maps" is shown in Figure A7. Although there is no appreciable varia-

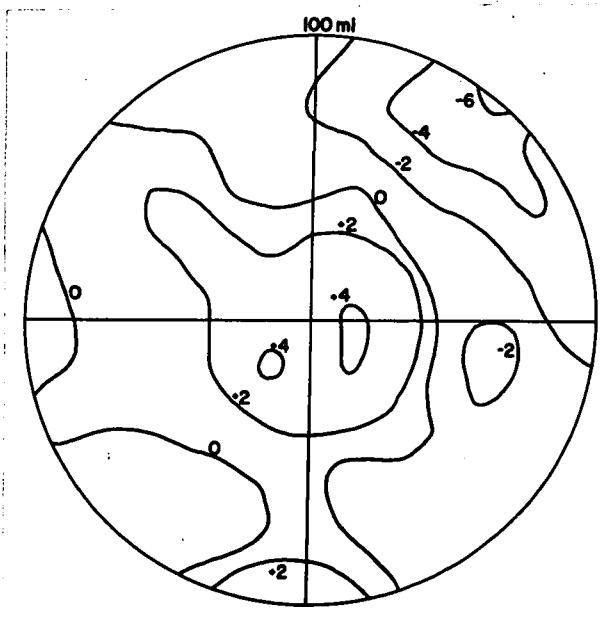


Figure A5. Correction field applied to radar data extracted from facsimile maps used in this study. (expressed in db of apparent radar-signal power).



Figure A6. Facsimile "map" produced by high-resolution scan of test-frame from cathode-current test of 6 February 1964. Thresholds 1', 3', 5' appear.

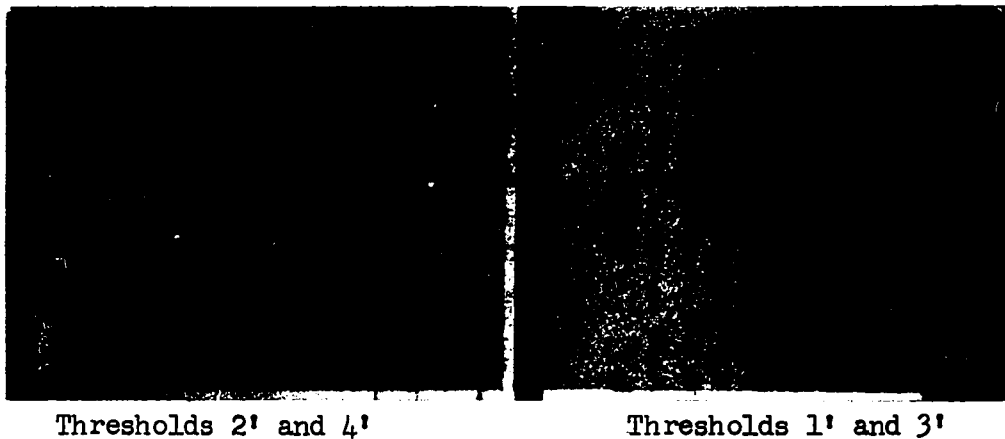


Figure A7. Facsimile "maps" ($\frac{1}{2}$ scale) produced during "clear" gate scan with high-resolution thresholds.

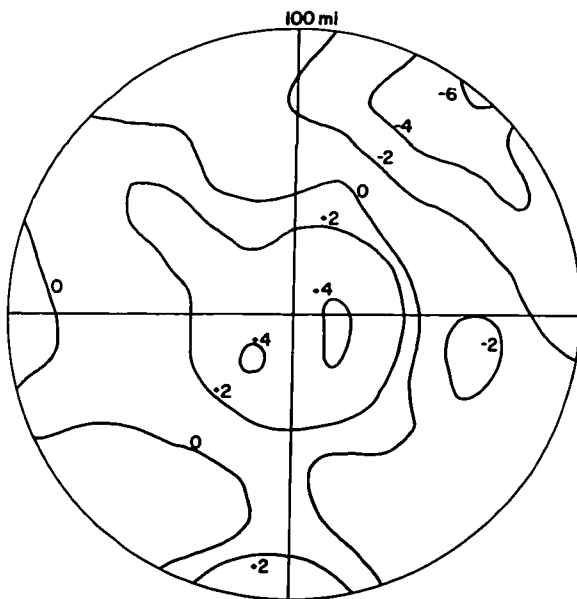


Figure A5. Correction field applied to radar data extracted from facsimile maps used in this study. (expressed in db of apparent radar-signal power).

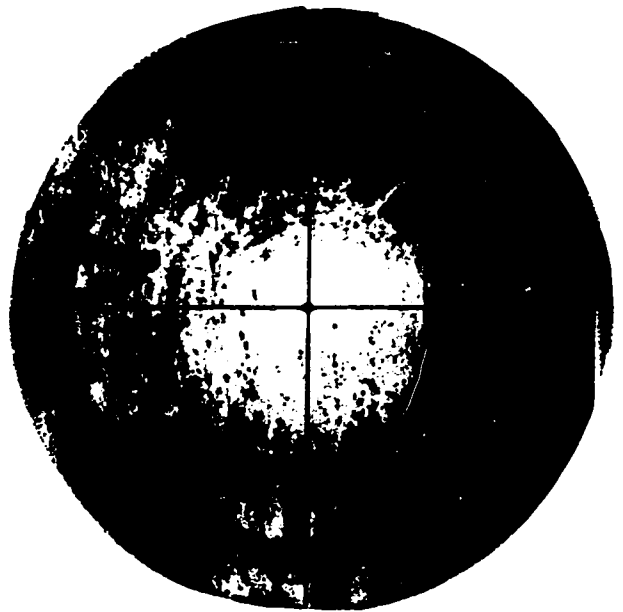


Figure A6. Facsimile "map" produced by high-resolution scan of test-frame from cathode-current test of 6 February 1964. Thresholds 1', 3', 5' appear.



Thresholds 2' and 4'



Thresholds 1' and 3'

Figure A7. Facsimile "maps" ($\frac{1}{2}$ scale) produced during "clear" gate scan with high-resolution thresholds.

tion from "north to south", the gradual variation from "west to east" corresponds to two of the high-resolution threshold steps, or 4 db in apparent radar-signal power on the facsimile maps. This variation is probably due to the electronics of the CRT on which the flying spot is generated in a rectangular raster. The ripples in the pattern appear to be related to undesirable 60-cycle modulation either in the scanner circuits, or in the facsimile system.

Appendix 2 - Effect of Shearing Winds on Falling Snow

Radar data for this storm, as recorded by the rapid-access display system, gave a better correlation between radar-measured and ground-measured amounts of snow when the relationship $Z = 1000 R^{2.67}$, rather than $Z = 2000 R^{2.0}$, was used. Later, it was found that the need for this change, particularly the change in the value of the exponent, was related to systematic non-uniformities within the rapid-access display system (Appendix 1). Prior to that finding, the need for changing the Z-R relationship was examined in terms of the effects of shearing winds on snow as it falls from heights at which radar observations are taken to the ground.

Gunn and Marshall (1955) found reason to expect a variation of Z-R relationship with height, for rain falling through shearing winds. They suggested that ground observations scattered about $Z = 200 R^{1.6}$, may be attributable to another locus aloft, such as $Z = 100 R^{1.8}$. The sense of that variation was such as would inter-relate $Z = 2000 R^{2.0}$ for snow at the ground to $Z = 1000 R^{2.67}$ aloft.

An average distribution with size of aggregate snowflakes (Gunn and Marshall, 1958) was coupled with the generating-cell concept (Marshall, 1953) to see whether the need for a modified Z-R relation in this study might be related to the size-sorting of snowflakes falling through shearing winds. Following the approach of Gunn and Marshall (1955), a pattern of snow generation was assumed to move with the wind at a specified generating height. In the first instance, a "point" generator (i.e., one of extent negligible in comparison with the resulting pattern of falling snow) at height 10 000 ft, was assumed to move with the air at that height while generating snow at a constant rate. This "point" generator is pictured as releasing snow through

a horizontal aperture of area 1 m^2 . At that aperture, and directly above it, a rate of snowfall of 1.1 mmw h^{-1} has been taken, with the Gunn and Marshall size-distribution appropriate to that rate. This is given by: $N_D = N_0 e^{-\Lambda D}$

$$\text{where } N_0 (\text{m}^{-3} \text{ mm}^{-1}) = 3.8 \times 10^3 R^{-0.87},$$

$$\Lambda (\text{cm}^{-1}) = 25.5 R^{-0.48},$$

$$R (\text{mmw h}^{-1}) = 1.1,$$

and D is diameter (cm) of spherical drops formed by melting flakes. Although this size-distribution resulted from measurements taken at the ground, it is introduced at a generating level, following the approach used by Marshall (1953).

Growth and evaporation, aggregation and break-up of snowflakes during their fall have been neglected, in line with the original generating-cell concept in which snow was considered to aggregate in generating cells and then fall with little further change.

Height 10 000 ft was used as the generating level for this storm because the radar records show that most of the snow was generated at heights between 10 000 and 15 000 ft. Estimates of the wind near the ground, and at heights of 5000 and 10 000 ft, were obtained from analyses of surface and upper-air reports for 0000Z 7 February 1964, as on the synoptic and upper-air maps. Interpolation between map heights gives the hodograph of Figure A8.

Figure A9 shows (in plan view) curving trails of snowflakes falling at 0.5 and 1.5 m sec^{-1} through the wind profile given by Figure A8. Mean winds were taken for ten 1000-ft layers between a "point" generator and the ground to obtain this pattern of snow trails. By taking reference axes fixed to the generator (and so fixed to the air at height 10 000 ft),

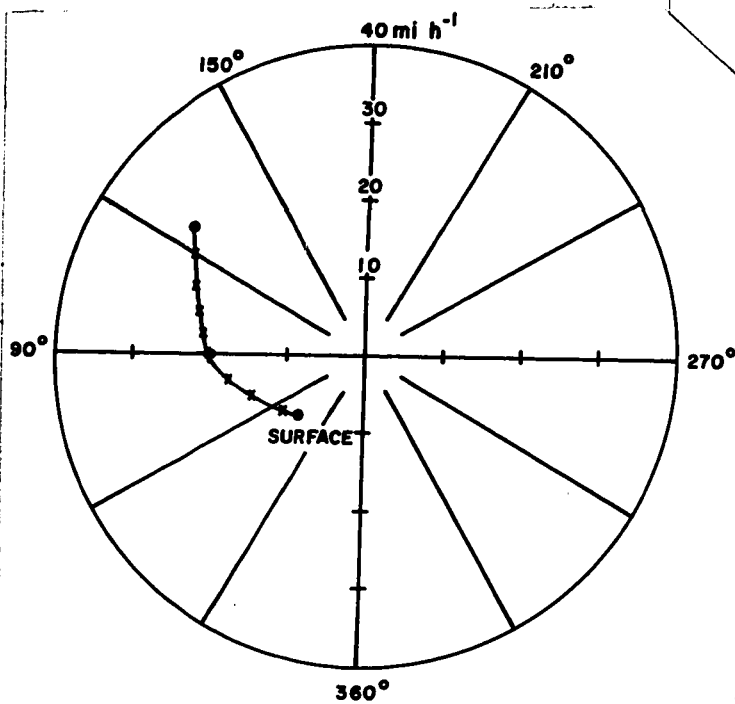


Figure A8. Hodograph derived from analyses of surface and upper-air reports for 0000Z 7 February 1964 (1900EST 6 February)

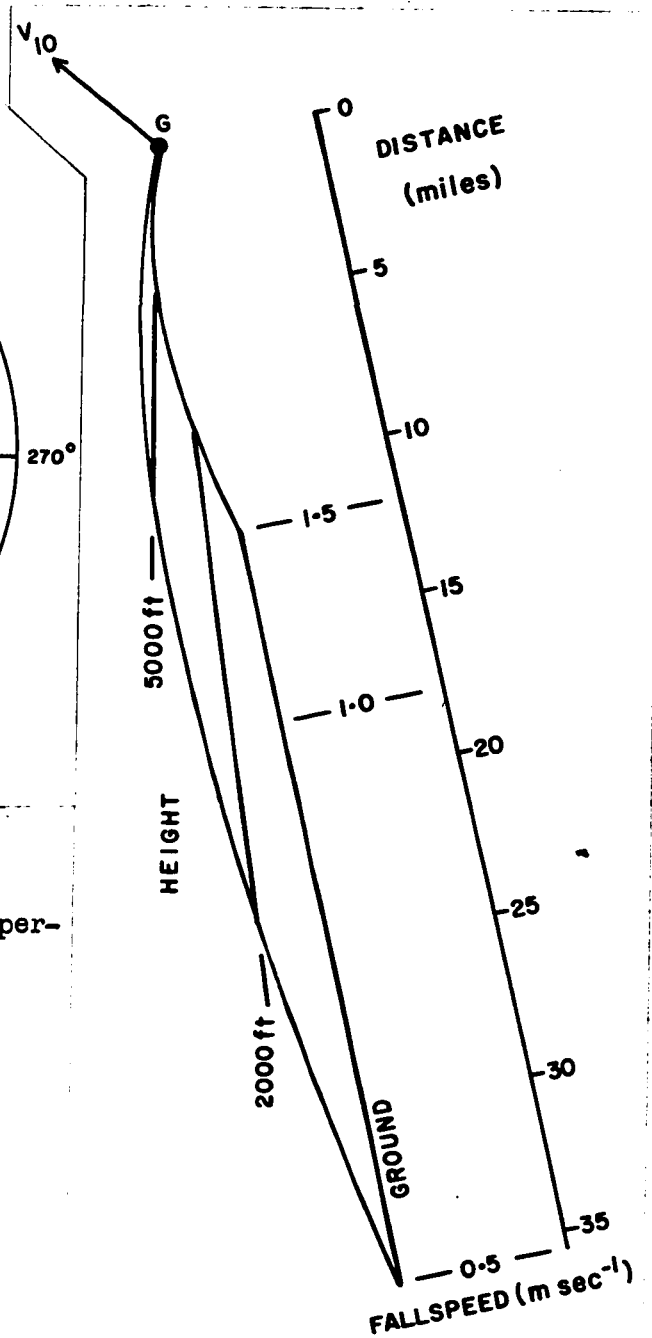


Figure A9. Curving trails of snowflakes falling at indicated speeds through wind field of Figure A8.

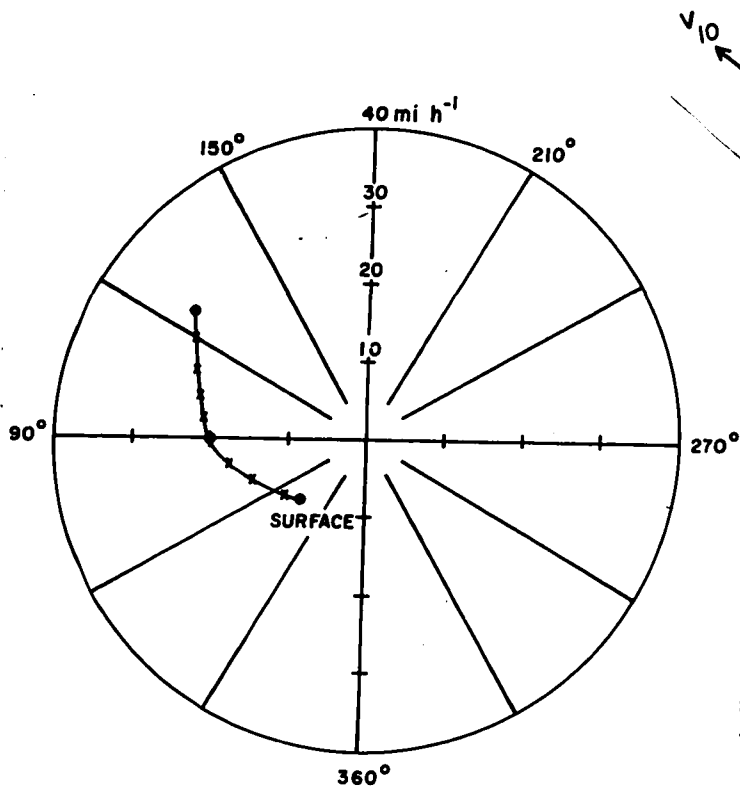


Figure A8. Hodograph derived from analyses of surface and upper-air reports for 0000Z 7 February 1964 (1900EST 6 February)

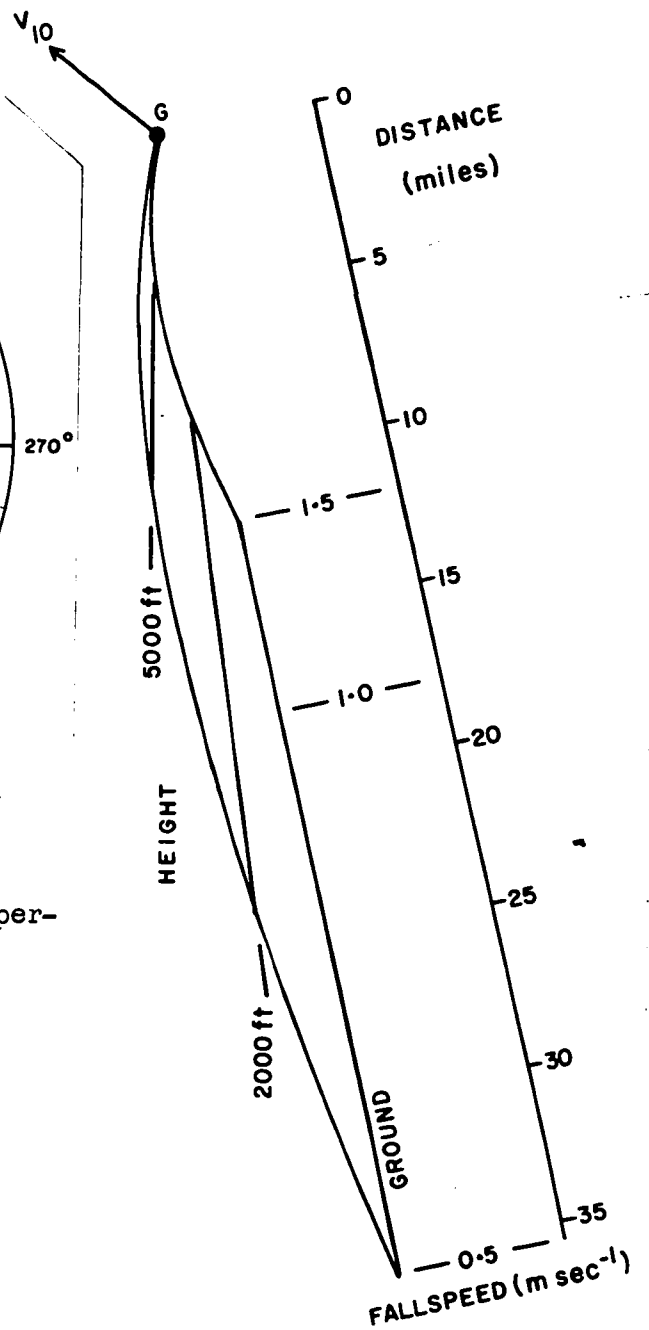


Figure A9. Curving trails of snowflakes falling at indicated speeds through wind field of Figure A8.

the trails become at the same time the trajectories followed by individual flakes having these fallspeeds. At all heights, it was assumed that the horizontal motion of the flakes was the same as that of the air through which they were falling.

For a continuous spectrum of fallspeeds, these trails form a curved sheet. The intercepts of the sheet with horizontal planes are sections of straight lines radiating from the plan position of the generator (G). In Figure A9, the intercepts at heights 5000 ft, 2000 ft and along the ground indicate the horizontal displacement and spread of snowflakes having fallspeeds between 0.5 and 1.5 m sec⁻¹. Along each of these intercepts, the horizontal separation of particular snowflakes from the plan position of the generator varies inversely with fallspeed.

Fallspeed has been related to size of snowflakes by $V(\text{m sec}^{-1}) = 2D^{1/3}$ (Langleben, 1954), where D is diameter (in cm) of spherical drops formed by melting of aggregate snowflakes. In this instance, the relation is assumed to apply at all heights.

Sizes and number densities of snowflakes along intercepts at selected heights below the generator were calculated using the foregoing size-intervals of 0.02 cm in D, taking into account the horizontal spreading due to the difference in fallspeed across each size interval. The sizes and number densities thus obtained were converted to distributions of $Z(\text{mm}^6 \text{ m}^{-3})$ and $R(\text{mmw h}^{-1})$. Figures A10 and A11 show distributions of Z and R, obtained in this manner along the intercepts at height 5000 ft, and at the ground, respectively.

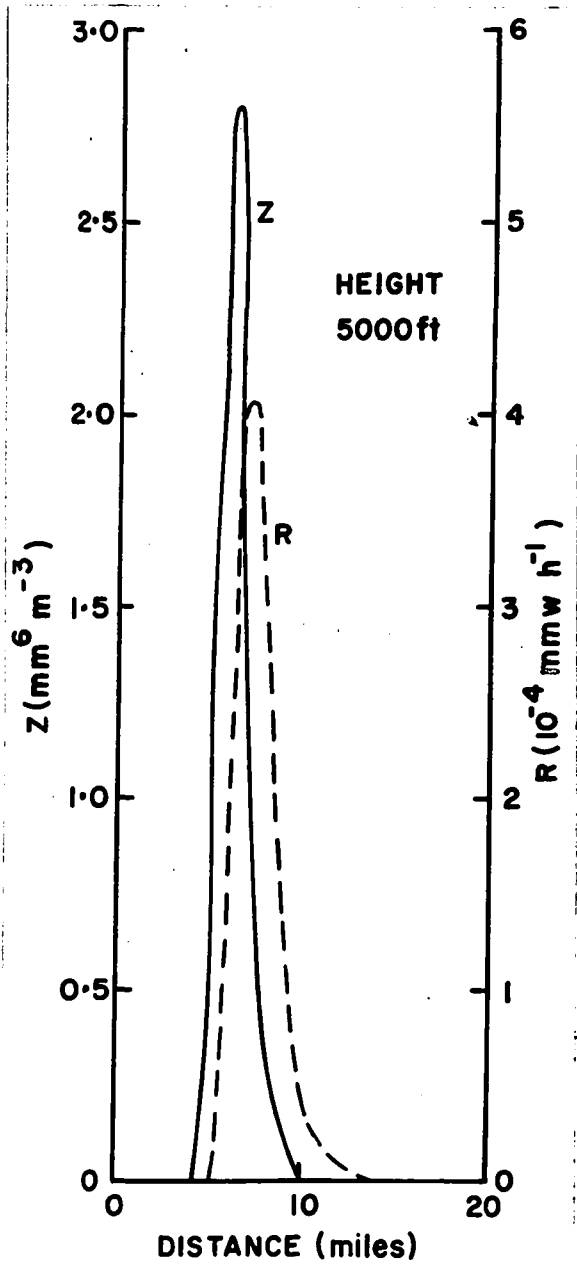
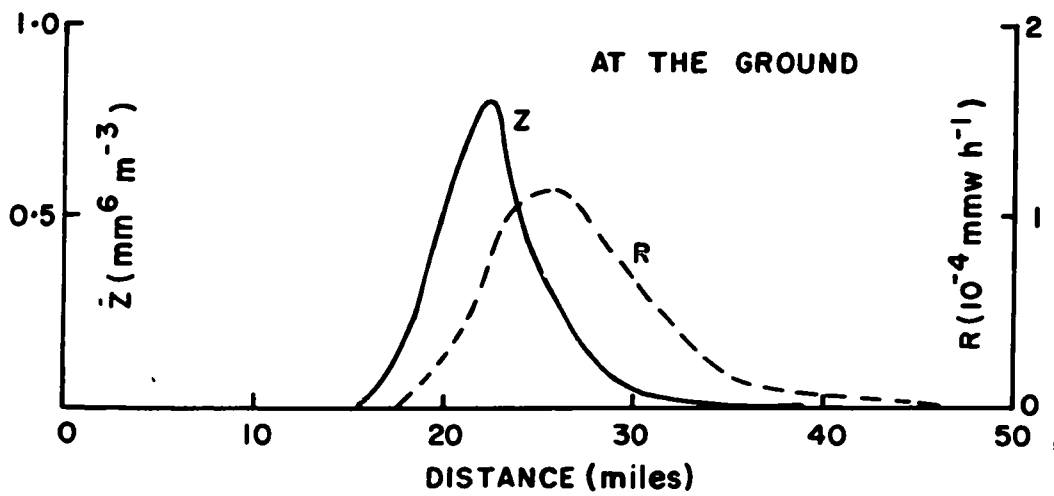


Figure A10. Distribution of Z and R with distance along 5000-ft intercept from plan position of point generator (Fig. A9).

Figure A11 (bottom). As above, for intercept along the ground.



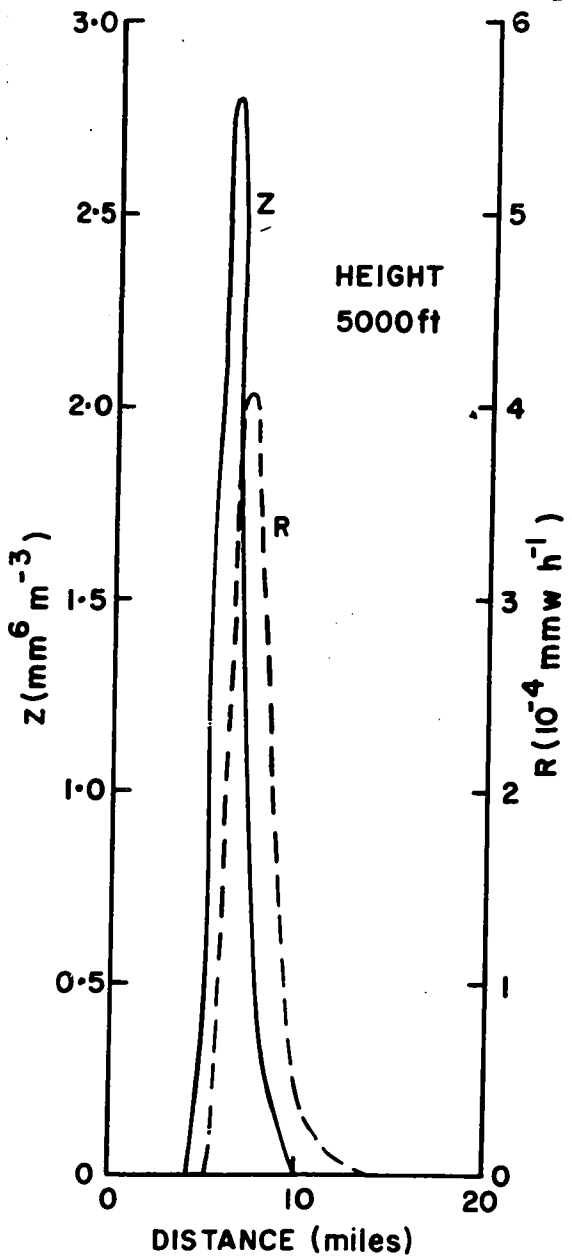
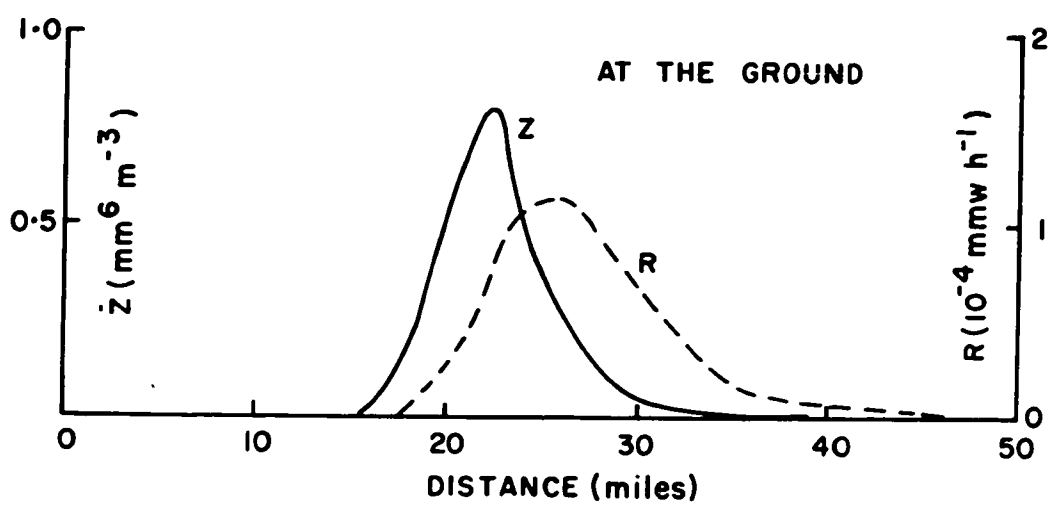


Figure A10. Distribution of Z and R with distance along 5000-ft intercept from plan position of point generator (Fig. A9).

Figure A11 (bottom). As above, for intercept along the ground.



The "point" generator, with its aperture of 1 m^2 , was then extended to deduce the distributions of Z and R below uniform generators of greater horizontal extent. First, the "point" generator was considered to be a 1-metre section of a long "line" generator, 1 metre wide. In this case, the areal pattern of snow at each height forms a parallelogram, in which flakes of each particular fallspeed fall through a strip 1-metre wide, which has the same length as the "line" generator and is oriented parallel to it. Figure A12 shows a rectangular pattern, at the ground, of flakes falling at speeds between 0.5 and 1.5 m sec^{-1} , from a "line" generator oriented at right angles to the intercept along the ground (Figure A9). Each section across this pattern (perpendicular to the line generator) has the same distributions of Z and R as those shown in Figure A11. The distributions of Z and R across the parallelograms at other heights, in this case, and for other orientations of the "line" generator, can be derived from the geometry of each particular situation.

The effect of changing from a "line" generator to rectangular generators of several widths was obtained by integrating under the Z and R curves of Figure A11. The resulting distributions of Z and R, along lines parallelling the intercept at the ground in Figure A9, are shown in Figure A13, for generators of width 0.6, 6, and 21 miles. At width 0.6 miles, all sizes (fallspeeds) of snowflakes in the generator never contribute simultaneously to $Z_{0.6}$ and $R_{0.6}$ at the ground, so the peak values fall short (by an order of magnitude) of the Z and R values in the generator. At width 6 miles, values of Z_6 and R_6 almost achieve the values in the generator over short distances. In each case, the Z and R values increase exponentially with distance along the intercept, and then go through a transition to an exponential decrease. At width 21 miles, values of Z_{21} and R_{21} increase

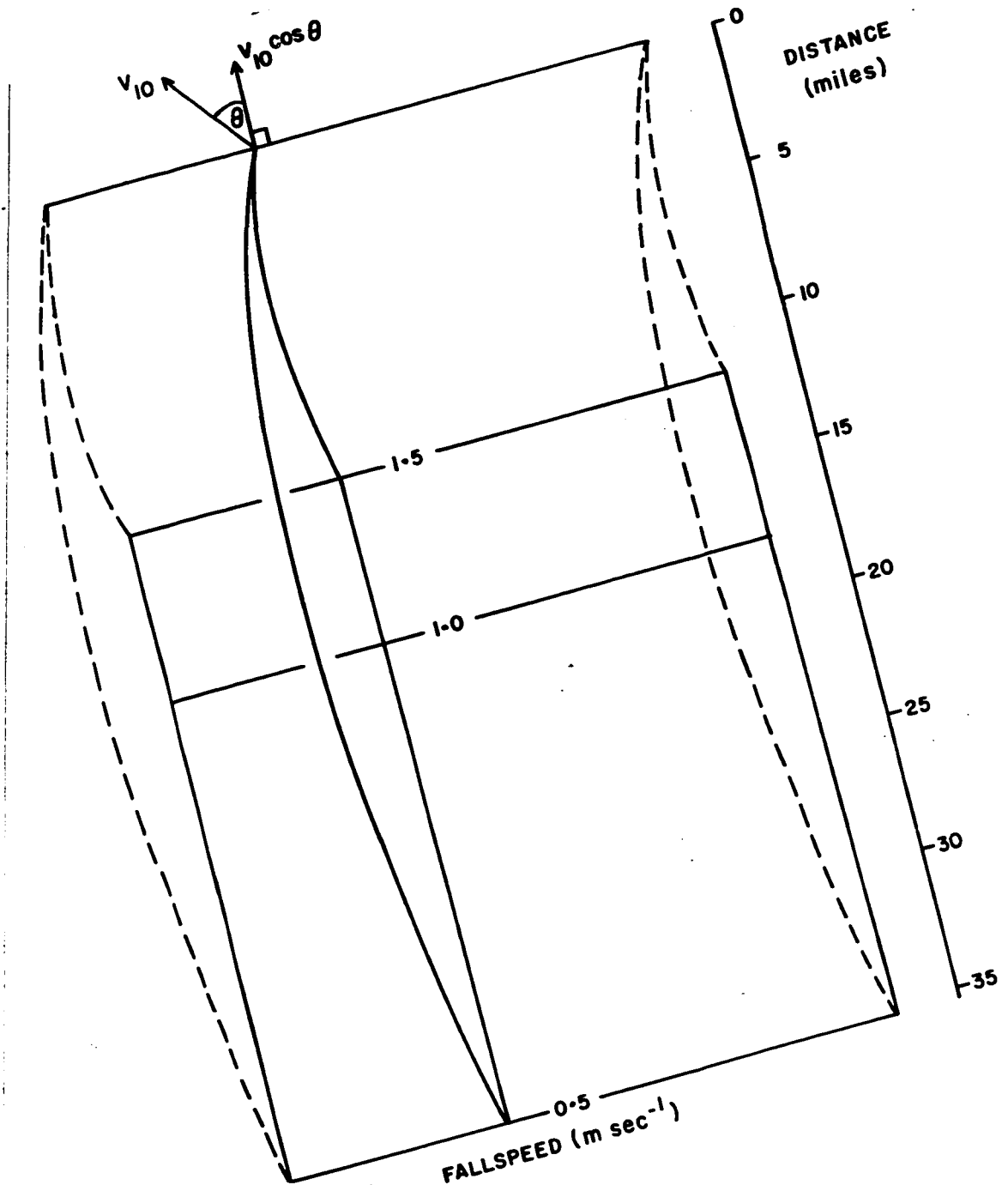


Figure A12. Rectangular pattern at the ground of snowflakes falling at indicated speeds from a "line" generator, and through the wind field of Fig. A8. Generator oriented at right angles to the intercept at the ground (Fig. A9).

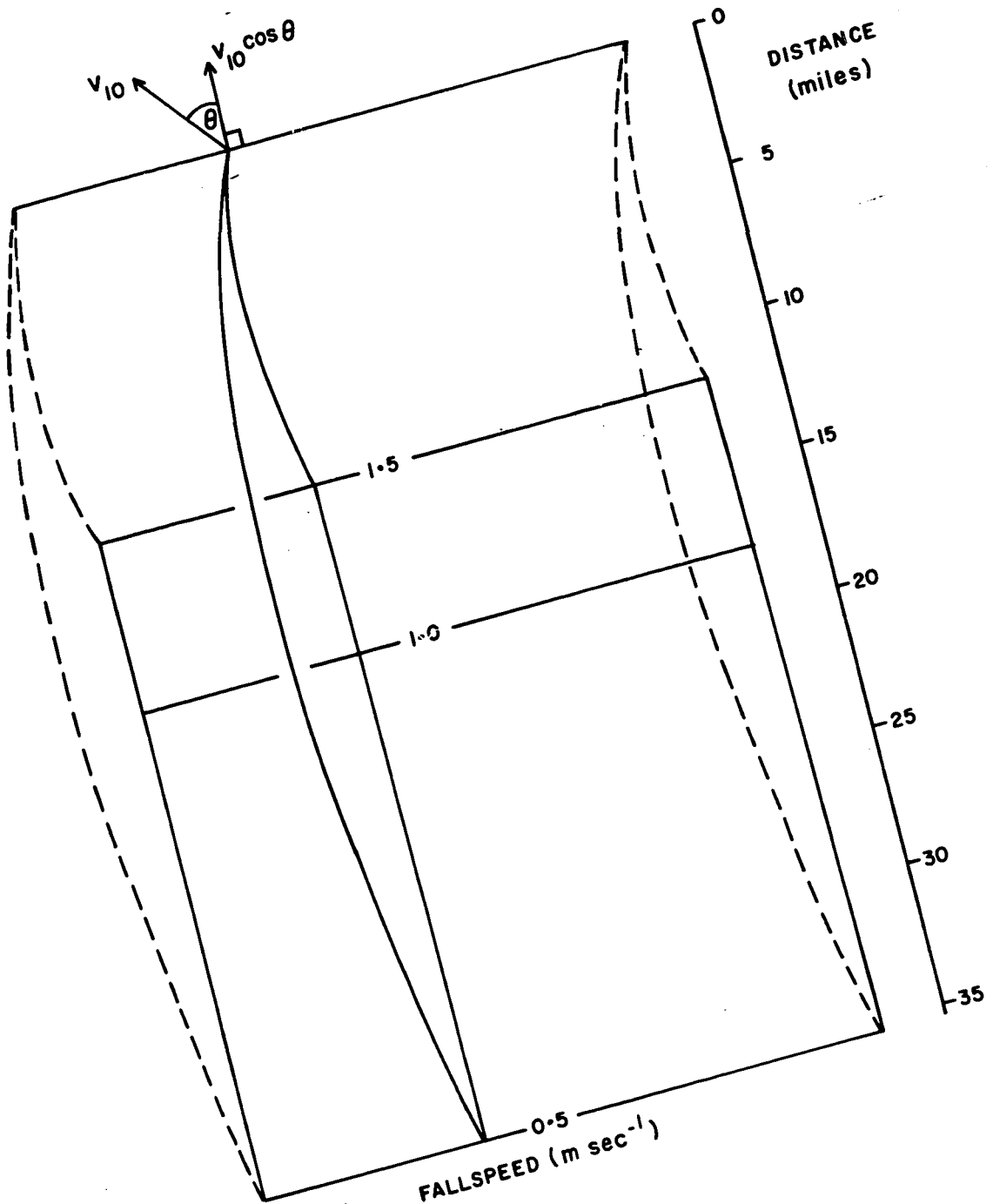


Figure A12. Rectangular pattern at the ground of snowflakes falling at indicated speeds from a "line" generator, and through the wind field of Fig. A8. Generator oriented at right angles to the intercept at the ground (Fig. A9).

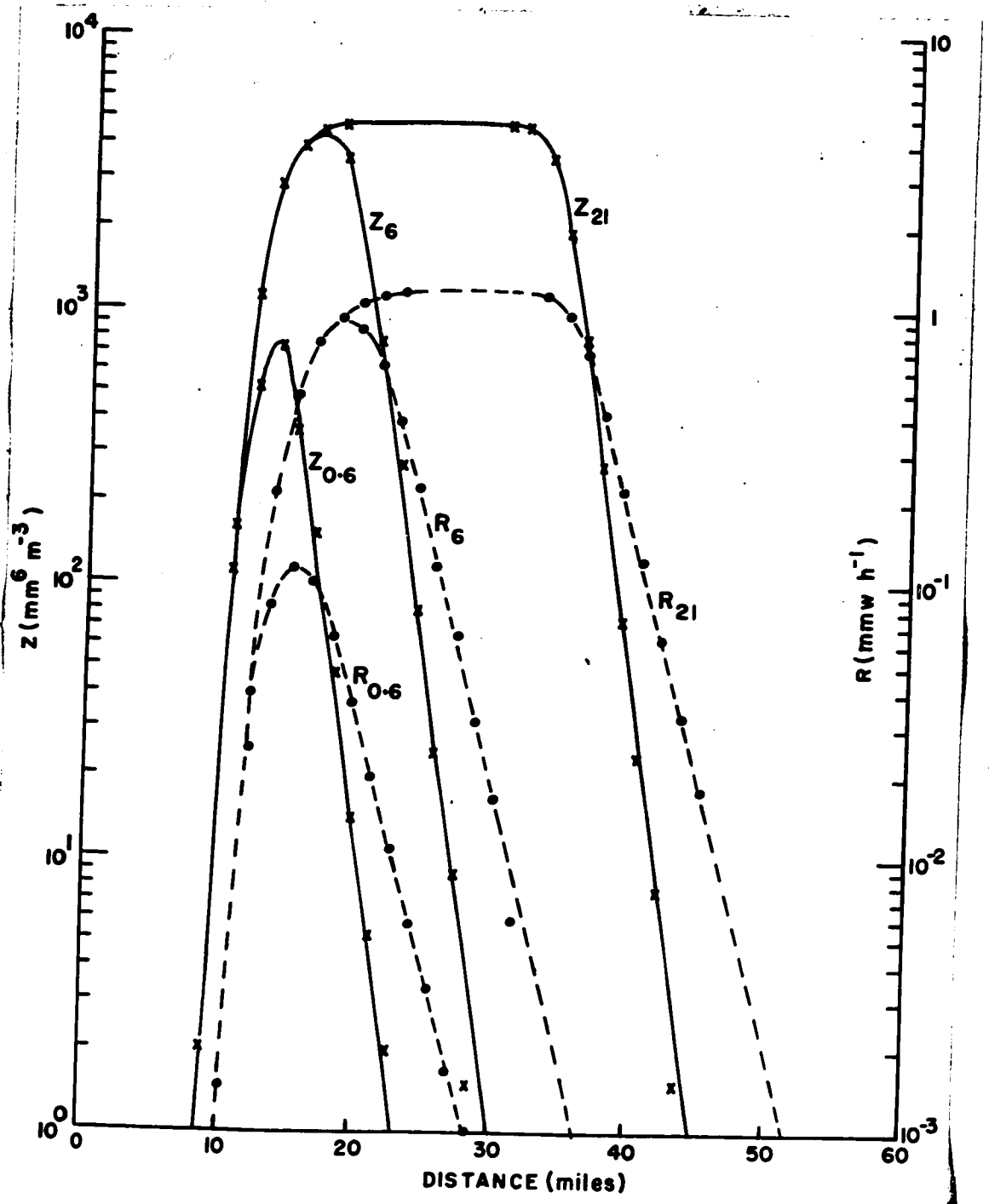


Figure A13. Distribution of Z and R at the ground with distance from plan position of leading edge of rectangular generator, for generator widths 0.6, 6, and 21 miles.

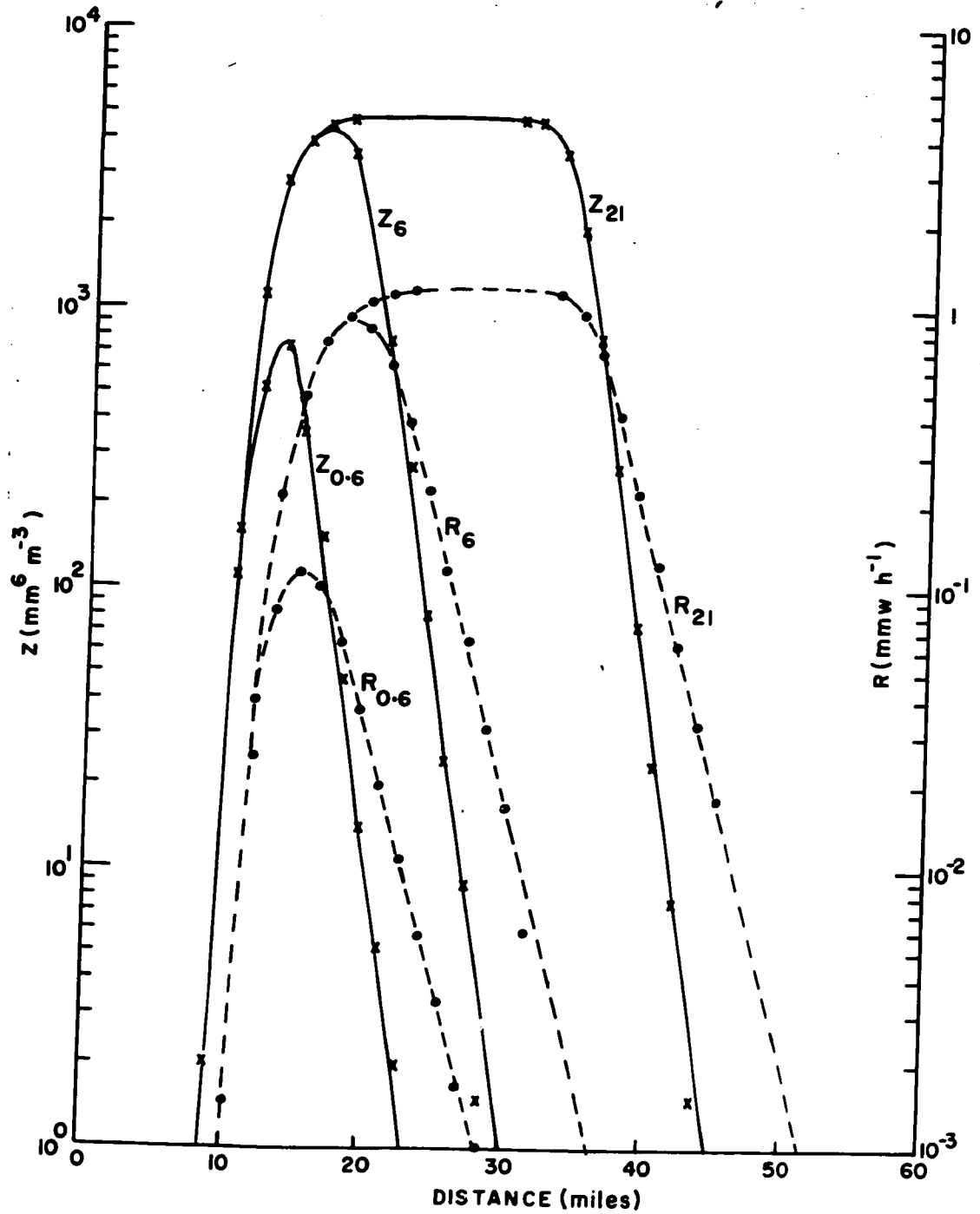


Figure A13. Distribution of Z and R at the ground with distance from plan position of leading edge of rectangular generator, for generator widths 0.6, 6, and 21 miles.

exponentially to plateau values equalling those in the generator, and then decrease exponentially in a region where the contributions of the larger sizes are eliminated progressively as distance from the generator increases. These regions of exponential increase, steady-state, and exponential decrease are labelled "leading edge", "plateau", and "trailing edge". This nomenclature indicates the order in which changes in Z and R values would occur at a fixed point on the ground, as this generator and its associated pattern of falling snow moved by.

How can the data of Figure A13 be interpreted in terms of the measurement of snowfall by radar? Any given value of Z occurs at just two points on the distance scale, once on the leading edge and once on the trailing edge. By plotting log Z against log R for paired values of Z and R taken at intervals along the horizontal axis of Figure A13, one obtains the scatter of Z-R data produced by the size-sorting effect of wind shear on falling snow. Figure A14 shows a log-log plot of Z_{21} and R_{21} values along the abscissa of Figure A13. In the leading edge, high values of Z are coupled with low values of R, but these quickly approach plateau values equalling those in the generator. The trailing-edge data fall away from the plateau values along a locus closely approximating the locus $Z = 2000 R^{2.0}$, for aggregate snow (Gunn and Marshall, 1958). This behaviour is similar to that of paired values of Z and R reported by Atlas and Plank (1953) from observations taken as an isolated rainshower passed overhead, and to that of theoretically-derived pairs of Z and R values below an isolated rainshower under specified conditions of wind shear (Gunn and Marshall, 1955). The data of Figure A14 indicate that, in the situation studied here at any rate, the effect of wind shear on falling snow is not such as would require a

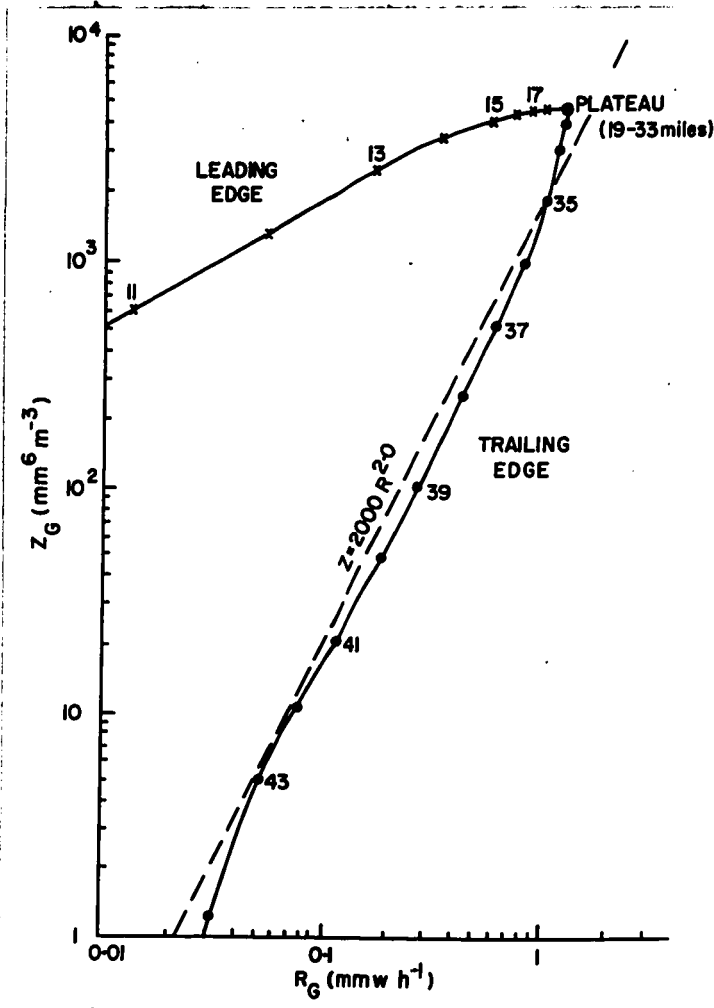


Figure A14. Log-log plot of paired values of Z_G and R_G at the ground, from Z_{21} and R_{21} curves of Figure A13.

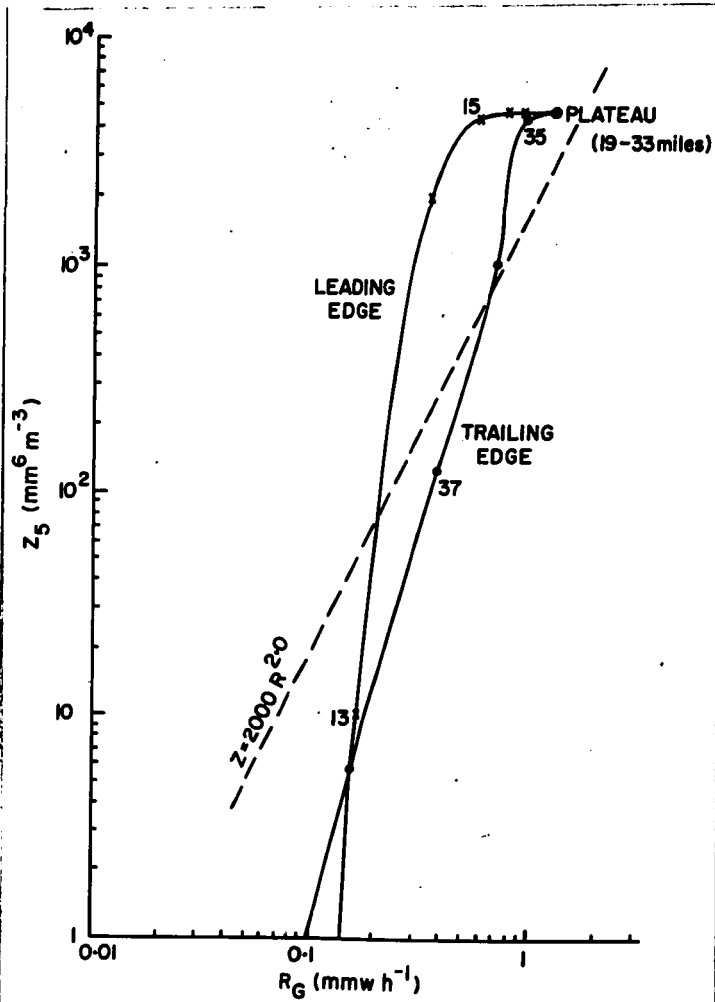


Figure A15. Log-log plot of paired values of Z_5 (Z_{21} at 5000 ft) and Z_G (Z_{21} at the ground). Z_5 curve was displaced 10.8 miles upwind to bring it into juxtaposition with the Z_G curve.

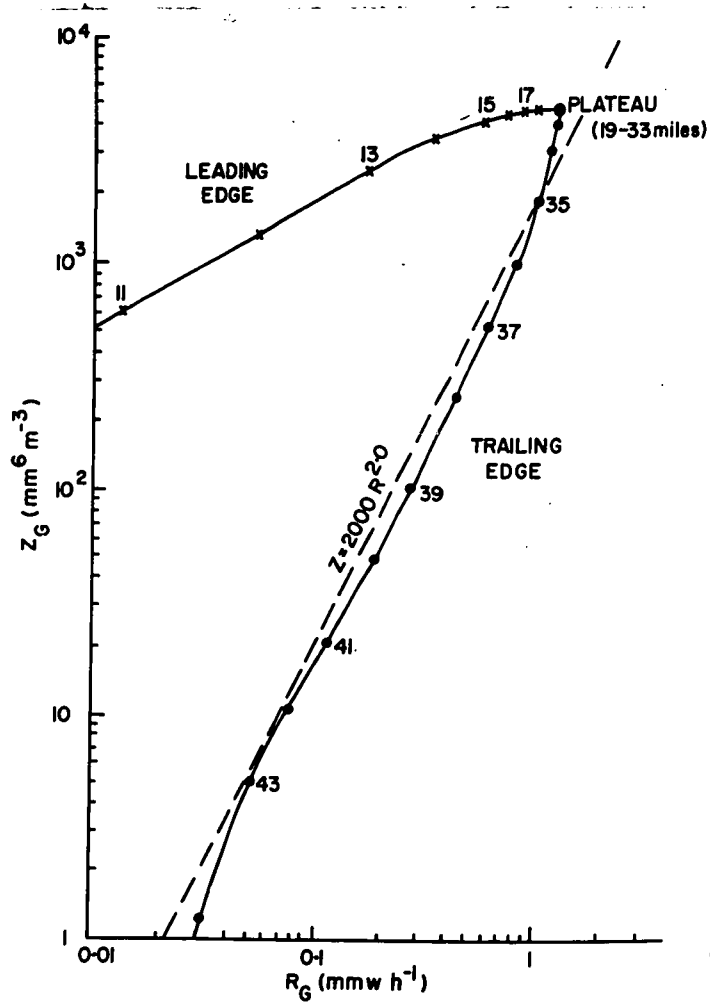


Figure A14. Log-log plot of paired values of Z_G and R_G at the ground, from Z_{21} and R_{21} curves of Figure A13.

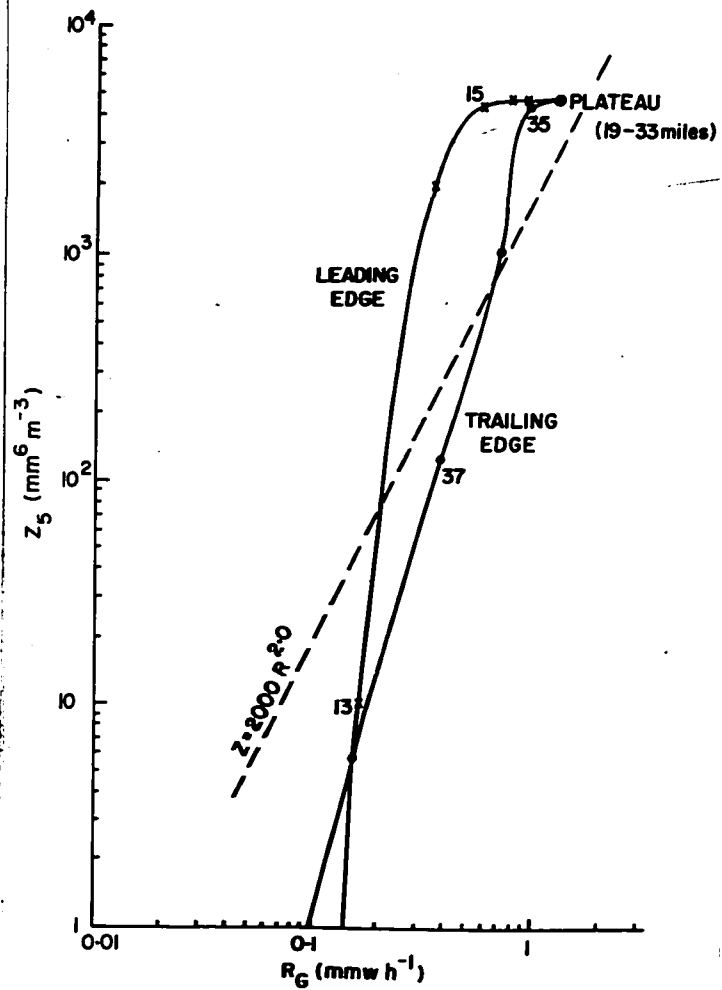


Figure A15. Log-log plot of paired values of Z_5 (Z_{21} at 5000 ft) and Z_G (Z_{21} at the ground). Z_5 curve was displaced 10.8 miles upwind to bring it into juxtaposition with the Z_G curve.

Z-R relation with an exponent greater than 2.0, when Z and R are measured simultaneously at the same height. In fact, the leading-edge data imply that a Z-R relation with an exponent of about 0.5 is required in that region. Leading-edge effects would be obscured in the storm under study by the subsequent heavier "plateau" snow.

Now, consider conditions in which reflectivity measurements at height 5000 ft are converted to snowfall rates and amounts, and compared to rates and amounts measured at the ground. The distribution of Z at height 5000 ft, below a generator of width 21 miles, was obtained by integrating under the Z-curve of Figure A10. The distribution thus obtained was displaced 10.8 miles upwind to the position it occupied 22 minutes earlier (i.e., time required for snow to fall, at 1.1 m sec^{-1} , from height 5000 ft to the ground) and correlated with the distribution of R_{21} (Figure A13) at the ground. A plot of paired values of Z and R is shown in Figure A15. The slope of the locus is approximately 8.0 at the leading edge and approximately 3.0 at the trailing edge. Thus, the correlation of radar data at one height with snowfall rates at a lower height could require the application of a Z-R relation with an exponent value greater than 2.0, at least for situations in which snow produced in discrete generating elements falls through shearing winds toward the ground. The magnitude of this effect depends upon such factors as:

1. The distribution of wind shear with height.

2. The degree of pattern in the process of snow generation i.e. Horizontal extent, and spacing, of generating cells relative to the horizontal spread in the pattern of falling snow.

3. The distribution with size of the snowflakes which largely determines the range of fallspeeds, and therefore

the horizontal spread of the snow during its fall.

4. The vertical distance between the height of radar observation and the height at which snowfall rates are measured.

The analysis indicates that it may be better to use shear-sorting considerations to convert radar observations aloft to snowfall estimates at ground level before correlating with snowfall measurements at the ground.

The rapid variations observed by Imai et al (1955) in the size distribution of snowflakes over a two-hour period may have been related to the size-sorting effect of wind shear on falling snow. Evidence given by the Japanese group, indicates that there was substantial wind shear, more or less constant in direction, in the layer from 25,000 ft to 6000 ft. The radar data show that there was a parallel-banded pattern in the snow aloft, as was described by the Japanese authors. The parallel bands were oriented almost at right angles to the direction of the wind, and they moved with the wind near the 500-mb level ($240^\circ / 70 \text{ mi h}^{-1}$).